IEEE Access
Multidisciplinary | Rapid Review | Open Access Journal

SPECIAL SECTION ON INDEX MODULATION TECHNIQUES FOR NEXT-GENERATION WIRELESS NETWORKS

Received December 25, 2017, accepted January 29, 2018, date of publication February 5, 2018, date of current version March 13, 2018.

Digital Object Identifier 10.1109/ACCESS.2018.2802863

Hierarchical Multi-Functional Layered Spatial Modulation

IBRAHIM A. HEMADEH, (Member, IEEE), MOHAMMED EL-HAJJAR, (Senior Member, IEEE), AND LAJOS HANZO, (Fellow, IEEE)

School of Electronics and Computer Science, University of Southampton, Southampton SO17 1BJ, U.K.

Corresponding author: Lajos Hanzo (lh@ecs.soton.ac.uk)

This work was supported in part by the European Research Council's Advanced Fellow Grant under the Beam-Me-Up Project and in part by the Royal Society's Wolfson Research Merit Award.

ABSTRACT In pursuit of optimal index modulation -aided multiple-input multiple-output (MIMO) systems, where information is implicitly conveyed by relying on the on/off mechanism of the system's components in addition to the classical amplitude, phase, or frequency components, we present in a tutorial style our novel multi-functional (MF) architecture of layered multi-set (LMS) modulation. This generalized framework subsumes various MIMO techniques exhibiting different multiplexing and diversity functionalities. Our LMS design relies on three constituents, namely the space-time (ST) unit, the layered unit and the spatial switching unit. More specifically, the ST unit relies on the generalized space-time shift keying (GSTSK) scheme, where P – rather than one – out of Q ST dispersion matrices are selected for dispersing an equivalent number of phase-shift keying/quadrature amplitude modulation symbols across the antennas and time-slots. In the layered unit, multiple GSTSK codewords are stacked within the layers of codewords spread over time and space. The spatial switching unit activates N_c^t out of N_t transmit antennas. Owing to its hierarchical MF architecture, our LMS system strikes a flexible design trade-off between the achievable throughput as well as the attainable diversity gain and it can potentially subsume various conventional MIMO schemes, such as Bell Lab's Layered Space-Time, space-time block codes, layered steered space-time codes, spatial modulation (SM), space-shift keying, linear dispersion codes, generalized SM, STSK, GSTSK, quadrature SM and multi-set STSK . Additionally, we derive the LMS system's discrete-input continuous-output memoryless channel capacity, which encompasses the capacity limit of all the LMS subsidiaries. We also propose a two-stage serially concatenated soft-decision (SD) based LMS detector by relying on an inner and an outer decoder that iteratively exchange their extrinsic information in order to achieve a near-capacity performance. Last but not least, we utilize the extrinsic information transfer charts for analyzing the convergence behavior of our SD-aided coded LMS scheme.

INDEX TERMS 5G, wireless networks, MIMO, index modulation, spatial modulation, space-time shift keying, MS-STSK, *M*PSK, *M*QAM, practical implementations, channel modulation, channel coding, near-capacity, EXIT charts, hard-decision detection, soft-decision detection.

GLOSSARY

NOMENCLATURE

AC	Antenna Combination
AE	Antenna Element
ASU	Antenna Selection Unit
AWGN	Additive White Gaussian Noise
BCJR	Bahl-Cocke-Jelinek-Raviv
BER	Bit Error Rate
BLAST	Bell-Labs Layered Space-Time
BPCU	Bits Per Channel Use
CC	Channel Coding
CSI	Channel State Information
DAC	Distinct AC
DCMC	Discrete-input Continuous-output Memoryless Channel

EXIT	EXtrinsic Information Transfer
GSTSK	Generalized Space-Time Shift Keying
GSM	Generalized Spatial Modulation
HD	Hard-Decision
I-AgC	Inter-AGglomerate Correlation
ICI	Inter-Channel Interference
I-CoC	Inter-COdeword Correlation
IM	Index Modulation
LDC	Linear Dispersion Coding
LLR	Log Likelihood Ratio
LMS	Layered Multi-Set
Log-MAP	Logarithmic Maximum *a posteriori*
LSSTC	Layered Steered Space-Time Coding
MF	Multi-Functional
MIMO	Multiple-Input Multiple-Output
ML	Maximum Likelihood
MSF-STSK	Multi-Space-Frequency Space-Time Shift Keying
MS-STSK	Multi-Set Space-Time Shift Keying
OFDM	Orthogonal Frequency-Division Multiplexing
OSTBC	Orthogonal STBC
PSK	Phase-Shift Keying
PDF	Probability Density Function
QAM	Quadrature Amplitude Modulation
QSM	Quadrature Spatial Modulation
RF	Radio Frequency
RSC	Recursive Systematic Convolutional
SAC	Shared AC
Semi-DAC	Semi-Distinct AC
SISO	Soft-Input Soft-Output
SD	Soft-Decision
SSK	Space-Shift Keying
ST	Space-Time
STBC	Space-Time Block Code
STSK	Space-Time Shift Keying
SM	Spatial Modulation
SNR	Signal-to-Noise Ratio
V-BLAST	Vertical Bell-Labs Layered Space-Time

LIST OF SYMBOLS

N_c^t	Number of transmit RF chains
N_c^r	Number of receive RF chains
N_t	Number of transmit AE
n_t	n_t-th transmit AE index
N_r	Number of receive AE
n_r	n_t-th receive AE index
M	STSK spatial dimension
Q	Number of dispersion matrices
$\mathcal{L}$	PSK/QAM constellation size
T	Number of STSK time slots
N_c	Number of ACs
P	Number of non-zero symbols in the GSM/GSTSK symbol vector
K	Number of layers
$\boldsymbol{A}_q$	The q-th space-time dispersion matrix of the set $\left\{\boldsymbol{A}_q \in \mathbb{C}^{M\times T}\right\}_{q=1}^{Q}$
$\boldsymbol{A}\,(p)$	The p-th selected dispersion matrix
$\tilde{\boldsymbol{A}}_{q,c}$	The $(N_t \times T)$-element q-th dispersion matrix $\boldsymbol{A}_q$ associated with c-th AC
x_l	l-th PSK/QAM symbol, where $l = 1, \ldots, \mathcal{L}$
$x\,(p)$	The p-th selected PSK/QAM symbol
$\bar{q}$	The q-th index of the p-th selected disperion matrix in the k-th layer $\left\{\left\{\left\{q_{k,p}\right\}_{p=1}^{P}\right\}_{k=1}^{K}\right\}_{q=1}^{Q}$
$\bar{l}$	The l-th PSK/QAM symbol of the p-th selected element in the k-th layer $\left\{\left\{\left\{l_{k,p}\right\}_{p=1}^{P}\right\}_{k=1}^{K}\right\}_{l=1}^{\mathcal{L}}$
$\left\langle \hat{\bar{q}}, \hat{\bar{l}}, \hat{c} \right\rangle$	Estimated values of $\langle \bar{q}, \bar{l}, c \rangle$
$\boldsymbol{S}_k$	Codeword generated by the k-th layer encoder - no AC information
$\bar{\boldsymbol{S}}_k$	Constitutes both $\boldsymbol{S}_k$ and its associated set of M RF chains - no AC information
$\bar{\boldsymbol{S}}$	The K stack of generated codeword by all layers - no AC information
$\mathring{\boldsymbol{S}}$	Transmitted agglomerate of the K generated codewords associated with the activated AC
$\boldsymbol{Y}$	Received block symbol
$\boldsymbol{V}$	AWGN noise
$\boldsymbol{H}$	Channel matrix
$\mathbf{K}$	Transmit symbol vector
a_q	The q-th symbol of $\mathbf{K}$ the symbol vector
$\mathcal{X}$	Matrix of Q vectorized dispersion matrices
$\bar{\boldsymbol{H}}$	$\boldsymbol{I} \otimes \boldsymbol{H}$ equivalent channel matrix
$\mathcal{I}$	AC activation matrix
$\bar{\boldsymbol{Y}}$	The $(N_r T \times 1)$-element vector-based received representation of $\boldsymbol{Y}$
$\bar{\boldsymbol{V}}$	Vectorized representation of $\boldsymbol{V}$
$\hat{\boldsymbol{A}}_{q,c}$	The vectorized form of $\tilde{\boldsymbol{A}}_{q,c}$
$\boldsymbol{F}_c$	The c-th AC ones-and-zeros activation matrix
$\bar{\boldsymbol{H}}_c$	The vectorized representation of the equivalent channel between the activated N_c^t transmit AEs and the N_r receive AEs
B_{SM}	Number of bits transmitted in an SM vector symbol
B_{GSM}	Number of bits transmitted in a GSM vector symbol
B_{QSM}	Number of bits transmitted in a QSM vector symbol
B_{STSK}	Number of bits transmitted in an STSK codeword
B_{GSTSK}	Number of bits transmitted in a GSTSK codeword
$B_{MS-STSK}$	Number of bits transmitted in an MS-STSK codeword
$B_{L-GSTSK}$	Number of bits transmitted in an L-GSTSK codeword

B_{ASU}	Number of bits fed into the ASU
B	Number of bits transmitted in an LMS agglomerate
R	The normalized throughput of the LMS system over T time slots
$\mathcal{D}$	Diversity order
C	System capacity
$L(b)$	LLR representation of a bit b
θ_c	Phase-shift rotation
$\bigwedge\theta_c$	Phase-shift difference between two ACs

MATHEMATICAL OPERATORS AND FUNCTIONS

$f(n, r)$	Returns the number of possible combinations $\binom{n}{r}$ of r objects from a set of n objects
2^{ι}	An order of two positive integer, where $\iota = 0, 1, 2, \ldots$
$\lfloor(\cdot)\rfloor_{2^{\iota}}$	Flooring to the nearest 2^{ι} integer operation
$\lfloor . \rceil$	The rounding operation of a real number to the nearest integer
$\Re\{x\}$	Real part of the complex value x
$\Im\{x\}$	Imaginary part of the complex value x
x^*	The conjugate of the complex value x
$(\cdot)_{q,c}$	A parameter that is associated with the q-th dispersion matrix and the c-th AC
$(\cdot)_{n_t}$	A parameter that is associated with the n_t-th transmit AE
$(\cdot)_{n_r}$	A parameter that is associated with the n_r-th receive AE
$\Theta^{(k)}$	A parameter Θ that is associated with the k-th layer
$\Theta(p)$	A parameter Θ that is associated with the p-th element of a P-sized set
$\Theta^{(DAC)}$	A parameter Θ that is associated with the DAC allocation technique
$\Theta^{(SAC)}$	A parameter Θ that is associated with the SAC allocation technique
$\Theta^{(Semi-DAC)}$	A parameter Θ that is associated with the Semi-DAC allocation technique
$vec(\cdot)$	Vectorization operation
$\mathcal{O}(\cdot)$	Complexity order
$\min(a, b)$	Returns the minimum between a and b
$\prod$	The multiplication operation
$\|\cdot\|$	The Frobenius norm
$\|\cdot\|$	The modulus of a complex number
$(\cdot)^T$	The transpose operation
$(\cdot)^H$	The Hermitian transpose
$(\cdot)^{\dagger}$	The Pseudo-inverse
$\mathrm{tr}\{\cdot\}$	The *trace* operator
$\log_2(\cdot)$	Logarithm to base 2
$\mathrm{jac}(\cdot)$	The Jacobian maximum operator
$p(a)$	Probability of a
$p(a\|b)$	Probability of a given b
$\arg\min_{x\in\mathcal{S}}\{\cdot\}$	Argument $x_i \in \mathcal{S}$ yielding the minimum

CONSTANTS AND SETS

π	The number pi
e	The Euler number
$\mathbb{C}$	Complex numbers
$\mathbb{R}$	Real numbers
$\mathbb{Z}$	Integer numbers
$\mathbf{0}$	All-zero matrix

I. INTRODUCTION

The 5th generation (5G) wireless technology [1]–[3] is expected to support a minimum downlink peak-rate of 20 Gbps and a minimum uplink peak-rate of 10 Gbps as set by the International Telecommunications Union (ITU) in their latest report in June 2017. The research community is relentlessly working on sophisticated Multiple-Input Multiple-Output (MIMO) techniques [4]–[9], Millimeter-Wave (mmWave) communications [6], [10]–[12], Massive MIMOs [13]–[15], small cells [16], Heterogeneous Networks (HetNets) [17] and so on, as detailed in [18]. A specific class of MIMO techniques, referred to as Multi-Functional MIMO (MF-MIMO) [2], [19], which relies on an amalgam of two or more design approaches in the space-time and/or-frequency dimensions has become a strong candidate for the next generation systems, because it amalgamates hybrid beamforming techniques conceived for mmWave communications [20], [21], hybrid MF-MIMO techniques [5]–[7], [22], [23], Index Modulation (IM)-based MIMOs [3], [9], [24]–[29] etc.

As shown in Figure 1, MIMO schemes can be categorized into classic co-located and distributed MIMOs [2]; the distributed class of MIMO schemes is beyond the scope of this paper. In particular, co-located MIMO techniques, where multiple AEs are employed at both the transmitter and the receiver can be further categorized into multiple access techniques [30], multiplexing techniques [31], [32], diversity techniques [33], [34] and beamforming techniques [35]. There is always a design trade-off between these techniques, as shown in Figure 1, which has been extensively covered by Xu *et al.* in [36]. Wireless systems are capable of achieving higher capacity with the aid of MIMO arrangements than by using Single-Input Single-output (SISO) arrangement [1], [2], [37].

In this treatise, we construct our novel Layered Multi-Set (LMS) architecture in a tutorial-based style, which belongs to the MF composite of MIMOs constituted by an amalgam of various MIMO techniques in Figure 1. This technique allows us to incorporate the merits of various MIMOs in a single system, namely Space-Time (ST) codes, transmission layering and IM-based schemes in order to boost the system capacity. In what follows, we briefly introduce each sub-class of the co-located MIMO techniques presented in Figure 1, namely the diversity, multiplexing, multiple access, beamforming as well as MF-MIMO classes, followed by introducing our LMS concept.

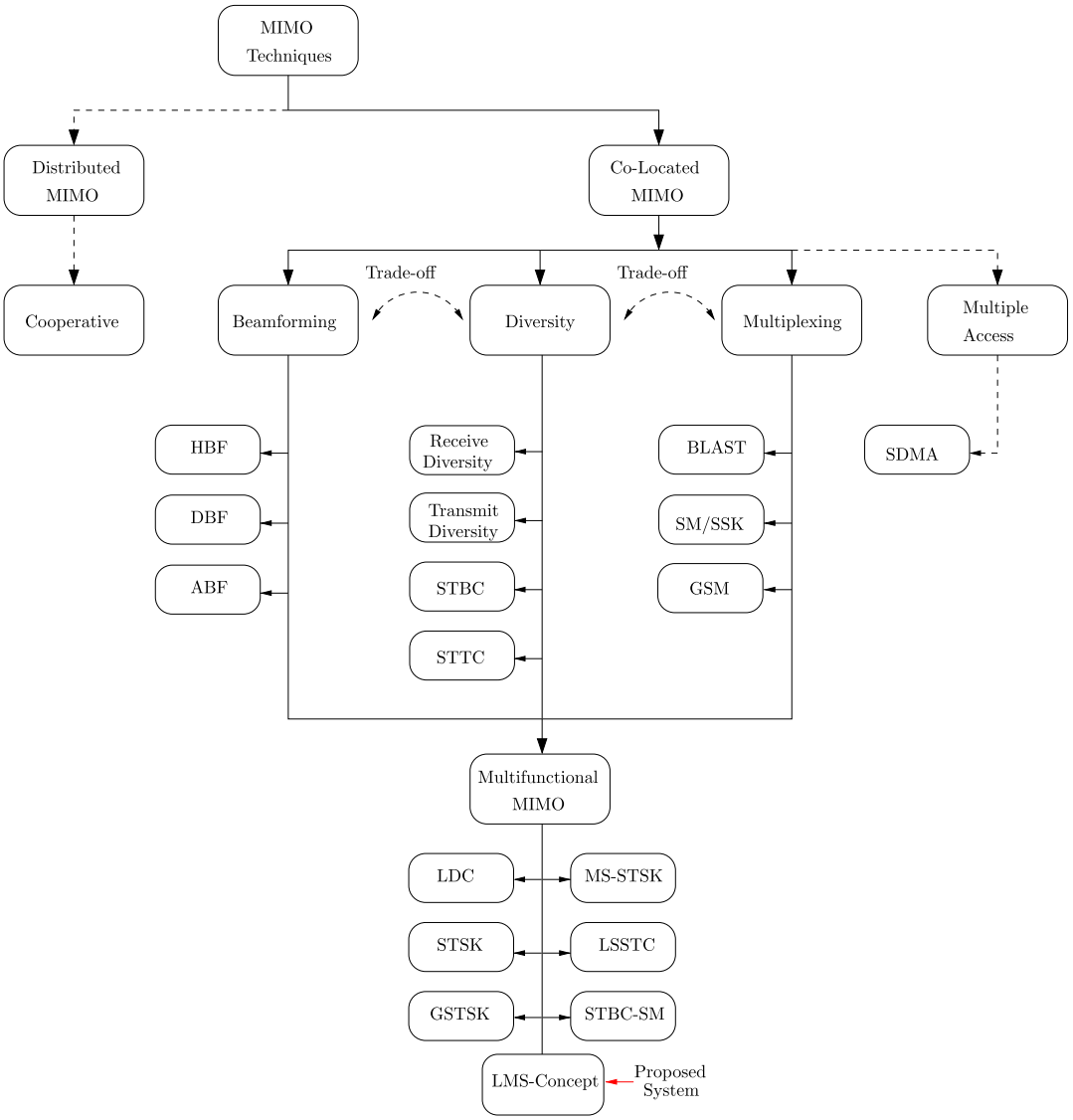

FIGURE 1. The family tree of MIMO techniques.

A. DIVERSITY TECHNIQUES

Diversity techniques are designed for enhancing the integrity of communications for transmission over fading channels by invoking multiple replicas of the transmitted and/or received signal over the space, time and/or frequency dimensions [37]. To elaborate further on the concept of diversity, let us consider the two signals shown in Figure 2, where each line in the figure corresponds to an independently fading replica of the same information. Furthermore, the signal power versus space/time/frequency variable represents the power normalized to the noise level, yielding the Signal-to-Noise Ratio (SNR). It is shown in the figure that when a specific signal suffers from deep fading at a specific instant, the corresponding lost information can be restored with the assistance of another replica or with the aid of an efficient combination of multiple replicas.

To expound a little further, spatial diversity can be achieved by positioning multiple AEs sufficiently far from each other at the transmitter and/or receiver in order experience independent fading [38]. The very first efforts dedicated to achieving spatial diversity were focused on the diversity concept intimated in Figure 1. This concept may be exploited by the Maximum Ratio Combining (MRC) technique [39] as well as by Brennan's classic Selection Combining (SEC) and Equal Gain Combining (EGC) techniques that were proposed as early as the 1950s [40], [41]. The MRC technique was then later also exploited at the transmitter side with the aid of the Maximum Ratio Transmission (MRT) scheme of [42] relying on transmit precoding. Furthermore, the Orthogonal Space-Time Block Code (OSTBC) was proposed by Alamouti [33] in the late 1990s, which is capable of achieving a diversity gain by jointly exploiting both the space- and

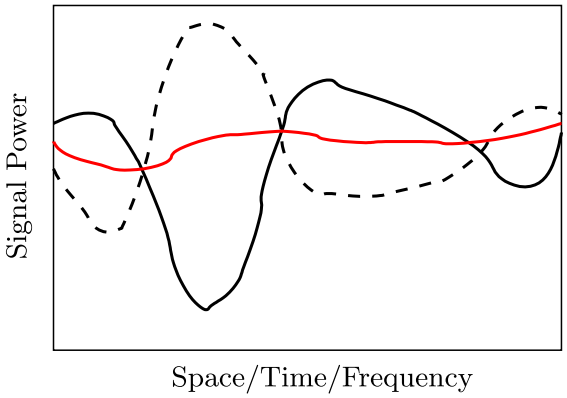

FIGURE 2. A diversity gain is attained when multiple replicas of the same signal are transmitted and received subjected to independent fading. The red curve denotes the combination of the two other curves.

time- domain using a (2×2)-MIMO configuration and orthogonal ST codes. Inspired by Alamouti's work, Tarokh *et al.* [34] generalized the OSTBC scheme by introducing the general STBC concept, which is capable of supporting multiple AE based arrangements. However, the family of STBCs shown in Figure 1 is incapable of attaining any coding gain and it is also severely affected by Inter-Symbol Interference (ISI). These limitations are resolved by introducing other schemes, such as the Space-Time Trellis Code (STTC) family, albeit at the cost of a higher decoding complexity [43], [44]. This is achieved by combining space-time coding with trellis coding. The capacity limitation of STBC was further resolved by introducing the Linear Dispersion Coding (LDC) scheme in [45], [46], where multiple PSK/QAM symbols are dispersed across both the space and time domains with the aid of dispersion matrices in order to achieve both an enhanced throughput and an improved diversity gain. This scheme is however considered under the multifunctional MIMO category in Figure 1, as it will be discussed later in Section I-E. By incorporating an additional dimension into the STBC framework, it was later extended to the frequency dimension in [47] with the aid of the Space-Frequency Coding (SFC) concept conceived for achieving frequency diversity. Furthermore, STBCs were amalgamated with Bit-Interleaved Coded Modulation (BICM) and OFDM in [48] and [49] for the sake of achieving space- time-and frequency-diversity gains.

B. MULTIPLEXING TECHNIQUES

The aforementioned diversity techniques, such as STBCs, are capable of attaining diversity gains, while typically sacrificing the achievable throughput [50]. For example, the OSTBC scheme associated with two transmit AEs arrangement achieves the highest possible normalized throughput of one information bit per channel use (bpcu) in the entire family of OSTBC schemes [33], [34]. Alternatively, the multiplexing branch of the MIMO family depicted in Figure 1 aims for attaining an enhanced normalized throughput by

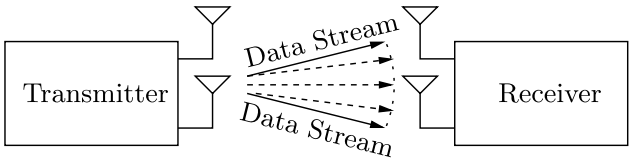

FIGURE 3. The MIMO concept of multiplexing.

simultaneously transmitting multiple data streams, as shown in Figure 3. The figure illustrates the concept of MIMO multiplexing, where a transmitter employs multiple AEs in order to transmit multiple independent data streams, which results in providing a beneficial multiplexing gain [6], [37]. Furthermore, the class of multiplexing techniques, in which the transmitted data streams are multiplexed over the spatial domain, is referred to as Spatial Division Multiplexing (SDM), which was first proposed by Paulraj and Kailath [51] in their US Patent 5,345,599 in a broadcasting context. However, the widespread consciousness of the benefits of SDM was later promoted by Bell Laboratories in the mid-1990s by introducing the concept of Bell-Labs Layered Space-Time (BLAST), scheme and the Diagonal BLAST (D-BLAST) arrangement of Foschini [52], as illustrated in Figure 1. Foschini's work was later extended by Wolniansky *et al.* in [31] to the Vertical BLAST (V-BLAST) concept, where independent data streams are transmitted over different AEs. The BLAST schemes are capable of approaching the capacity limits of MIMO systems [2].

Later, a new class of multiplexing techniques was introduced by Song *et al.* [53] in 2004, which is currently known as Spatial Modulation (SM), representing the spatial derivative of the multi-dimensional Index Modulation (IM) scheme [54]. In a nutshell, IM invokes the on/off mechanism of communications systems in order to reliably convey implicit information using transmit antennas, frequency subcarriers, time slots etc. in contrast to conventional modulation techniques, which rather rely on the amplitude, phase and/or frequency components of sinusoidal carriers. Basar *et al.* [28] has rigorously reviewed the IM concept's space- time -and frequency -domain representatives. However, in this treatise we specifically focus our attention on the spatial dimension of IM, as manifested in Figure 1.

Space Shift Keying (SSK) was originally proposed by Chau and Yu [55] in 2001 and then developed into its current form by Jeganathan *et al.* [56]. This scheme was then further refined by Mesleh *et al.* [32] in 2008, where a single AE is activated from a larger set of transmit AEs for the sake of implicitly conveying for example two bits of extra information by the index of the activated AEs in addition to the classic transmitted symbol itself. The SM philosophy has two substantial benefits, namely the reduced number of RF chains, which reduces both the cost and the complexity of the MIMO system, and the reduced single-stream detection complexity [57], [58]. However, it is widely agreed that in

its original form, SM does not achieve any transmit diversity gain, unless incorporated with other precoding technique, such as the space-time indexing SSK (ST-SSK) scheme proposed in [59], hence this has to be achieved at the receiver side. As a solution, Masouros and Hanzo [60] proposed a low complexity SM encoding technique by relying on Constellation Randomization (CR) at the transmitter side for the sake of striking a trade-off between the achievable transmit diversity gain and the detection complexity. Furthermore, it was demonstrated in [32], [56], and [61] that the SM/SSK scheme is capable of exhibiting benefits over many other MIMO arrangements.

Later on, the Generalized SM (GSM) concept shown in Figure 1 was proposed by Wang *et al.* [62] as a generalized version of the aforementioned single-AE SM scheme, where a specific fraction of the total number of antennas is activated in order to transmit a single or multiple PSK/QAM symbols, while additionally relying on implicit antenna index information. However, the GSM scheme suffers from Inter-Channel Interference (ICI), which may be mitigated with the aid of sophisticated receiver techniques [63], [64]. For the sake of further enhancing the performance of the GSM scheme, transmit precoding was applied to the transmitted symbols in [65]. For instance, Masouros [66] proposed a transmit precoding technique for SM by relying on symbol scaling and/or phase-alignment in order to retrieve a symbol constellation having uniform phase angles at the receiver side.

C. SPACE-DIVISION MULTIPLE ACCESS

The concept of SDM can be extended to the Space-Division Multiple Access (SDMA) concept presented in Figure 1 for supporting Multi-User (MU) scenarios, where the independent spatial streams of Figure 3 are assigned to multiple users, instead of a single user having multiple streams. This was achieved by exploiting the unique, user-specific CIRs of the users [67]. Hence, the spatial dimension is exploited in SDM for enhancing the achievable throughput, whereas in SDMA the spatial dimension is invoked for the sake of increasing the number of communicating users.

D. BEAMFORMING TECHNIQUES

The final direct branch of the co-located MIMO family classified in Figure 1 is Beamforming (BF), designed for the sake of attaining an improved SNR gain and/or to reduce the inter-user interference of MU scenarios [68]. Beamforming is achieved by focusing the transmitted and/or received beam in the direction of the transmitter or receiver [69]. This can be achieved with the aid of three main beamforming architectures, namely the Digital BF (DBF), Analogue BF (ABF) and Hybrid BF (HBF) arrangements [10]. The research of different types of BF techniques has flourished following the recent popularity of mmWaves [7].

In all of the aforementioned MIMO techniques, namely the diversity and multiplexing techniques, the AEs should be spaced sufficiently far apart in order to achieve independent fading on each transmit and receive AE. When the AEs are insufficiently far from to each other, correlation is imposed on the transmitted streams, which would reduce both the diversity gain [70] and the achievable capacity of MIMO systems [71], [72]. However, in the context of beamforming, the AEs are typically $\lambda/2$-spaced.

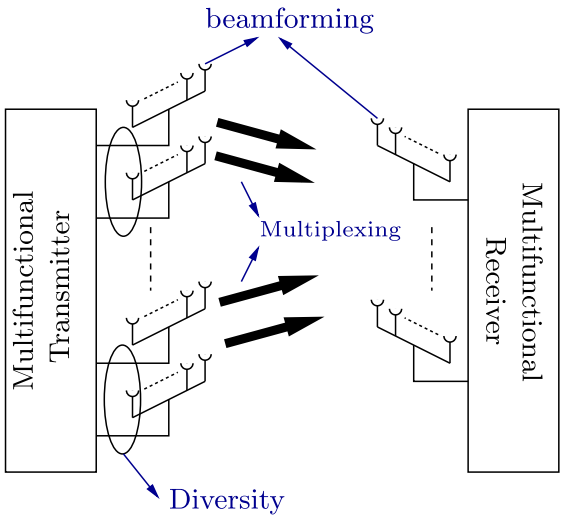

FIGURE 4. General architecture of a MFAA representing an amalgam of diversity, multiplexing and joint transmitter-receiver beamforming techniques.

E. MULTIFUNCTIONAL MIMO TECHNIQUES

When two or more MIMO techniques are combined in a single MIMO system, the system is referred to as a Multi-Functional MIMO (MF-MIMO) [1], [37]. The general architecture of a MF-MIMO is shown in Figure 4, where the transmitter is formed of multiple Transmit Antenna Arrays (TAAs), each equipped with multiple AEs used for achieving BF gain. Furthermore, each group of TAAs can be additionally harnessed for achieving diversity gain, while other TAAs may be invoked for transmitting independent signals in order to achieve a multiplexing gain, as shown in Figure 4. Similarly, the receiver employs multiple Receive Antenna Arrays (RAAs) for the sake of achieving further receive beamforming gain. For instance, Tarokh *et al.* [73] proposed a MF-MIMO in 1999, which combines V-BLAST and STBC in a layered structure, where the system is capable of achieving both enhanced diversity gain and improved capacity. Later in 2002, Jongren *et al.* [74] proposed an amalgam of OSTBC and transmit beamforming, where the system achieved compelling performance enhancements over the classical OSTBC scheme. El-Hajjar *et al.* [75] proposed a trimode system referred to as the Layered Steered Space-Time Codes (LSSTC) representing an amalgam of the OSTBC scheme, of V-BLAST as well as of transmit ABF. This LSSTC scheme is capable of benefiting from the enhanced diversity gain and low detection complexity of the OSTBC, from the improved throughput of V-BLAST and from the enhanced BF gain of ABF.

Another type of MF-MIMO can be digitally tuned. For example, the aforementioned LDC scheme proposed by Hassibi and Hochwald [45], is capable of attaining both full multiplexing gain and full diversity gain by dispersing multiple modulated MPSK/QAM symbols over both the space and time-domain using appropriately designed dispersion matrices. The LDC can strike a design trade-off between the attainable diversity gain and the achievable throughput [46]. The concept of SM was further enhanced also with the aid of SSK by Jeganathan *et al.* [56], where information is exclusively conveyed by the index of the activated AE. This scheme, as well as the LDC concept were later combined with the idea of SM by Sugiura *et al.* [76], resulting in the concept of Space-Time Shift Keying (STSK). Explicitly, in STSK, one out of Q dispersion matrices is activated for spreading a classical QAM/PSK symbol both over time and space, thus achieving an excellent performance associated with low-complexity detection. Furthermore, Sugiura *et al.* [77] and [78] investigated STSK in comparison to many other MIMO arrangements, such as V-BLAST, SM and LDC. Sugiura *et al.* demonstrated that STSK is capable of outperforming these systems, whilst imposing a lower detection complexity. The STSK scheme was further enhanced in [57], [79], [80] by reducing its computational complexity, while in [6], and [81]–[83] by supporting a MU scenario. The STSK scheme was then further developed by Sugiura *et al.* [63] to the generalized STSK (GSTSK) regime, where multiple dispersion matrices are simultaneously activated by different symbols.

Another MF-MIMO arrangement referred to as the STBC-SM arrangement was proposed by Basar *et al.* [24], where the low-complexity OSTBC concept was combined with SM in order to provide both multiplexing and diversity gains. Recall that the maximum normalized throughput of one symbol per channel use can only be achieved by Alamouti's 2×2 STBC. In order to improve the throughput of STBC-SM, an increased number of antenna combinations should be employed, which would impose an increased complexity. More recently, Datta *et al.* [84] proposed Generalized Spatial Index Modulation (GSIM), which exploits the philosophy of SM by transmitting over multiple antennas in order to implicitly convey the activated antenna indices. The second technique was also proposed in [84], which is referred to as Generalized Space-Frequency Index Modulation (GSFIM), because it utilizes both the space and frequency indices of an OFDM symbol for enhancing the attainable throughput by conveying additional information over the combination of antennas and sub-carrier frequency indices. Furthermore, both the GSIM and GSFIM schemes increase the attainable throughput without affecting the diversity order.

Due to the limited achievable throughput of OSTBC, attaining an increased throughput in SM-OSTBC relies on invoking additional transmit AEs. To circumvent this problem in SM-aided MIMO structures, we proposed the Multi-Set STSK (MS-STSK) [85] concept of Figure 1 as an amalgamation of SM and STSK. In MS-STSK, a carefully selected combination from a larger set of AEs is invoked for transmitting an STSK codeword associated with the implicit AE combination index, which leads to an enhanced throughput and to an improved integrity over the classical STSK scheme, while flexibly adjusting the number of RF chains and the detection complexity order. The MS-STSK scheme strikes a design trade-off between the achievable throughput and diversity gain, which was shown to outperform the conventional STSK scheme [85], with the additional advantage of avoiding the ICI issues imposed both by GSM and GSTSK. Hence, MS-STSK has the potential of outperforming other conventional MIMO arrangements, such as STSK, LDC, SM/SSK, OSTBC and V-BLAST, which can be achieved by carefully tunning the MS-STSK's parameters, namely the number of RF-chains, the number of dispersion matrices Q and the constellation size $\mathcal{L}$. The MS-STSK scheme was later extended to exploit the frequency dimension [9] and to support a MU scenario in the downlink [8].

Owing to their flexible structure, we opt for the MF-MIMO framework of co-located MIMO techniques for the proposed LMS architecture, which is capable of striking a design trade-off between the achievable throughput and the attainable diversity gain. Against this background, the novelty of this treatise is detailed in the following section.

F. NOVELTY STATEMENT

In the light of the above MIMO techniques, the novelty of this treatise can be summarized as follows:

1) We present an insightful tutorial over several IM-assisted techniques, namely the SM/SSK, GSM/QSM, STSK, GSTSK and MS-STSK arrangements as well as the V-BLAST and LSSTC techniques, with focusing on their functionalities, system models and on their interrelationships.
2) We propose the novel MF architecture of LMS, which is a sophisticated amalgam of space-time processing, layered designs as well as of spatial domain index modulation. The LMS is a hierarchical MIMO framework that incorporates several classical MIMO schemes as special cases, such as BLAST, STBC, SM/SSK, LDC, STSK and MS-STSK as well as their generalized interpretations, such as LSSTC, GSTSK and GSM/QSM.
3) The proposed LMS architecture accommodates multiple novel standalone MIMO architectures. More specifically, the layered-and/or-generalized constructions of the aforementioned MIMO arrangements can be considered as a unique system, such as the L-LDC, L-STSK, L-GSTSK etc.
4) We derive the Discrete-input Continuous-output Memoryless Channel (DCMC) capacity for our LMS system, which is a generalized capacity formulation of all its subsidiaries.
5) We propose a two-stage serially concatenated Soft-Decision (SD) based LMS detector for our LMS arrangement, which constitutes a pair of inner and outer decoders that iteratively exchange their extrinsic

information in order to achieve a near-capacity performance. The proposed detection technique is extended to all other MIMO arrangements.

6) We utilize the powerful tool of EXtrinsic Information Transfer (EXIT) charts for analyzing the convergence behavior of our LMS scheme, which achieves an infinitesimally low BER.

In the remainder of this treatise, we device our LMS system concept in Section II. Then, we introduce the LMS transceiver design in Section III, with a detailed insight into the different pconstituent MIMO schemes. Next we detail the LMS receiver's operation in Section IV, where we present both a Hard-Decision (SD)-aided detector and a soft-aided-decision detector as well as a two-stage serially concatenated design followed by a detailed derivation of the LMS system's DCMC capacity in Section V. In Section VI, we present our performance results and discussion. Then, the EXIT chart tool is utilized to evaluate the convergence behavior of the system in Section VII. Finally, we conclude in Section VIII. The structure of this treatise is outlined in Figure 5.

II. THE LMS CONCEPT

In what follows, we commence by introducing the classical SM system model and then proceed by presenting the logic behind the model-vectorization applied to the STSK, GSTSK and MS-STSK systems, before we detail our LMS-GSTSK system model.

In this section, we construct our LMS framework, which is an amalgam of multiple MIMO arrangements, namely of ST coding, of IM in its spatial form as well as of MIMO layering, where we separately introduce each of the components' features. We commence by introducing the philosophy of implicit information transmission attained by exploiting the on/off mechanism of the available AEs in SM [32]. Then, we extend our discussions to its generalized forms of GSM [62] and QSM [86], [87]. Subsequently, we present the STSK [78] and GSTSK [76], both of which utilize the on/off status of SM and GSM by activating a carefully chosen fraction of the dispersion matrices in favor of an enhanced throughput and/or improved diversity gain. After that, we present the concept of MS-STSK [85], which utilizes the on/off philosophy both in the time- and spatial-domain, by activating a single antenna combination and a single dispersion matrix as an amalgam of SM and STSK. Next, we detail the layering philosophy of MIMO systems and finally, we introduce the general structure of our LMS scheme.

Let us first consider a general MIMO system having N_t transmit and N_r receive AEs. Let $\boldsymbol{H} \in \mathbb{C}^{N_r \times N_t}$ describe the zero-mean and unity-power channel matrix between the system's transmit and receive AEs and $\boldsymbol{V}$ the zero-mean Additive White Gaussian Noise (AWGN) obeying $\mathcal{CN}(0, N_0)$ with N_0 being the noise power. The received signal $\boldsymbol{Y}$ can be formulated as

$$\boldsymbol{Y} = \boldsymbol{H}\,\mathring{\boldsymbol{S}} + \boldsymbol{V}. \tag{1}$$

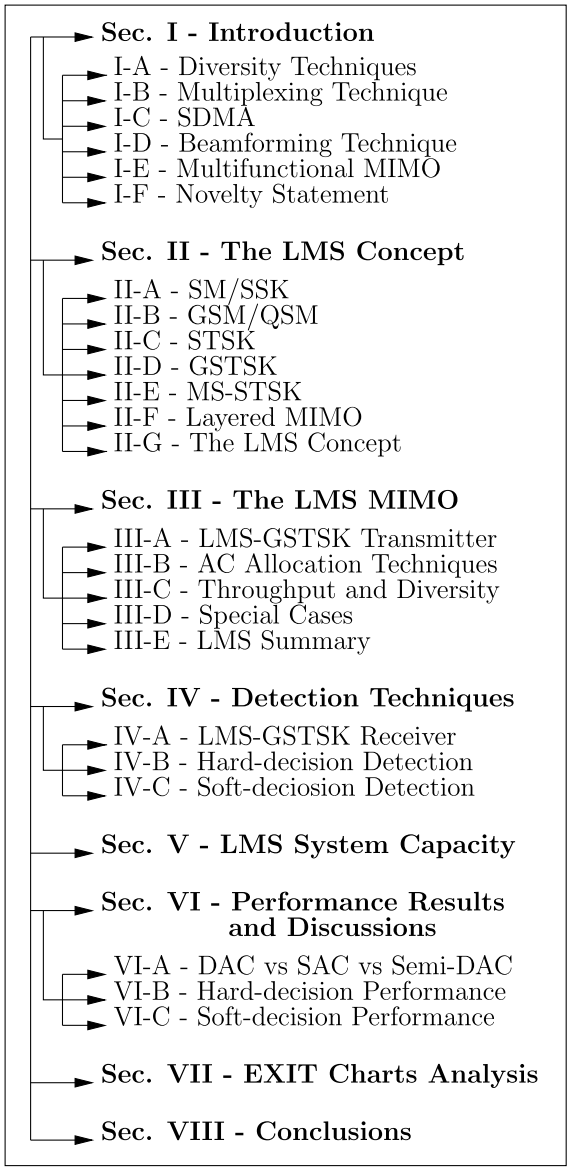

FIGURE 5. Treatise Structure.

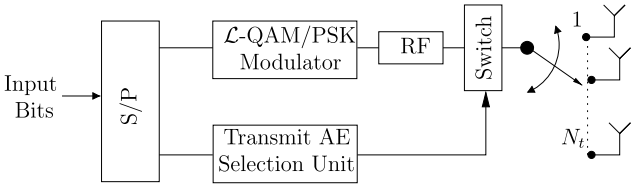

FIGURE 6. SM transmitter block diagram.

The system model presented in (1) serves here as a general MIMO system and can be used for any of the following systems.

A. SM/SSK

Consider the single-RF-chain based $(N_t \times N_r)$-element SM system of Figure 6. In classical SM [32], only one AE out of $N_t = 2^t$ AEs is activated with the aid of both a transmit

AE selection unit as well as a sufficiently fast switch for transmitting a single PSK/QAM symbol x_l at the activated AE, while $\iota \in \mathbb{Z}$ denotes any positive integer number. This allows the system to implicitly convey $\log_2(N_t)$ bits of the activated AE index information in addition to $\log_2(\mathcal{L})$ bits of the transmitted symbol information, where the total number of transmitted bits B_{SM} is expressed as

$$B_{SM} = \log_2(N_t) + \log_2(\mathcal{L}), \tag{2}$$

where the SM system degenerates into a conventional SISO system, when $N_t = 1$. Furthermore, when no information is conveyed over the classic PSK/QAM constellation, yielding $\mathcal{L} = 1$ and t $x_l = 1$, then the only information is transmitted by the activated AE. Hence, the system becomes a simple form SSK[1] arrangement [56].

The SM scheme exhibits several advantageous features over other classical MIMO schemes. For instance, SM is capable of achieving a higher throughput than either the single-antenna systems relying on PSK/QAM modulations or OSTBC, while benefiting from a single RF-chain based implementation [88]. Furthermore, in addition to the transmitter's simple design shown in Figure 6, SM requires a lower transmit power, hence relaxing the linearity requirements of the power amplifiers [3]. At the receiver side, a single-stream ML detector maybe employed as a benefit of activating a single-AE per channel use, because no ICI is imposed. Furthermore, SM benefits from a wide range of optimum and sub-optimum low complexity detectors, which strike a BER performance versus detection complexity trade-off, as discussed in [36] and in the citations therein. The ML search-space in the SM arrangement relies both on N_t and on $\mathcal{L}$, where the complexity order achieved is $\mathcal{O}(N_t \cdot \mathcal{L})$, while for the SSK system it is rather $\mathcal{O}(N_t)$.

To elaborate further, the system model of (1) can be formulated as

$$\boldsymbol{Y} = \underbrace{\begin{bmatrix} \boldsymbol{H}_1 & \cdots & \boldsymbol{H}_{n_t} & \cdots & \boldsymbol{H}_{N_t} \end{bmatrix}}_{\boldsymbol{H}} \underbrace{\begin{bmatrix} 0 \\ \vdots \\ x_l \\ \vdots \\ 0 \end{bmatrix}}_{\mathring{\boldsymbol{S}}} + \boldsymbol{V}, \tag{3}$$

$$= \underbrace{\begin{bmatrix} \boldsymbol{H}_1 & \cdots & \boldsymbol{H}_{n_t} & \cdots & \boldsymbol{H}_{N_t} \end{bmatrix}}_{\boldsymbol{H}} \cdot \underbrace{\begin{bmatrix} \underbrace{0, \ldots, 0}_{q-1}, x_l, \underbrace{0, \ldots, 0}_{N_t - q} \end{bmatrix}^T}_{\mathring{\boldsymbol{S}}} + \boldsymbol{V}, \tag{4}$$

where the position of x_l at the q-th index of the transmit vector $\boldsymbol{S} \in \mathbb{C}^{N_t \times 1}$ activates the q-th column vector $\boldsymbol{H}_q$ out of $n_t = 1, \ldots, q, \ldots N_t$ of $\boldsymbol{H}$. Hence, the q-th transmit AE is activated to transmit x_l and the implicit index information within. In the following, we introduce an example for further illustrating the concept of SM.

Example 1: consider a SM system associated with $N_t = 4$ transmit antennas, where the $(N_r = 4 \times N_t = 4)$-element channel matrix of (1) is defined as

$$\boldsymbol{H} = \begin{bmatrix} h_{1,1} & h_{1,2} & h_{1,3} & h_{1,4} \\ h_{2,1} & h_{2,2} & h_{2,3} & h_{2,4} \\ h_{3,1} & h_{3,2} & h_{3,3} & h_{3,4} \\ h_{4,1} & h_{4,2} & h_{4,3} & h_{4,4} \end{bmatrix}, \tag{5}$$

while the PSK/QAM symbol x_l is located at $q = 2$ in $\mathring{\boldsymbol{S}}$ as

$$\mathring{\boldsymbol{S}} = \begin{bmatrix} 0 & x_l & 0 & 0 \end{bmatrix}^T. \tag{6}$$

Hence, the received signal $\boldsymbol{Y}$ can be expressed as

$$\boldsymbol{Y} = \begin{bmatrix} h_{1,2} \\ h_{2,2} \\ h_{3,2} \\ h_{4,2} \end{bmatrix} x_l + \boldsymbol{V}. \tag{7}$$

B. GSM/QSM

In the classical SM presented in [32], a single RF chain has to be switched between $N_t = 2^\iota$ AEs[2] to transmit a single PSK/QAM symbol as well as the implicit antenna index information. The spectral efficiency of SM is hence bounded by $\log_2(N_t)$, which cannot be improved by any additional AEs disobeying the equality rule of $N_t = 2^\iota$. To overcome this constraint, Younis *et al.* [89] and Fu *et al.* [90] proposed that a combination of P AEs can be activated in the Generalized SM (GSM) scheme of Figure 7(a), which enhances the spectral efficiency at the cost of employing extra RF chains. Hence, the total number of bits transmitted B_{GSM} by the GSM scheme based on B_{SM} of (2) is

$$B_{GSM} = \log_2 f(N_t, P) + \log_2(\mathcal{L}), \tag{8}$$

when a single $\mathcal{L}$PSK/QAM symbol is transmitted over the P activated AEs [89] and

$$B_{GSM} = \log_2 f(N_t, P) + P \cdot \log_2(\mathcal{L}). \tag{9}$$

when P independent symbols are transmitted over the P activated AEs [91], where the function $f(N_t, P)$ is used for calculating the number of available combinations of P out of N_t AEs as

$$f(N_t, P) = \left\lfloor \binom{N_t}{P} \right\rfloor_{2^\iota}. \tag{10}$$

Observe here that both interpretations of B_{GSM} in (8) and (9) are equivalent to B_{SM} of (2), when $P = 1$, hence SM may be considered as a special case of GSM under the same constraint. In the following we introduce an example to further illustrate the concept of GSM. The ML search-space in the GSM arrangement relies both on $f(N_t, P)$ and on $\mathcal{L}$, where the complexity order achieved is $\mathcal{O}\left(f(N_t, P) \cdot \mathcal{L}^P\right)$.

[1] In this treatise, we use 1PSK to indicate that no information is transmitted over the PSK/QAM symbol, yielding $x_l = 1 \forall l = \mathcal{L} = 1$.

[2] The notation of 2^ι regards a power of two number, such as 0, 2, 4, 8 etc.

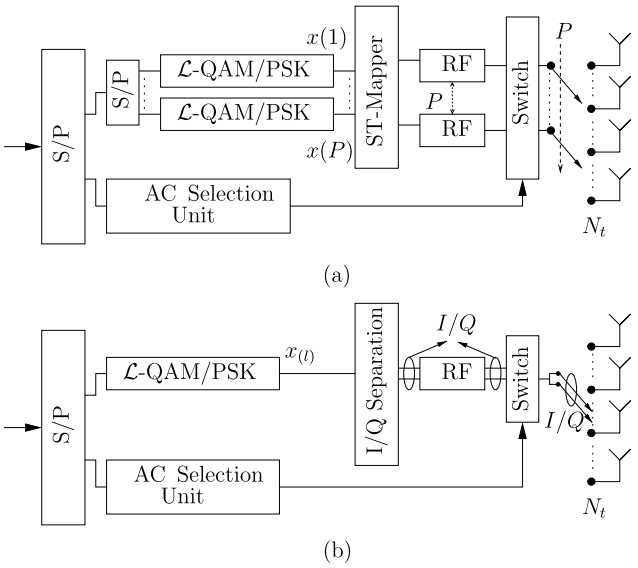

FIGURE 7. Transmitter structures of (a) GSM and (b) QSM.

The downside of simultaneously transmitting several symbols over the P activated AEs is the ICI problem, which resurfaces again in GSM systems after being eradicated in their conventional SM counterparts. This leads to an increased detection complexity at the receiver required for eliminating the $(P-1)$ ICI contributions. As a remedy, Younis *et al.* [89] suggested that a single symbol could be transmitted over the activated AEs, which completely removes the ICI and attains a beneficial transmit diversity gain, however at the expense of eroding the multiplexing gain.

Example 2: consider a GSM system associated with $N_t = 4$ transmit AEs and $N_c^t = 2$ RF chains, where the $(N_r = 4 \times N_t = 4)$-element channel matrix is identical to the one used in (5), while the PSK/QAM symbol vector $\mathring{\boldsymbol{S}} \in \mathbb{C}^{N_t \times 1}$ containing the $P = N_c^t$ transmitted symbols is given by

$$\mathring{\boldsymbol{S}} = \begin{bmatrix} x(1) & 0 & x(2) & 0 \end{bmatrix}^T, \tag{11}$$

where we have $x(1) = x(2) = x_l$ in case of transmitting the same symbol over the two activated AEs, while $x(1) \neq x(2)$ otherwise.

The transmitted symbol $\mathring{\boldsymbol{S}}$ of (11) activates the 1st and 3rd AEs of the system, corresponding to the locations of $x(1)$ and $x(2)$ respectively. Hence, the received signal $\boldsymbol{Y}$ can be expressed as

$$\boldsymbol{Y} = \begin{bmatrix} h_{1,1} & h_{1,3} \\ h_{2,1} & h_{2,3} \\ h_{3,1} & h_{3,3} \\ h_{4,1} & h_{4,3} \end{bmatrix} \begin{bmatrix} x(1) \\ x(2) \end{bmatrix} + \boldsymbol{V}. \tag{12}$$

Another enhanced SM design is proposed by Mesleh *et al.* [86] referred to as the Quadrature SM (QSM) scheme, which can be considered as a special case of the aforementioned GSM, given that a special type of RF chains is used, as shown in Figure 7(b). In the QSM system depicted in Figure 7(b), the SM constellation symbols are divided into in-phase and quadrature components and transmitted over separate AEs. This can be achieved with the aid of a specific single-RF chain, where the in-phase and quadrature components are switched to different AEs, given that the implicit antenna information is conveyed separately by each of the components' activated antennas, as shown in Figure 7(b).

The number of bits conveyed by the QSM system can be expressed as

$$B_{QSM} = 2 \cdot \log_2(N_t) + \log_2(\mathcal{L}), \tag{13}$$

which is equivalent to B_{GSM} of (8), when $f(N_t, P) = N_t^2$.

Example: consider the aforementioned example used for GSM, but with a $N_c^t = 1$ RF chain of a special type having separate outputs for the in-phase and quadrature parts. Here, we use the same pattern of the symbol vector $\mathring{\boldsymbol{S}}$ of (11), given that either $x(1)$ or $x(2)$ in (11) and (12) can be 0, $\Re\{x\}$, $j \cdot \Im\{x\}$ or $(\Re\{x\} + j \cdot \Im\{x\})$, where $\Re\{x\}$and $\Im\{x\}$ denote the real and imaginary parts of the complex symbol x and we have $j = \sqrt{-1}$.

C. STSK

Inspired by the philosophy of SM, Sugiura *et al.* [78] extended the idea of activating a single AE to activating a single space-time dispersion matrix for the sake of attaining multiplexing and diversity gains, given that SM lacked any transmit diversity gain.

In a nutshell, dispersion matrices are typically constructed prior to the commencement of transmission in order to disperse for example a set of PSK/QAM symbols over both time and space for either improving the achievable capacity or enhancing the attainable diversity order. A widely known type of dispersion matrices is the symbol-based family of matrices used in OSTBCs [33]. More explicitly, in OSTBC dispersion matrices are constructed using orthogonal column vectors of PSK/QAM symbols over T time slots in return for an increased diversity gain. By contrast, another class of dispersion matrices that was originally proposed for LDCs [45], [46] is based on randomly generated blocks of chaotic complex information without any orthogonality constraints, which can be used to disperse PSK/QAM symbols over the time and space dimensions, hence achieving either a maximized multiplexing gain or an improved diversity gain. Further insights into the diversity-multiplexing trade-off of dispersion matrices may be found in [80] and [36]. In STSK, LDC-based dispersion matrices are employed in the context of SM.

To expound a little further, let us consider the STSK transmitter block diagram of Figure 8, where the input bit sequence B_{STSK} is partitioned into two streams; the first sequence is invoked to obtain the PSK/QAM symbol x_l using the classical PSK/QAM modulator of Figure 8, while the other is used for selecting one out of Q space-time dispersion matrices

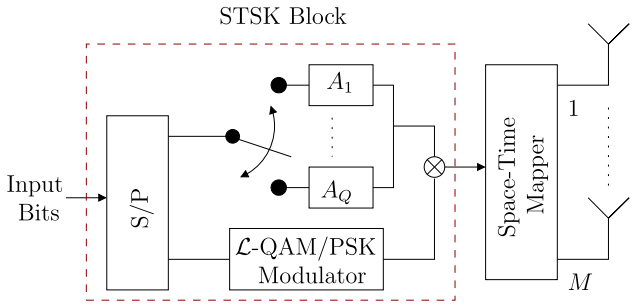

FIGURE 8. STSK transmitter block diagram.

as [46], [77], and [78]

$$\boldsymbol{A}_q \in \left\{\boldsymbol{A}_q \in \mathbb{C}^{M\times T}\right\}_{q=1}^{Q}, \tag{14}$$

which adhere to the power constraint of trace $\left[\boldsymbol{A}_q\boldsymbol{A}_q^H\right] = T$.

The l-th PSK/QAM symbol x_l is then dispersed over T time slots and M space dimensions using the q-th selected dispersion matrix $\boldsymbol{A}_q \in \mathbb{C}^{M\times T}$ and then fed into a space-time mapper, which maps the single-streamed output of the STSK block of Figure 8 into $(M \times T)$-element matrix. The symbol $\boldsymbol{S} \in \mathbb{C}^{M\times T}$ transmitted over the $N_t = M$ AEs at the output of the space-time mapper of Figure 8 can be expressed as

$$\boldsymbol{S} = \boldsymbol{A}_q x_l. \tag{15}$$

The STSK system is generally represented as STSK(M, N_r, T, Q, $\mathcal{L}$-PSK/QAM) [6], [77], [78], where $N_t = M$ denotes the number of both the transmit AEs and the RF chains,[3] while T indicates the number of time slots over which the STSK codeword $\boldsymbol{S}$ is transmitted.

In the light of SM, the STSK scheme can be viewed as an amalgam of LDC [45], [46] and SM [32]. In LDC, Q PSK/QAM symbols are dispersed over time and space using all of the available Q dispersion matrices, while in STSK only a single symbol is used to activate a single dispersion matrix, where the dispersion matrices generated can be interchangeably used for both schemes.

Furthermore, the number of bits B_{STSK} conveyed in a single STSK codeword over T time slots can be expressed as

$$B_{STSK} = \log_2(Q) + \log_2(\mathcal{L}), \tag{16}$$

$$= \log_2(Q \cdot \mathcal{L}), \tag{17}$$

which is equivalent to B_{SM} of (2) with the difference of having Q in place of N_t. In fact, the STSK system becomes an SM system, when $N_t = Q$ and $T = 1$.

Let us now consider an STSK system based on Figure 8 having the system model of (1), given that $\boldsymbol{S}$ of (15) is now the $(M \times T)$-element transmitted STSK codeword. Based on [77], the STSK system model of (1) can be transformed into an SM-equivalent linear model by simply applying the vectorial stacking operation $vec(.)$, which transforms any $(X \times Y)$-element matrix into an $(XY \times 1)$-element vector. This allows the STSK scheme to invoke all the optimum as well as the reduced complexity sub-optimum detection techniques of SM [36]. Hence, the $(N_rT \times 1)$-element vector-based received STSK signal $\bar{\boldsymbol{Y}}$ can be expressed as

$$\bar{\boldsymbol{Y}} = \bar{\boldsymbol{H}}\mathcal{X}\mathbf{K} + \bar{\boldsymbol{V}}, \tag{18}$$

$$= \underbrace{\left[\left(\bar{\boldsymbol{H}}\mathcal{X}\right)_1 \quad \cdots \quad \left(\bar{\boldsymbol{H}}\mathcal{X}\right)_q \quad \cdots \quad \left(\bar{\boldsymbol{H}}\mathcal{X}\right)_Q\right]}_{\left(\bar{\boldsymbol{H}}\mathcal{X}\right)} \cdot \underbrace{\left[\underbrace{0,\ldots,0}_{q-1},\ x_l,\underbrace{0,\ldots,0}_{Q-q}\right]^T}_{\mathbf{K}} + \bar{\boldsymbol{V}}, \tag{19}$$

where $\bar{\boldsymbol{H}} = \boldsymbol{I}_T \otimes \boldsymbol{H}$ denotes the $(N_rT \times N_tT)$-element equivalent channel matrix, with $\boldsymbol{I}_T$ being an $(T \times T)$-element identity matrix and $\otimes$ the Kronecker product. Furthermore, $\chi \in \mathbb{C}^{(MT)\times Q}$ represents a matrix hosting the Q dispersion matrices in the form of:

$$\chi = \left[vec(\boldsymbol{A}_1), \ldots, vec(\boldsymbol{A}_Q)\right], \tag{20}$$

while $\mathbf{K} = [\underbrace{0,\ldots,0}_{q-1}, x_l, \underbrace{0,\ldots,0}_{Q-q}]^T$ represents the $(Q \times 1)$-element transmit symbol vector and $\bar{\boldsymbol{V}} = vec(\boldsymbol{V})$ is the $(N_tT \times 1)$-element vectorized form of $\boldsymbol{V}$. Observe in (19) that the position of x_l at the q-th index of $\mathbf{K}$ would select the q-th column vector $\left(\bar{\boldsymbol{H}}\mathcal{X}\right)_q \in \mathbb{C}^{(MT)\times 1}$ denoting the SM-equivalent effective channel, which represents both to activating the q-th dispersion matrix and dispersing the l-th PSK/QAM symbol over time and space using the dispersion matrix selected. This allows the system to mimic the SM system of Figure 6 associated with $N_t = Q$ transmit AEs, based on the model shown in (3), where a single dispersion matrix is activated rather than activating a single transmit AE. The size of the ML search-space in the STSK scheme relies both on Q and on $\mathcal{L}$, where the complexity order achieved is $\mathcal{O}(Q \cdot \mathcal{L})$. In the following, we introduce an example to further illustrate the concept of STSK.

Example 3: consider an STSK(2, 2, 2, 2, $\mathcal{L}$-PSK/QAM) system where the $(N_r = 2 \times N_t = 2)$-element channel matrix is defined as

$$\boldsymbol{H} = \begin{bmatrix} h_{1,1} & h_{1,2} \\ h_{2,1} & h_{2,2} \end{bmatrix}, \tag{21}$$

while the PSK/QAM symbol x_l is located at $q = 2$ in $\mathbf{K}$ as

$$\mathbf{K} = \begin{bmatrix} 0 & x_l & 0 & 0 \end{bmatrix}^T. \tag{22}$$

[3] Here, we use M rather than just N_t to make a distinct separation between the number of transmit AEs and the STSK space dimension, since STSK is embedded into other schemes, where N_t is different from M, as described later in this paper.

Hence, based on (18) the SM-equivalent received signal can be expressed as

$$\bar{\boldsymbol{Y}} = \underbrace{\begin{bmatrix} h_{1,1} & h_{1,2} & 0 & 0 \\ h_{2,1} & h_{2,2} & 0 & 0 \\ 0 & 0 & h_{1,1} & h_{1,2} \\ 0 & 0 & h_{2,1} & h_{2,2} \end{bmatrix}}_{\bar{\boldsymbol{H}}} \cdot \underbrace{\begin{bmatrix} a_{1,1} & a_{1,2} & a_{1,3} & a_{1,4} \\ a_{2,1} & a_{2,2} & a_{2,3} & a_{2,4} \\ a_{3,1} & a_{3,2} & a_{3,3} & a_{3,4} \\ a_{4,1} & a_{4,2} & a_{4,3} & a_{4,4} \end{bmatrix}}_{\mathcal{X}} \cdot \underbrace{\begin{bmatrix} 0 & x_l & 0 & 0 \end{bmatrix}^T}_{\mathbf{K}} + \bar{\boldsymbol{V}}, \tag{23}$$

where after converting $\bar{\boldsymbol{Y}}$ into its matrix form, the received block $\boldsymbol{Y}$ can be expressed as

$$\boldsymbol{Y} = \begin{bmatrix} h_{1,1} & h_{1,2} \\ h_{2,1} & h_{2,2} \end{bmatrix} \begin{bmatrix} a_{1,2} & a_{3,2} \\ a_{2,2} & a_{4,2} \end{bmatrix} x_l + \boldsymbol{V}, \tag{24}$$

given that x_l is dispersed by the 2-nd dispersion matrix.

D. GSTSK

The above-mentioned STSK concept was further extended by Sugiura *et al.* [76] to include both the time and space dimensions in the proposed GSTSK scheme. In a similar manner to GSM, P out Q dispersion matrices[4] are simultaneously activated in GSTSK rather than only the single dispersion matrix activated in STSK. To elaborate a little further, let us consider the GSTSK transmitter block diagram of Figure 9. The B_{GSTSK} input bits of Figure 9 are partitioned into two streams, the first is used for selecting P out of Q dispersion matrices, which are used to spread P PSK/QAM modulated symbols over both space and time. Given that the system model of (1) is employed here, the $(M \times T)$-element GSTSK codeword $\mathring{\boldsymbol{S}}$ may be expressed as

$$\mathring{\boldsymbol{S}} = \sum_{p=1}^{P} \boldsymbol{A}(p)\, x(p), \tag{25}$$

where $\boldsymbol{A}(p) \in \mathbb{C}^{M \times T}$ is the p-th selected dispersion matrix of the set $\{\boldsymbol{A}_q\}_{q=1}^{Q}$, M is the GSTSK spatial dimension, T denotes the codeword's duration and its time dimension, while $x(p)$ is the p-th selected symbol of the $\mathcal{L}$-PSK/QAM constellation, given that $p = 1, \ldots, P$. In order to maintain a unity transmission power per channel use, the dispersion matrix selected should obey the constraint of [76], [92], and [93]

$$\text{trace}\left[\boldsymbol{A}_{q'}\boldsymbol{A}_{q'}^H\right] = \frac{T}{P} \quad (q' = 1, \ldots, Q). \tag{26}$$

[4]The letter P is usually used in characterizing the chosen combination of both the transmit AEs in GSM and the dispersion matrices in GSTSK.

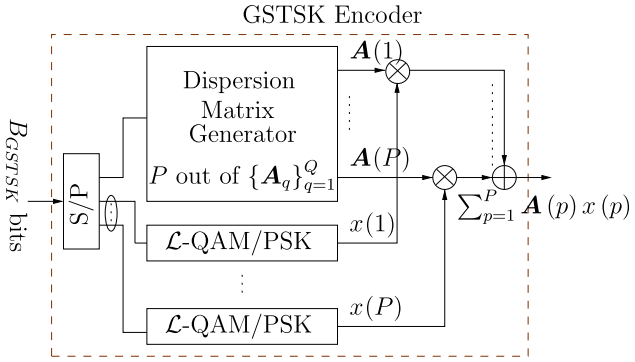

FIGURE 9. GSTSK transmitter block diagram.

The total number of bits transmitted per GSTSK codeword is equivalent to

$$B_{GSTSK} = \log_2 f(Q, P) + P \cdot \log_2(\mathcal{L}), \tag{27}$$

which is equivalent to the function B_{GSM} in (9), when substituting N_t of (9) by Q. The number of available combinations of the P dispersion matrices activated can be determined using (10).

Again, given that STSK can be considered as a special case of GSTSK, when $P = 1$, both B_{GSTSK} and B_{STSK} are equivalent under the same constraint. Furthermore, the GSTSK system transforms into a GSM system, when $N_t = Q$ and $T = 1$. In fact, the GSTSK system naturally subsumes STSK, GSM, QSM and SM as special cases and it is capable of potentially outperforming them at the cost of an additional computational complexity and/or an increased number of RF chains – except for GSM, where both may impose a similar complexity order at an equivalent number of RF chains.

In the light of the SM-representation of STSK provided in (18), the difference between the GSTSK and STSK systems lies in the transmitted symbol vector $\mathbf{K}$, where multiple symbols are hosted by the symbol vector $\mathbf{K}$ in GSTSK instead of the STSK's single symbol of (18). Hence, the GSTSK symbol vector can be expressed as

$$\mathbf{K} = \left[a_1, \ldots, a_q, \ldots, a_Q\right]^T, \tag{28}$$

where the q-th dispersion matrix is activated when $a_q \neq 0$, given that the total number of non-zero components of $\mathbf{K}$ is P, which is equal to the number of dispersion matrices activated. The BER performance of GSTSK was shown to be better than that of STSK [76], which came at the expense of an increased detection complexity. This additional complexity is due to eliminating the ICI imposed by the transmitted vector, given that several non-zero symbols are transmitted in $\mathbf{K}$ of (28), which leads to $(P-1)$ ICI contributions. The size of the ML search-space in the GSTSK arrangement relies both on $f(Q, P)$ and on $\mathcal{L}$, where the complexity order achieved is $\mathcal{O}\left(f(Q, P) \cdot \mathcal{L}^P\right)$. A GSTSK system is generally denoted as GSTSK(M, N_r, T, Q, $\mathcal{L}$-PSK/QAM, P). In the following, we introduce an example for further illustrating the concept of GSTSK.

Example 4: consider a GSTSK(2, 2, 2, 2, $\mathcal{L}$-PSK/QAM, 2) system, where the $(N_r = 2 \times N_t = 2)$-element channel matrix is equivalent to that in (21). Let us select the 3-rd and 4-th dispersion matrices with the aid of placing the PSK/QAM symbols $x(1)$ and $x(2)$ into their corresponding position in $\mathbf{K}$ of (28) as

$$\mathbf{K} = \begin{bmatrix} 0 & 0 & x(1) & x(2) \end{bmatrix}^T. \tag{29}$$

Hence, based on (23) the SM-equivalent received signal of the associated GSTSK system can be expressed as

$$\bar{\boldsymbol{Y}} = \underbrace{\begin{bmatrix} h_{1,1} & h_{1,2} & 0 & 0 \\ h_{2,1} & h_{2,2} & 0 & 0 \\ 0 & 0 & h_{1,1} & h_{1,2} \\ 0 & 0 & h_{2,1} & h_{2,2} \end{bmatrix}}_{\bar{\boldsymbol{H}}} \cdot \underbrace{\frac{1}{\sqrt{2}} \begin{bmatrix} a_{1,1} & a_{1,2} & a_{1,3} & a_{1,4} \\ a_{2,1} & a_{2,2} & a_{2,3} & a_{2,4} \\ a_{3,1} & a_{3,2} & a_{3,3} & a_{3,4} \\ a_{4,1} & a_{4,2} & a_{4,3} & a_{4,4} \end{bmatrix}}_{\mathcal{X}} \cdot \underbrace{\begin{bmatrix} 0 & 0 & x(1) & x(2) \end{bmatrix}^T}_{\mathbf{K}} + \bar{\boldsymbol{V}}, \tag{30}$$

where after converting $\bar{\boldsymbol{Y}}$ into its matrix form, the received block $\boldsymbol{Y}$ can be expressed as

$$\boldsymbol{Y} = \begin{bmatrix} h_{1,1} & h_{1,2} \\ h_{2,1} & h_{2,2} \end{bmatrix} \cdot \frac{1}{\sqrt{2}} \left(\begin{bmatrix} a_{1,3} & a_{3,3} \\ a_{2,3} & a_{4,3} \end{bmatrix} x(1) + \begin{bmatrix} a_{1,4} & a_{3,4} \\ a_{2,4} & a_{4,4} \end{bmatrix} x(2) \right) + \boldsymbol{V}. \tag{31}$$

E. MS-STSK

Another STSK enhancement approach we proposed in [85] is the MS-STSK concept, where the compelling merits of SM and STSK are amalgamated into a single system in order to achieve an increased throughput and enhanced BER performance compared to both techniques without any extra RF-chain requirement. The MS-STSK block diagram is shown in Figure 10, which incorporates the STSK encoder depicted earlier in Figure 8. The input bit sequence is partitioned into two parts, where the first one is utilized for generating the STSK codeword, while the other for selecting a specific Antenna Combination (AC) of M AEs with the aid of the Antenna Selection Unit (ASU) of Figure 10. The number of transmit RF-chains is equal to that of the STSK spatial dimension M, while the number of transmit AEs N_t should be higher than M in order to achieve a multiplexing gain in the activated antenna index domain, yielding $N_t \geq M$. The MS-STSK system is represented as MS-STSK($N_t, M, N_r, T, Q, \mathcal{L}$PSK/QAM).

The total number of bits $B_{MS-STSK}$ transmitted within each MS-STSK codeword over T time slots can be expressed as

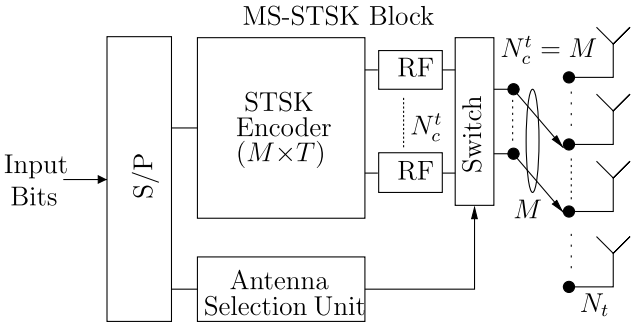

FIGURE 10. MS-STSK transmitter block diagram.

$$B_{MS-STSK} = \log_2 f(N_t, M) + \log_2(Q \cdot \mathcal{L}), \tag{32}$$

where the total number N_c of the available ACs has a maximum of $\log_2 f(N_t, M)$, as formulated in (10). The ML search-space in the MS-STSK system relies on $Q, \mathcal{L}$ as well as on N_c, where the complexity order achieved is $\mathcal{O}(Q \cdot \mathcal{L} \cdot N_c)$. The number of ACs is typically determined using one of two allocation techniques, namely the Distinct Antenna Combination (DAC) and Shared Antenna Combination (SAC) techniques presented in [85], which will be discussed later in Section III-B.

The MS-STSK scheme subsumes STSK and all of its subsidiaries, such as SM and SSK [85]. For instance, the MS-STSK system scales down: to STSK when $N_c^t = N_t$, to SM when $N_c^t = N_t = Q$ and $T = 1$ as well as to SSK when $N_c^t = N_t = Q, T = 1$ and $\mathcal{L} = 1$.

In what follows, we present a pair of approaches to model the MS-STSK system. The first one was previously presented in [85], where the available ACs are embedded into the equivalent dispersion matrix. However, we conceive in this treatise a new modeling approach for MS-STSK, where the ACs are represented in a distinct matrix, which is more suitable for modeling our LMS system.

1) In the first approach, the STSK system model of (18) is used for MS-STSK with an additional matrix $\mathcal{I}$ characterizing the AC selection as

$$\bar{\boldsymbol{Y}} = \bar{\boldsymbol{H}} \mathcal{X} \mathcal{I} \mathbf{K} + \bar{\boldsymbol{V}}, \tag{33}$$

$$= \underbrace{\begin{bmatrix} \boldsymbol{H} & \cdots & \boldsymbol{0} \\ \vdots & \ddots & \vdots \\ \boldsymbol{0} & \cdots & \boldsymbol{H} \end{bmatrix}}_{\bar{\boldsymbol{H}}} \cdot \underbrace{\begin{bmatrix} \cdots & \begin{bmatrix} \hat{\boldsymbol{A}}_{1,c} & \cdots & \hat{\boldsymbol{A}}_{Q,c} \end{bmatrix} & \cdots \end{bmatrix}}_{\mathcal{X}}$$

$$\cdot \underbrace{\begin{bmatrix} \mathbf{0} \\ \vdots \\ \boldsymbol{I}_Q^c \\ \vdots \\ \mathbf{0} \end{bmatrix}}_{\mathcal{I}} \cdot \underbrace{\begin{bmatrix} \underbrace{0,\ldots,0}_{q-1},\ x_l, \underbrace{0,\ldots,0}_{Q-q} \end{bmatrix}^T}_{\mathbf{K}} + \bar{\boldsymbol{V}}, \tag{34}$$

where $\hat{\boldsymbol{A}}_{q,c} = vec(\tilde{\boldsymbol{A}}_{q,c}) \in \mathbb{C}^{N_t T \times 1}$ is the vectorized form of $\tilde{\boldsymbol{A}}_{q,c} \in \mathbb{C}^{N_t \times T}$ denoting the q-th dispersion matrix $\boldsymbol{A}_q \in \mathbb{C}^{M \times T}$ associated with c-th AC. Furthermore, $\mathcal{X} \in \mathbb{C}^{(N_t T) \times (QN_c)}$ of (34) constitutes the Q matrices associated with the N_c ACs $\left\{ \left\{ \hat{\boldsymbol{A}}_{q,c} \right\}_{q=1}^{Q} \right\}_{c=1}^{N_c}$ and $\mathcal{I} \in \mathbb{C}^{(QN_c) \times (Q)}$ denotes the AC activation matrix, given that the c-th component $\boldsymbol{I}_Q^c$ of $\mathcal{I} = [\mathbf{0} \ldots \boldsymbol{I}_Q^c \ldots \mathbf{0}]^T$ represents a $(Q \times Q)$-element identity matrix that activates the c-th AC of $\mathcal{X}$ with $\mathbf{0}$ being a $(Q \times Q)$-element zero matrix corresponding to the inactive ACs. Now, the MS-STSK system model of (34) can be formulated as

$$\bar{\boldsymbol{Y}} = \underbrace{\left[\left(\bar{\boldsymbol{H}}\mathcal{X}\mathcal{I}\right)_{1,c} \quad \cdots \quad \left(\bar{\boldsymbol{H}}\mathcal{X}\right)_{q,c} \quad \cdots \quad \left(\bar{\boldsymbol{H}}\mathcal{X}\right)_{Q,c} \right]}_{\left(\bar{\boldsymbol{H}}\mathcal{X}\right)} \cdot \underbrace{\begin{bmatrix} \underbrace{0,\ldots,0}_{q-1},\ x_l, \underbrace{0,\ldots,0}_{Q-q} \end{bmatrix}^T}_{\mathbf{K}} + \bar{\boldsymbol{V}}, \tag{35}$$

where the q-th dispersion matrix and the c-th AC are selected by relying on the SM-equivalent channel column vector $\left(\bar{\boldsymbol{H}}\mathcal{X}\right)_{q,c} \in \mathbb{C}^{(N_t T) \times 1}$ of (35). Hence, the MS-STSK system can be represented as an SM-equivalent system. In the following, we introduce an example to further illustrate the concept of MS-STSK associated with the first modeling approach.

Example 5: consider an MS-STSK(4, 2, 2, 2, 2, $\mathcal{L}$-PSK/QAM) system associated with the SAC arrangement, where the $(N_r = 4 \times N_t = 4)$-element channel matrix is equivalent to that given in (5), while the AC activation matrix $\mathcal{I}$ selecting the $c = 1$ AC out of $N_c = 2$ ACs is given by

$$\mathcal{I} = \begin{bmatrix} \underbrace{\begin{bmatrix} 1 & 0 \\ 0 & 1 \end{bmatrix}}_{\boldsymbol{I}_Q^1} \\ \begin{bmatrix} 0 & 0 \\ 0 & 0 \end{bmatrix} \end{bmatrix}, \tag{36}$$

and the matrix $\mathcal{X}$ including all dispersion matrices and ACs is expressed as

$$\mathcal{X} = \begin{bmatrix} a_{1,1} & a_{1,2} & 0 & 0 \\ a_{2,1} & a_{2,2} & 0 & 0 \\ a_{3,1} & a_{3,2} & 0 & 0 \\ a_{4,1} & a_{4,2} & 0 & 0 \\ 0 & 0 & a_{1,3} & a_{1,4} \\ 0 & 0 & a_{2,3} & a_{2,4} \\ 0 & 0 & a_{3,3} & a_{3,4} \\ \underbrace{0}_{\hat{\boldsymbol{A}}_{1,1}} & \underbrace{0}_{\hat{\boldsymbol{A}}_{2,1}} & \underbrace{a_{4,3}}_{\hat{\boldsymbol{A}}_{1,2}} & \underbrace{a_{4,4}}_{\hat{\boldsymbol{A}}_{2,2}} \end{bmatrix}. \tag{37}$$

Hence, after placing x_l at the $q = 2$ position of $\mathbf{K}$, the received SM-equivalent signal based on Equation (34) can be expressed as

$$\bar{\boldsymbol{Y}} = \underbrace{\begin{bmatrix} \boldsymbol{H} & \mathbf{0} \\ \mathbf{0} & \boldsymbol{H} \end{bmatrix}}_{\bar{\boldsymbol{H}}} \cdot \underbrace{\begin{bmatrix} \hat{\boldsymbol{A}}_{1,1} & \hat{\boldsymbol{A}}_{2,1} & \hat{\boldsymbol{A}}_{1,2} & \hat{\boldsymbol{A}}_{2,2} \end{bmatrix}}_{\mathcal{X}} \cdot \underbrace{\begin{bmatrix} \underbrace{\begin{bmatrix} 1 & 0 \\ 0 & 1 \end{bmatrix}}_{\boldsymbol{I}_Q^1} \\ \begin{bmatrix} 0 & 0 \\ 0 & 0 \end{bmatrix} \end{bmatrix}}_{\mathcal{I}} \cdot \underbrace{\begin{bmatrix} 0 & x_l & 0 & 0 \end{bmatrix}^T}_{\mathbf{K}} + \bar{\boldsymbol{V}}, \tag{38}$$

where after converting $\bar{\boldsymbol{Y}}$ into its MS-STSK matrix form, the received block $\boldsymbol{Y}$ can be expressed as

$$\boldsymbol{Y} = \begin{bmatrix} h_{1,1} & h_{1,2} & h_{1,3} & h_{1,4} \\ h_{2,1} & h_{2,2} & h_{2,3} & h_{2,4} \\ h_{3,1} & h_{3,2} & h_{3,3} & h_{3,4} \\ h_{4,1} & h_{4,2} & h_{4,3} & h_{4,4} \end{bmatrix} \cdot \begin{bmatrix} a_{1,2} & a_{3,2} \\ a_{2,2} & a_{4,2} \\ 0 & 0 \\ 0 & 0 \end{bmatrix} x_l + \boldsymbol{V}, \tag{39}$$

where it is shown that the second dispersion matrix associated with the first antenna combination $\left[\hat{\boldsymbol{A}}_{2,1}\right]$ is selected.

2) In our new approach,[5] we introduce the AC selection matrix at the channel side prior to applying the vectorization operation. This approach allows us to further

[5]The second approach of modeling the MS-STSK system is proposed in this treatise.

simplify the system model by distinctively showing each of the system's components, which is more suitable for our LMS system model. For instance, let us rewrite the system model of (33) as

$$\boldsymbol{Y} = \boldsymbol{H}\boldsymbol{F}_c \underbrace{\boldsymbol{A}_q x_l}_{\mathring{\boldsymbol{S}}} + \boldsymbol{V}, \tag{40}$$

where $\boldsymbol{F}_c \in \mathbb{C}^{N_t \times M}$ is an AC activation matrix containing ones-and-zeros that produces the channel matrix $(\boldsymbol{H}\boldsymbol{F}_c) \in \mathbb{C}^{N_r \times M}$ between the M activated transmit AEs and the N_r receive AEs, when multiplied by $\boldsymbol{H}$. Now, Equation (33) appears as

$$\begin{aligned}\bar{\boldsymbol{Y}} &= \bar{\boldsymbol{H}}_c \mathcal{X} \mathbf{K} + \bar{\boldsymbol{V}}, \qquad (41)\\ &= \underbrace{\begin{bmatrix} (\boldsymbol{H}\mathbf{F}_c) & \cdots & \mathbf{0} \\ \vdots & \ddots & \vdots \\ \mathbf{0} & \cdots & (\boldsymbol{H}\mathbf{F}_c) \end{bmatrix}}_{\bar{\boldsymbol{H}}} \cdot \underbrace{\left[vec\left(\boldsymbol{A}_1\right), \ldots, vec(\boldsymbol{A}_Q)\right]}_{\mathcal{X}} \\ &\quad \cdot \underbrace{\begin{bmatrix} \underbrace{0, \ldots, 0}_{q-1}, x_l, \underbrace{0, \ldots, 0}_{Q-q} \end{bmatrix}^T}_{\mathbf{K}} + \bar{\boldsymbol{V}}, \qquad (42)\end{aligned}$$

where $\bar{\boldsymbol{H}}_c = \boldsymbol{I}_T \otimes (\boldsymbol{H}\boldsymbol{F}_c) \in \mathbb{C}^{N_r T \times MT}$ is the equivalent channel matrix, while $\mathcal{X} \in \mathbb{C}^{(MT)\times(Q)}$ is the matrix of the Q STSK dispersion matrices, with $\boldsymbol{I}_T$ being an $(T \times T)$-element identity matrix. By observing Equation (42), the position of x_l in $\mathbf{K}$ activates the q-th column vector $\mathcal{X}$, while the pattern of $\mathbf{F}_c$ (or the position of the ones in $\mathbf{F}_c$) activates the M selected AEs. In the following, we introduce an example to further illustrate the concept of MS-STSK associated with the second modeling approach.

It is worth noting that as per the two modeling approaches presented above, which imply that the MS-STSK can be viewed as an SM system, the MS-STSK system may benefit from all the optimum and sub-optimum reduced complexity techniques proposed in the literature for both SM and STSK [85].

Example 6: consider an MS-STSK(4, 2, 2, 2, 2, $\mathcal{L}$-PSK/QAM) system similar to the one given above, where the $(N_r = 4 \times N_t = 4)$-element channel matrix is equivalent to that given in (5), while the first AC activation matrix $\boldsymbol{F}_1$ associated with $c = 1$, which incorporates both the first and the second AEs, is given by

$$\boldsymbol{F}_1 = \begin{bmatrix} 1 & 0 \\ 0 & 1 \\ 0 & 0 \\ 0 & 0 \end{bmatrix}. \tag{43}$$

Hence, the $(N_r = 4 \times M = 2)$-element channel matrix of the link between the $M = 2$ activated transmit AEs and the $N_r = 4$ receive AEs becomes:

$$(\boldsymbol{H}\boldsymbol{F}_1) = \begin{bmatrix} h_{1,1} & h_{1,2} \\ h_{2,1} & h_{2,2} \\ h_{3,1} & h_{3,2} \\ h_{4,1} & h_{4,2} \end{bmatrix}. \tag{44}$$

Based on the system model of (41), the SM-equivalent signal can be expressed as

$$\begin{aligned}\bar{\boldsymbol{Y}} = &\underbrace{\begin{bmatrix} h_{1,1} & h_{1,2} & 0 & 0 \\ h_{2,1} & h_{2,2} & 0 & 0 \\ h_{3,1} & h_{3,2} & 0 & 0 \\ h_{4,1} & h_{4,2} & 0 & 0 \\ 0 & 0 & h_{1,1} & h_{1,2} \\ 0 & 0 & h_{2,1} & h_{2,2} \\ 0 & 0 & h_{3,1} & h_{3,2} \\ 0 & 0 & h_{4,1} & h_{4,2} \end{bmatrix}}_{\bar{\boldsymbol{H}}_1} \\ &\cdot \underbrace{\begin{bmatrix} a_{1,1} & a_{1,2} & a_{1,3} & a_{1,4} \\ a_{2,1} & a_{2,2} & a_{2,3} & a_{2,4} \\ a_{3,1} & a_{3,2} & a_{3,3} & a_{3,4} \\ a_{4,1} & a_{4,2} & a_{4,3} & a_{4,4} \end{bmatrix}}_{\mathcal{X}} \\ &\cdot \underbrace{\begin{bmatrix} 0 & x_l & 0 & 0 \end{bmatrix}^T}_{\mathbf{K}} + \bar{\boldsymbol{V}}, \qquad (45)\end{aligned}$$

where upon converting $\bar{\boldsymbol{Y}}$ into its MS-STSK matrix form, the received block $\boldsymbol{Y}$ can be expressed as

$$\boldsymbol{Y} = \begin{bmatrix} h_{1,1} & h_{1,2} \\ h_{2,1} & h_{2,2} \\ h_{3,1} & h_{3,2} \\ h_{4,1} & h_{4,2} \end{bmatrix} \begin{bmatrix} a_{1,2} & a_{3,2} \\ a_{2,2} & a_{4,2} \end{bmatrix} x_l + \boldsymbol{V}. \tag{46}$$

Observe that Equations (39) and (46) exhibit some similarities, albeit two different system modeling techniques were used. However, the second approach is more compatible with our LMS system, as it will be shown later in this paper. In the following section, we introduce the concept of multiple layers into our MIMO system, which represents one of the key features of our LMS concept.

F. LAYERED MIMO

The layering arrangement partitions the system's resources into parallel components, where each component is regarded as a single layer that functions independently from other layers for transmitting a separate information stream, and hence maximizing the system's spectral efficiency. To expound a little further, the OSTBC system [33] or the above SM and STSK systems for example cannot be considered as layered systems, since each codeword is generated as a single self-contained block. By contrast, the V-BLAST [52] depicted in Figure 11 is considered as a layered system, where each

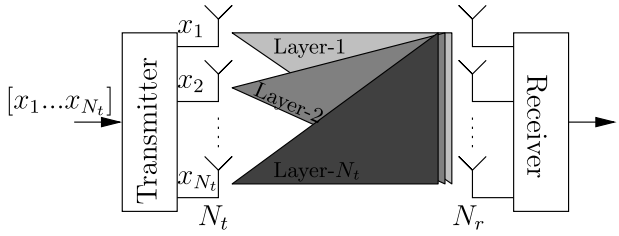

FIGURE 11. The layered architecture of the BLAST system.

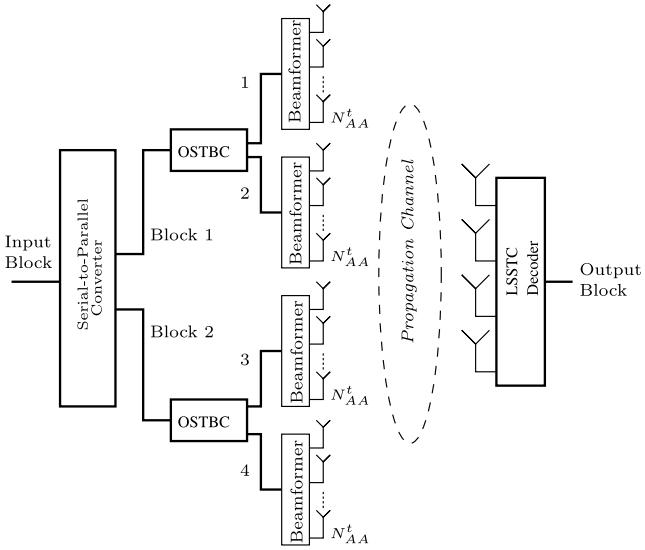

FIGURE 12. The LSSTC system block diagram.

n_t-th transmit AE simultaneously transmits a symbol $x_{n_t} \in \{x_1, \ldots, x_{N_t}\}$ independent of other AEs over time and frequency. This allows the receiver to detect the received multi-stream signals separately, for example by using interference cancellation techniques, such as the classic Successive Interference Cancellation (SIC) technique [38]. We may regard the V-BLAST system as a special case of the above-mentioned GSM system, especially when $N_c^t = N_t$. Hence the GSM system can be considered as a multi-layered SM system.

The layering ideology was also incorporated into more sophisticated MIMO schemes in contemplation of improved multiplexing gain, such as the LSSTC system proposed by El-Hajjar *et al.* [75]. In LSSTC, the system is partitioned into K layers, where each layer has a separate STC encoder as well as a specific set of antenna arrays. This layered structure allows the transmitter to simultaneously convey multiple STBC blocks, hence achieving an enhanced multiplexing gain, while maintaining the OSTBC's diversity gain. In the following, we introduce an example to further illustrate the concept of LSSTC.

Example 7: Consider the LSSTC system depicted in Figure 12, where the system is constituted by $K = 2$ layers of OSTBC encoders, as well as four transmit AEs, where each OSTBC encoder is assigned two antenna arrays, given that we have $N_{AA}^t = 1$ AEs. The transmitted symbol can be

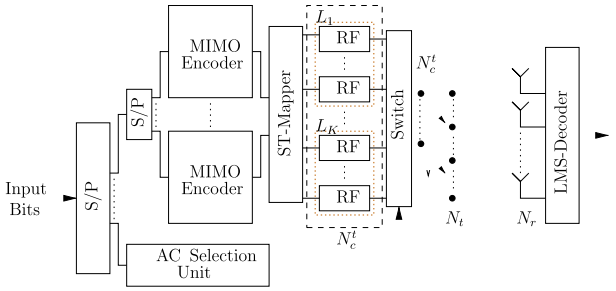

FIGURE 13. LMS system architecture.

expressed as

$$\mathring{\boldsymbol{S}} = \left[\begin{array}{cc} x_1^{(1)} & x_2^{(1)} \\ -x_2^{(1)*} & x_1^{(1)*} \\ \hline x_1^{(2)} & x_2^{(2)} \\ -x_2^{(2)*} & x_1^{(2)*} \end{array}\right], \tag{47}$$

where the k-th postscript of $x_l^{(k)}$ denotes the k-th transmission layers of the l-th PSK/QAM symbol, while the horizontal line is used for visually separating both layers.

Now, at the receiver of Figure 12, which is for instance equipped with $N_r = 4$ AEs, the received symbol can be expressed as

$$\boldsymbol{Y} = \left[\begin{array}{cc|cc} h_{1,1} & h_{1,2} & h_{1,3} & h_{1,4} \\ h_{2,1} & h_{2,2} & h_{2,3} & h_{2,4} \\ h_{3,1} & h_{3,2} & h_{3,3} & h_{3,4} \\ h_{4,1} & h_{4,2} & h_{4,3} & h_{4,4} \end{array}\right], \cdot \left[\begin{array}{cc} x_1^{(1)} & x_2^{(1)} \\ -x_2^{(1)*} & x_1^{(1)*} \\ \hline x_1^{(2)} & x_2^{(2)} \\ -x_2^{(2)*} & x_1^{(2)*} \end{array}\right] + \boldsymbol{V}. \tag{48}$$

The receiver of the layered system of Figure 12 is now capable of simultaneously detecting the information conveyed over each layer. In the following section, we introduce our LMS concept based on all the systems and examples presented in this section.

G. THE LMS CONCEPT

The above-mentioned MIMO concepts incorporate the main features of our LMS system. To elaborate further, let us consider the $(N_t \times N_r)$-element LMS system of Figure 13, where the transmitter is equipped with N_t transmit AEs and $N_c^t \leq N_t$ RF chains, while the receiver is equipped with N_r receive AEs and N_c^r RF chains.

The first key feature of our LMS system is its layered architecture, where the system constitutes multiple independent MIMO encoders, as shown in Figure 13, given that each encoder is associated with a specific layer selected out of K layers. The layering concept is employed with the aid of

partitioning the input information stream into multiple sub-streams, where each stream is conveyed through a distinct layer for attaining a substantial multiplexing gain.

Another key feature of the LMS system is its index modulation based architecture, capable of choosing a specific combination out of many antenna combinations, following the philosophy of the above-mentioned SM, GSM, QSM and MS-STSK systems. More specifically, the number of transmit RF chains shown in Figure 13 can potentially be lower than the number of the transmit AEs available, which allows the system to convey the implicit information of the activated AC index.

In a nutshell, the LMS transmitter simultaneously activates K layers of M AEs, denoting a specific AC with the aid of the $N_c^t = K \cdot M$ transmit RF chains available in order to transmit a single LMS agglomerate,[6] which is a layered combination of space-time complex codewords. This allows the system to convey both the implicit information of the activated ACs indices as well as the modulated information spread over the multiplexed codewords. Furthermore, the choice of the specific MIMO encoding scheme plays a major influential factor, when designing the LMS system, hence in what follows we present the MIMO scheme selected followed by a detailed insight into the transmitter's behavior.

III. THE LMS MIMO

In this section we introduce our novel LMS system transceiver design. We commence by introducing the LMS transmitter design, while elaborating on why we choose GSTSK as the core information encoder. Next, we present the AC allocation schemes proposed for selecting the activated AE before transmission. Then, we quantify the LMS system's achievable throughput and the attainable diversity order, followed by a detailed discussion on all of the LMS framework's special cases and finally, we present an overall summary of our LMS system.

A. THE LMS-GSTSK TRANSMITTER

Motivated by its appealing characteristics, we invoke our sophisticated MS-STSK scheme of Figure 10 for the MIMO encoding section of our LMS system shown in Figure 13, which is potentially capable of outperforming other MIMO schemes, as an explicit benefit of its flexible architecture striking a diversity-multiplexing trade-off. However, for the sake of generalizing our scheme we adopt the GSTSK scheme of Figure 9 rather than the STSK of Figure 8 as the core encoder of the MS-STSK scheme of Figure 10. This further refine our LMS system by incorporating more MIMO schemes as special cases. For example, it was confirmed by Sugiura *et al.* [76] that STSK constitutes a special case of GSTSK and can be outperformed by its generalized architecture. Hence, we refer to our system as LMS-GSTSK, where the transmitter's block diagram of Figure 13 is now shown

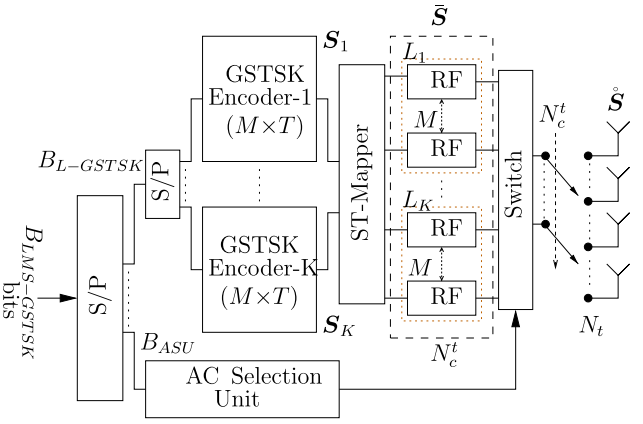

FIGURE 14. Block diagram of the proposed LMS-GSTSK transmitter.

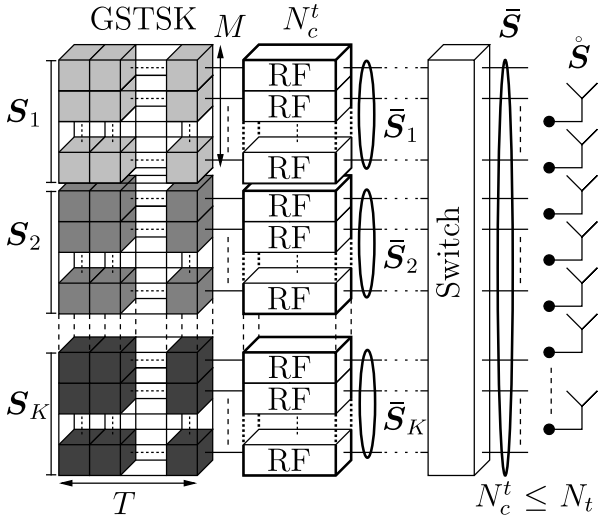

FIGURE 15. A visualization of the LMS-GSTSK codeword agglomerate generation.

in Figure 14 relying on the GSTSK encoders employed, given that each layer is assisted by M RF chains, where the total number of the transmitter's RF chains is $N_c^t = (K \cdot M)$. The ASU of Figure 14 is responsible for mapping the GSTSK agglomerate into the AC's activated AEs with the aid of an agile switch.

According to Figure 14, the input bit sequence is partitioned into two streams with the aid of a serial-to-parallel converter (S/P), where the first $B_{L-GSTSK}$ bit stream is utilized for encoding the Layered GSTSK (L-GSTSK) codeword agglomerate,[7] while the other B_{ASU} bits stream is used for selecting the activated AC.

To expound a little further, the first $B_{L-GSTSK}$ bits are fed into K layers of GSTSK encoders, where each layer generates an $(M \times T)$-element space-time GSTSK codeword $\boldsymbol{S}_k$ $(k = 1, \ldots, K)$, as visualized in Figure 15 by

[6]We defined by a transmitted agglomerate an amalgam of independent encoded codewords transmitted simultaneously over space and time.

[7]An L-GSTSK codeword agglomerate denotes a stack of K GSTSK codewords packed into a single super-codeword.

selecting P out of Q dispersion matrices to spread a sequence of P classic $\mathcal{L}$ -PSK/QAM symbols over time and space, as shown by the GSTSK encoder of Figure 9. The k-th layer GSTSK codeword may be expressed as

$$\boldsymbol{S}_k = \sum_{p=1}^{P} \boldsymbol{A}^{(k)}(p)\, x^{(k)}(p), \tag{49}$$

where $\boldsymbol{A}^{(k)}(p) \in \mathbb{C}^{M\times T}$ is the p-th selected dispersion matrix of the set $\{\boldsymbol{A}_q\}_{q=1}^{Q}$ at the k-th layer, M represents the GSTSK spatial dimension, T denotes the codeword's duration and its time dimension, while $x^{(k)}(p)$ is the p-th selected symbol of the $\mathcal{L}$-PSK/QAM constellation at the k-th layer, as illustrated in Figure 9. In order to maintain a unity transmission power per channel use, the dispersion matrix selected should obey the constraint of [76], [92], and [93]

$$\text{trace}\left[\boldsymbol{A}_{q'}\boldsymbol{A}_{q'}^{H}\right] = \frac{T}{P} \left(\text{where } q' = 1, \ \ldots, Q\right). \tag{50}$$

After mapping each layer of the K available GSTSK encoders of Figures 14 and 15, the L-GSTSK codeword agglomerate output of all the K available GSTSK encoders, which represents an amalgam of the $\boldsymbol{S}_k$ GSTSK codewords denoted by $\bar{\boldsymbol{S}} \in \mathbb{C}^{N_c^t\times T}$, may be expressed as

$$\bar{\boldsymbol{S}} = \sum_{k=1}^{K} \bar{\boldsymbol{S}}_k, \tag{51}$$

where $N_c^t = (K \cdot M)$ represents the total number of RF chains, while $\bar{\boldsymbol{S}}_k$ encompasses both $\boldsymbol{S}_k$ and its position within the L-GSTSK agglomerate as $\bar{\boldsymbol{S}}_k = \left[\cdots \boldsymbol{0} \cdots \boldsymbol{S}_k \cdots \boldsymbol{0} \cdots\right]^T$, given that $\boldsymbol{0} \in \mathbb{C}^{M\times T}$ is a matrix of zeros entered into $\bar{\boldsymbol{S}}_k$ in order to ensure that none of the K GSTSK codewords $\boldsymbol{S}_k$ overlap with one another in $\bar{\boldsymbol{S}}$, as shown in Figure 15.

Now, the total number of bits conveyed over each GSTSK layer may be formulated as

$$B_{GSTSK} = \log_2 f(Q,\ P) + P \cdot \log_2(\mathcal{L}), \tag{52}$$

where $f(Q,\ P)$ is the function defining the total number of P out of Q dispersion matrix combinations available, which may be expressed as

$$f(Q,\ P) = \left\lfloor \binom{Q}{P} \right\rfloor_{2^\iota}, \tag{53}$$

where $\lfloor . \rfloor_{2^\iota}$ denotes flooring to the nearest smallest 2^ι integer for ensuring that we have an integer number of bits B_{GSTSK}. Therefore, the total number of bits conveyed over the L-GSTSK agglomerate is defined as

$$B_{L-GSTSK} = (K \cdot B_{GSTSK}). \tag{54}$$

Meanwhile, the other bit stream B_{ASU} is simultaneously fed into the ASU of Figure 14, which has $(K \cdot M)$ inputs as well as $(K \cdot M)$ outputs and is used for selecting one out of N_c ACs in order to activate $N_c^t = K \cdot M$ AEs out of N_t AEs for transmitting the L-GSTSK agglomerate $\bar{\boldsymbol{S}}$ using an identical number of RF chains. Hence, the total number of implicitly bits transmitted over the selected AC index is defined as

$$B_{ASU} = \log_2(N_c), \tag{55}$$

where the ACs construction mechanisms are detailed in the following subsection.

Lastly, the switch block of the LMS system of Figure 14 multiplexes the L-GSTSK codeword agglomerate $\bar{\boldsymbol{S}}$ over space by switching the output of the N_c^t RF chains to the input of N_c^t AEs of the selected AC. Hence, the LMS codeword agglomerate conveyed by the LMS transmitter of Figure 14 is defined as

$$\mathring{\boldsymbol{S}} = \begin{bmatrix} \cdots & \boldsymbol{0} & \cdots & \boldsymbol{S}_1 & \cdots & \boldsymbol{0} & \cdots \\ \cdots & \boldsymbol{0} & \cdots & \boldsymbol{S}_k & \cdots & \boldsymbol{0} & \cdots \\ \cdots & \boldsymbol{0} & \cdots & \boldsymbol{S}_K & \cdots & \boldsymbol{0} & \cdots \end{bmatrix}^T, \tag{56}$$

or as

$$\mathring{\boldsymbol{S}} = \begin{bmatrix} \cdots & \boldsymbol{0} & \cdots & \bar{\boldsymbol{S}}_1 & \cdots & \boldsymbol{0} & \cdots \\ \cdots & \boldsymbol{0} & \cdots & \bar{\boldsymbol{S}}_k & \cdots & \boldsymbol{0} & \cdots \\ \cdots & \boldsymbol{0} & \cdots & \bar{\boldsymbol{S}}_K & \cdots & \boldsymbol{0} & \cdots \end{bmatrix}^T, \tag{57}$$

where $\mathring{\boldsymbol{S}} \in \mathbb{C}^{N_t\times T}$ represents the entire LMS-GSTSK agglomerate depicted in Figure 15, which includes both the L-GSTSK agglomerate as well as the AC index activated. The zero matrix $\boldsymbol{0} \in \mathbb{C}^{M\times T}$ describes the deactivated set of M AEs over the T transmission time slots. Some further examples are provided in the following section.

Our LMS-GSTSK scheme is associated with the following parameters, N_t, N_c, K, M, N, T, Q, P and $\mathcal{L}$-PSK/QAM, which can be represented as LMS-GSTSK(N_t : N_c^t, N_c, K, M, N_r, T, P:Q, $\mathcal{L}$-PSK/QAM).[8]

B. AC ALLOCATION TECHNIQUES

In this treatise, we present three AC allocation techniques, namely the DAC and SAC techniques presented in [85] as well as the new Semi-SAC or Semi-DAC techniques, which are used for activating N_c^t of N_t transmit AEs in order to transmit the L-GSTSK codeword agglomerate $\bar{\boldsymbol{S}}$ of Figure 15.

More specifically, the DAC relies on a strictly unique combinations of different AEs, as shown in Figure 16(a), where each AE is explicitly assigned to a single M-sized AC layer subsumed by a combination of N_c^t activated AEs. The total number of ACs available in an LMS system associated with the DAC technique is then given by

$$N_c^{(DAC)} = \left\lfloor \frac{N_t}{N_c^t} \right\rfloor_{2^\iota} = \left\lfloor \frac{N_t}{(K \cdot M)} \right\rfloor_{2^\iota}. \tag{58}$$

In the following, we introduce an example to further illustrate the DAC technique.

Example 8: consider the LMS-GSTSK(16:4, $N_c = 4$, $K = 2$, $M = 2$, N_r, T, P:Q, $\mathcal{L}$-PSK/QAM) system of Figure 14

[8]We use LMS-GSTSK(N_t, N_c, K, M, N_r, T, P:Q, $\mathcal{L}$-PSK/QAM) instead, when the value of N_c^t is not required.

associated with the DAC allocation technique. The ASU of Figure 14 is capable of generating $N_c^{(DAC)} = \left\lfloor \frac{16}{(2\cdot 2)} \right\rfloor_{2^\iota} = 4$ distinct ACs. The L-GSTSK agglomerate $\bar{\boldsymbol{S}}$ of (51) and of Figure 15 can be expressed as

$$\begin{aligned}\bar{\boldsymbol{S}} &= \bar{\boldsymbol{S}}_1 + \bar{\boldsymbol{S}}_2 \\ &= \begin{bmatrix} \boldsymbol{S}_1 \\ \mathbf{0}_{M\times T} \end{bmatrix} + \begin{bmatrix} \mathbf{0}_{M\times T} \\ \boldsymbol{S}_2 \end{bmatrix} \\ &= \begin{bmatrix} \boldsymbol{S}_1 \\ \boldsymbol{S}_2 \end{bmatrix}, \end{aligned} \tag{59}$$

where $\boldsymbol{S}_1$ and $\boldsymbol{S}_2$ denote the $(M \times T)$-element GSTSK codewords of the first and second layers, respectively, $\bar{\boldsymbol{S}}_1$ and $\bar{\boldsymbol{S}}_2$ denote the $(K \cdot M \times T)$-element GSTSK codewords with their location in the agglomerate, given that $\mathbf{0}_{M\times T}$ is an $(M \times T)$-element zero matrix. To be able to view the row vector $\boldsymbol{s}_{k,m}$ representation of the m-th row of the k-th $\boldsymbol{S}_k$ GSTSK codeword, $\bar{\boldsymbol{S}}$ can be rewritten as

$$\bar{\boldsymbol{S}} = \begin{bmatrix} \boldsymbol{s}_{1,1} \\ \boldsymbol{s}_{1,2} \\ \boldsymbol{s}_{2,1} \\ \boldsymbol{s}_{2,2} \end{bmatrix}. \tag{60}$$

Now, given that the final LMS agglomerate $\mathring{\boldsymbol{S}}$ of Figure 15 can be transmitted over $N_c = 4$ ACs, the row vectors of $\bar{\boldsymbol{S}}$ of (60) can be mapped to four distinct combinations as follows:

$$\begin{aligned}\mathring{\boldsymbol{S}} = &\left[\begin{bmatrix} \boldsymbol{s}_{1,1} \\ \boldsymbol{s}_{1,2} \\ \boldsymbol{s}_{2,1} \\ \boldsymbol{s}_{2,2} \end{bmatrix}, \begin{bmatrix} \mathbf{0} \\ \mathbf{0} \\ \mathbf{0} \end{bmatrix}\right]_1, \left[\begin{bmatrix} \mathbf{0} \\ \boldsymbol{s}_{1,1} \\ \boldsymbol{s}_{1,2} \\ \boldsymbol{s}_{2,1} \\ \boldsymbol{s}_{2,2} \end{bmatrix}, \begin{bmatrix} \mathbf{0} \\ \mathbf{0} \end{bmatrix}\right]_2, \\ &\left[\begin{bmatrix} \mathbf{0} \\ \mathbf{0} \\ \boldsymbol{s}_{1,1} \\ \boldsymbol{s}_{1,2} \\ \boldsymbol{s}_{2,1} \\ \boldsymbol{s}_{2,2} \end{bmatrix}, \begin{bmatrix} \mathbf{0} \end{bmatrix}\right]_3, \text{or} \left[\begin{bmatrix} \mathbf{0} \\ \mathbf{0} \\ \mathbf{0} \\ \boldsymbol{s}_{1,1} \\ \boldsymbol{s}_{1,2} \\ \boldsymbol{s}_{2,1} \\ \boldsymbol{s}_{2,2} \end{bmatrix}\right]_4, \end{aligned} \tag{61}$$

where $\mathbf{0}$ is an $(K \cdot M \times T)$-element zero matrix denoting the deactivated transmit AEs. It is shown in Equation (61) that the L-GSTSK agglomerate of (60) is mapped into four distinct sets of AEs in each AC.

By contrast, the ACs constructed using the SAC allocation technique may have common AEs in different ACs, given that they are not utilized simultaneously, as depicted in Figure 16(b), where it is shown that the second AE is assigned to both the n_{sc}-th and $(n_{sc}+1)$-st ACs. Hence, the total number of ACs associated with the SAC allocation technique is expressed as

$$N_c^{(SAC)} = \left\lfloor \binom{N_t}{N_c^t} \right\rfloor_{2^\iota}. \tag{62}$$

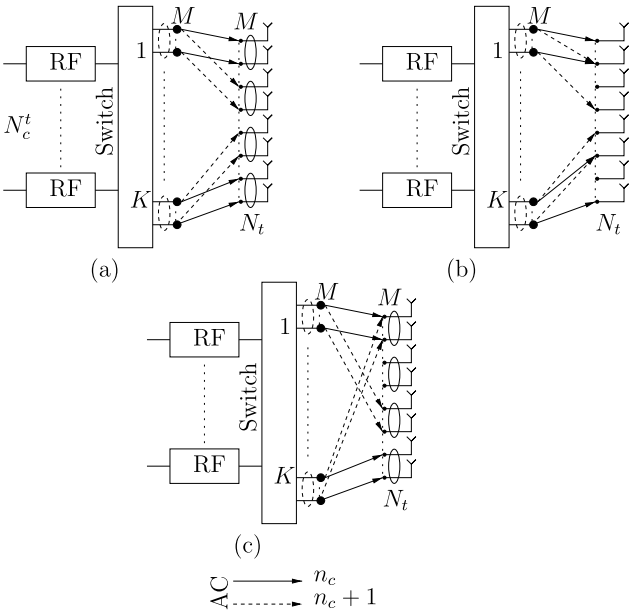

FIGURE 16. LMS system associated with (a) DAC, (b) SAC and (c) Semi-SAC/Semi-DAC antenna allocation techniques.

In the following, we introduce an example for further illustrating the SAC technique.

Example 9: consider the LMS-GSTSK(6:4, $N_c = 4$, $K = 2$, $M = 2$, N_r, T, P:Q, $\mathcal{L}$-PSK/QAM) system of Figure 14 associated with the SAC allocation technique. We reduced N_t here to arrange for having the same number of ACs as in the Example 8. The ASU of Figure 14 is capable of generating a total of $\binom{6}{4} = 15$ ACs that share some common AEs and up to $N_c^{(SAC)} = \lfloor 15 \rfloor_{2^\iota} = 8$ effective ACs. However we will only utilize $N_c = 4$ ACs to have a comparable number of ACs to that of Example 8. Given the same L-GSTSK agglomerate of (59) and (60), the LMS agglomerate $\mathring{\boldsymbol{S}}$ can be transmitted over $N_c = 4$ shared-AEs ACs as

$$\begin{aligned}\mathring{\boldsymbol{S}} = &\left[\begin{bmatrix} \boldsymbol{s}_{1,1} \\ \boldsymbol{s}_{1,2} \\ \boldsymbol{s}_{2,1} \\ \boldsymbol{s}_{2,2} \\ 0 \\ 0 \end{bmatrix}\right]_1, \left[\begin{bmatrix} \boldsymbol{s}_{1,1} \\ 0 \\ \boldsymbol{s}_{1,2} \\ \boldsymbol{s}_{2,1} \\ \boldsymbol{s}_{2,2} \\ 0 \end{bmatrix}\right]_2, \left[\begin{bmatrix} \boldsymbol{s}_{1,1} \\ 0 \\ \boldsymbol{s}_{1,2} \\ \boldsymbol{s}_{2,1} \\ 0 \\ \boldsymbol{s}_{2,2} \end{bmatrix}\right]_3, \\ &\text{or} \left[\begin{bmatrix} \boldsymbol{s}_{1,1} \\ 0 \\ \boldsymbol{s}_{1,2} \\ 0 \\ \boldsymbol{s}_{2,1} \\ \boldsymbol{s}_{2,2} \end{bmatrix}\right]_4, \end{aligned} \tag{63}$$

where the scalar zero 0 denotes the deactivated AE. It can be clearly seen in (63) that by employing SAC, the same AE might be activated as part of the various ACs to transmit the same row-vector of the L-GSTSK agglomerate, such as the first AE transmitting $\boldsymbol{s}_{1,1}$ in all ACs and the sixth AE transmitting $\boldsymbol{s}_{2,2}$ in the third and fourth AC. Note here that

other ACs are also available, but they are not altered by the ASU, since only 2^{ι} ACs are required for characterizing B_{ASU}.

Finally, the ACs constructed using the Semi-DAC allocation technique features both of the aforementioned DAC and SAC techniques. To elaborate a little further on the Semi-DAC technique, the AEs are partitioned into groups of M distinct AEs, as seen in Figure 16(c). Now, each group of M distinct AEs is used for transmitting a specific GSTSK codeword in one or more ACs and can be used for transmitting another GSTSK codeword in other ACs. Naturally, an AE element assigned to a specific group of M AEs cannot be assigned to another group, hence LMS agglomerates represent a total of $N_c^t = K \cdot M$ AEs having groups of M AEs shared among them. Therefore, the total number of ACs now depends on how many sets of M AEs and RF chains are available

$$N_c^{(Semi-DAC)} = \left\lfloor \binom{N_t/M}{N_c^t/M} \right\rfloor_{2^{\iota}}. \tag{64}$$

Both the DAC and the Semi-DAC techniques represent special cases of the SAC, where amongst all combinations obtained from $\binom{N_t}{N_c^t}$, only those satisfying the conditions of DAC or Semi-DAC are considered. In the following, we introduce an example for further illustrating the Semi-DAC technique.

Example 10: consider the LMS-GSTSK(8:4, $N_c = 4$, $K = 2$, $M = 2$, N_r, T, P:Q, $\mathcal{L}$-PSK/QAM) system of Figure 14 associated with the Semi-DAC allocation technique. We increase N_t used in Example 9 to arrange for the same number of ACs used in the Examples 8 and 9. Here the ASU of Figure 14 is capable of generating a total of $\binom{8/2}{4/2} = 6$ ACs that share distinct sets of $M = 2$ AEs and $N_c^{(Semi-DAC)} = \lfloor 6 \rfloor_{2^{\iota}} = 4$ effective ACs. Given the same L-GSTSK agglomerate as used in Example 8 in (59) and (60), the LMS agglomerate $\mathring{\boldsymbol{S}}$ can now be transmitted over $N_c = 4$ Semi-shared-AEs ACs, where the row-vector representation of $\mathring{\boldsymbol{S}}$ is expressed as

$$\mathring{\boldsymbol{S}} = \begin{bmatrix} s_{1,1} \\ s_{1,2} \\ s_{2,1} \\ s_{2,2} \\ 0 \\ 0 \\ 0 \\ 0 \end{bmatrix}_1, \begin{bmatrix} s_{1,1} \\ s_{1,2} \\ 0 \\ 0 \\ s_{2,1} \\ s_{2,2} \\ 0 \\ 0 \end{bmatrix}_2, \begin{bmatrix} s_{1,1} \\ s_{1,2} \\ 0 \\ 0 \\ 0 \\ 0 \\ s_{2,1} \\ s_{2,2} \end{bmatrix}_3, \text{ or } \begin{bmatrix} 0 \\ 0 \\ s_{1,1} \\ s_{1,2} \\ 0 \\ 0 \\ s_{2,1} \\ s_{2,2} \end{bmatrix}_4, \tag{65}$$

while the codeword representation of $\mathring{\boldsymbol{S}}$ can be viewed as

$$\mathring{\boldsymbol{S}} = \begin{bmatrix} \boldsymbol{S}_1 \\ \boldsymbol{S}_2 \\ \boldsymbol{0}_{M\times T} \\ \boldsymbol{0}_{M\times T} \end{bmatrix}_1, \begin{bmatrix} \boldsymbol{S}_1 \\ \boldsymbol{0}_{M\times T} \\ \boldsymbol{S}_2 \\ \boldsymbol{0}_{M\times T} \end{bmatrix}_2, \begin{bmatrix} \boldsymbol{S}_1 \\ \boldsymbol{0}_{M\times T} \\ \boldsymbol{0}_{M\times T} \\ \boldsymbol{S}_2 \end{bmatrix}_3, \text{ or } \begin{bmatrix} \boldsymbol{0}_{M\times T} \\ \boldsymbol{S}_1 \\ \boldsymbol{0}_{M\times T} \\ \boldsymbol{S}_2 \end{bmatrix}_4. \tag{66}$$

Observe that in (65) and (66) $M = 2$ distinct sets of AEs are shared among the ACs to transmit $\boldsymbol{S}_1$ and $\boldsymbol{S}_2$ over distinct AEs, such as the first and second AEs transmitting $\boldsymbol{s}_{1,1}$ and $\boldsymbol{s}_{1,2}$ ($\boldsymbol{S}_1$) in the first, second and third ACs as well as the seventh and eighth AEs transmitting $\boldsymbol{s}_{2,1}$ and $\boldsymbol{s}_{2,2}$ ($\boldsymbol{S}_2$) in the third and fourth AC. Furthermore, the third and fourth AEs transmitting $\boldsymbol{s}_{1,1}$ and $\boldsymbol{s}_{1,2}$ ($\boldsymbol{S}_1$) in the fourth AC are also used for transmitting $\boldsymbol{s}_{2,1}$ and $\boldsymbol{s}_{2,2}$ ($\boldsymbol{S}_2$) in the first AC.

C. LMS SYSTEM THROUGHPUT AND DIVERSITY ORDER

The LMS system proposed employs a sophisticated MIMO encoding principle, where a specific combination out of N_c ACs is activated to transmit a multi-layered GSTSK codeword agglomerate containing the information bits in addition to the activated AC index. In this section, we expand on the number of bits conveyed by each of the LMS-GSTSK components, namely the number of ACs N_c, the number of layers K, the P out of Q selected dispersion matrices of the GSTSK codeword as well as on the $\mathcal{L}$PSK/QAM constellation size.

The number of bits transmitted by our LMS system is given by

$$B = B_{L-GSTSK} + B_{ASU}, \tag{67}$$

where $B_{L-GSTSK}$ and B_{ASU} were defined in (52) and (55), respectively, and the total number of LMS bits can be formulated as

$$\begin{aligned} B &= (K \cdot B_{GSTSK}) + \log_2(N_c) \\ &= \log_2 f(Q, P)^K + K \cdot P \cdot \log_2(\mathcal{L}) + \log_2(N_c). \end{aligned} \tag{68}$$

Hence, the normalized throughput R of the LMS-GSTSK system of Figure 14, which transmits over T time slots can be expressed as

$$R = \frac{B}{T} \text{ (bpcu)}, \tag{69}$$

in terms of bits-per-channel-use (bpcu). Furthermore, the maximum achievable diversity order of the LMS-GSTSK scheme of Figure 14 can be expressed as

$$\mathcal{D} = N_r \cdot \min(M, T), \tag{70}$$

which is equivalent to a single layer GSTSK/STSK/MS-STSK system.

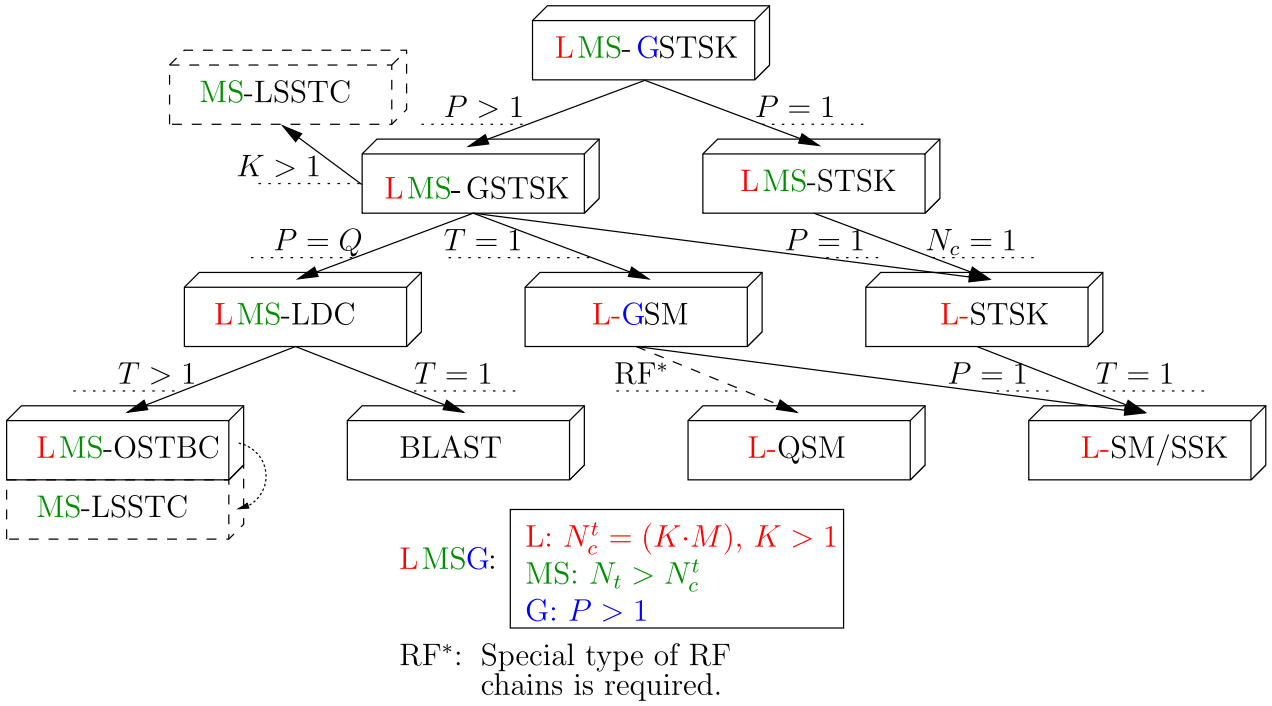

FIGURE 17. Other MIMO schemes are subsumed within the LMS-GSTSK framework. The colored annotations (LMS-G) denote the optional Layered (L), Multi-Set (MS) and Generalized (G) features of the LMS system based on the configuration shown in Table 1.

TABLE 1. The LMS system frequently used annotations (LMS-G) represent the optional Layered (L), Multi-Set (MS) and Generalized (G) system features, when $K = 1$, $N_t \geq N_c^t$ and $P > 1$, respectively.

Acronym	K	N_t	P
L:	> 1		
MS:		$\geq N_c^t$	
G:			$1 < P \leq Q$

D. SPECIAL CASES

We opt for the GSTSK arrangement of Figure 9 as our main encoding scheme in order to further generalize our system and improve its flexibility. Based on the specific choice of the LMS-GSTSK system parameters, as illustrated in Figure 17, we can obtain many other conventional as well as further novel MIMO arrangements as follows. Note here that the colored letters shown in Figure 17 as Layered (e.g. $K \geq 1$) Multi-Set (e.g. $N_t \geq N_c^t$) Generalized (e.g. $1 > P > Q$) represented by the nomenclature of LMS-G are all optional, where the schemes referring to each letter, multiple letters, all letters and/or none of them can be activated, as presented in Table 1. Furthermore, the set of different systems parameters is provided in Table 2. In the following, we expound on how to arrive at each of the LMS concept's special cases presented in Figure 17 and Table 2.

1) MS-GSTSK/GSTSK

Based on the illustration provided in Figure 17 and on the parameters presented in Table 2, let us consider the case of $K = 1$ of LMS-GSTSK, where a single-layer is available at the transmitter relying on $N_c^t = M$ RF chains. The system then scales down to the MS-GSTSK scheme, which is a generalized form of the MS-STSK scheme of Figure 10 proposed in [85], where M AEs are activated for transmitting a single GSTSK codeword. Hence, the source bits are conveyed over the GSTSK codeword as well as by the implicit information of the activated AC index. The transmitted symbol of (51) can now be expressed as

$$\bar{\boldsymbol{S}} = \sum_{k=1}^{K=1} \bar{\boldsymbol{S}}_k = \bar{\boldsymbol{S}}_1, \tag{71}$$

and the total number of bits per MS-GSTSK codeword is

$$B = \log_2 f\,(Q,\ P) + P \cdot \log_2\,(\mathcal{L}) + \log_2\,(N_c)\,. \tag{72}$$

Furthermore, when the number of RF chains N_c^t is equal both to the number of spatial dimensions of a single layer GSTSK and to the number of transmit AEs, as encapsulated in $N_c^t = M = N_t$, observe in Table 2 that the number of ACs reduces to $N_c = 1$ AC, which down-grades the system to the conventional GSTSK scheme proposed in [76]. The GSTSK scheme subsumes other conventional MIMO arrangements, which are presented below.

TABLE 2. Other MIMO schemes as special cases of the LMS-GSTSK system.

Section	Scheme	K	N_t	N_c^t	$P(\leq Q)$	M	Q	T
III	LMS-GSTSK	>1	$\geq N_c^t$	KM	≥ 1	≥ 1	≥ 1	≥ 1
III-D1	MS-GSTSK	1	$\geq N_c^t$	KM	≥ 1	≥ 1	≥ 1	>1
III-D2	LMS-STSK	>1	$\geq N_c^t$	KM	1	≥ 1	≥ 1	>1
	MS-STSK	1	$\geq N_c^t$	M	1	≥ 1	≥ 1	>1
III-D3	L-GSTSK	>1	KM	KM	≥ 1	≥ 1	≥ 1	>1
	GSTSK	1	M	M	≥ 1	≥ 1	≥ 1	>1
	L-STSK	>1	KM	KM	1	≥ 1	≥ 1	>1
	STSK	1	M	M	1	≥ 1	≥ 1	>1
III-D4	LSSTC	>1	KM	KM	Q	≥ 1	≥ 1	>1
	OSTBC	1	M	M	Q	≥ 1	≥ 1	2
III-D5	L-GSM	>1	KM	KP	≥ 1	Q	M	1
	GSM	1	M	P	≥ 1	Q	M	1
	L-SM/L-SSK	>1	KM	K	1	Q	M	1
	SM/SSK	1	M	1	1	Q	M	1
III-D6	L-QSM	>1	KM	K	2	Q	M	1
	QSM	1	M	1	2	Q	M	1
III-D7	LMS-LDC	>1	$\geq N_c^t$	KM	Q	Q	≥ 1	>1
	L-LDC	>1	KM	KM	Q	≥ 1	≥ 1	>1
	LDC	1	M	M	Q	≥ 1	≥ 1	>1
III-D8	BLAST	1	M	M	Q	Q	M,1	1

2) LMS-STSK/MS-STSK

We may also view the proposed LMS system as LMS-STSK, by setting $P = 1$, as depicted in Figure 17 and Table 2. The conventional STSK scheme of [77] is subsumed by GSTSK [76], where upon selecting $P = 1$ out of Q dispersion matrices and a single PSK/QAM symbol by the GSTSK encoder of Figure 14, we obtain an STSK codeword, which transforms into an MS-STSK codeword, when associated with an AC. Hence, the system may be viewed as LMS-STSK.

In an LMS-STSK system, the traditional MS-STSK scheme's behavior is evolved to operating over multiple layers, rather than using a single layer only. More specifically, in the traditional MS-STSK a specific AC of M AEs out of the available AEs is activated to implicitly include the activated AC index. Similarly, the N_t transmit AEs available in LMS-STSK are partitioned into layers of N_t^v AEs in order to associate the generated STSK codeword with an AC within each of the N_t/N_t^v AE layers, as shown both in Figure 18 and Table 2. In this figure we show that only M out of N_t^v transmit AEs are activated within each layer, which facilitates for the scheme to have reduced number of RF chains, where only the required M ACs are activated at each MS-STSK transmission.

3) L-GSTSK/GSTSK AND L-STSK/STSK

Both the MS-STSK and STSK schemes of Figure 10 and Figure 8 are subsumed by MS-GSTSK and GSTSK, respectively, upon using $P = 1$. The LMS-GSTSK system of Figure 14 subsumes the MS-STSK arrangement of Figure 10 upon setting $P = 1$, $K = 1$ as well as the STSK arrangement of Figure 8 when additionally using a single AC of $N_c = 1$, where in addition to LMS-STSK a layered arrangement can be used for the latter referred to as L-STSK. Likewise, by setting $P > 1$ in a single layered LMS-GSTSK system, we may arrive at a layered arrangement of GSTSK referred to as L-GSTSK. Hence, the LMS-GSTSK system encompasses both L-STSK and STSK as well as both L-GSTSK and GSTSK schemes as special cases, which is illustrated in Figure 17 and Table 2, while ignoring the transmit AEs partitioning used for LMS-STSK of Figure 18 by setting $N_t^v = M$.

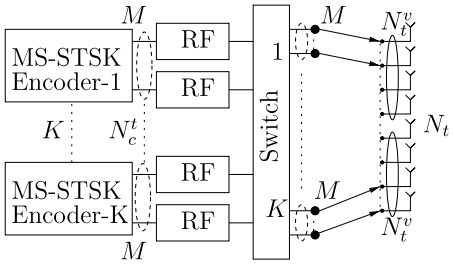

FIGURE 18. Layered MS-STSK system block diagram.

4) GENERALIZED LSSTC/OSTBC

The LSSTC scheme belongs to the class of multi-functional MIMOs that combines for example V-BLAST and STCs for enhancing the achievable performance. More specifically, the LSSTC system of Figure 12 resembles the multiplexing architecture of V-BLAST by transmitting independent STC block streams over different layers of AEs. This concept is reciprocated by the aforementioned L-GSTSK, where independent GSTSK block streams are transmitted over different layers, which may be transformed into LSSTC, when using a special type of STSK codewords, namely those of STBCs, as shown in Figure 17 and Table 2. For instance, consider an LSSTC system associated with twin OSTBC encoders relying on a PSK/QAM symbol constellation and with two pairs of antenna layers, yielding $N_t = 4$ and $M = 2$. Hence, the transmitted double-layered LSSTC codeword $\bar{\boldsymbol{S}} \in \mathbb{C}^{(N_t=2)\times(T=2)}$ can be expressed as:

$$\bar{\boldsymbol{S}} = \left[\begin{array}{cc} x_1^{(1)} & x_2^{(1)} \\ -x_2^{(1)*} & x_1^{(1)*} \\ \hline x_1^{(2)} & x_2^{(2)} \\ -x_2^{(2)*} & x_1^{(2)*} \end{array}\right], \tag{73}$$

where the k-th postscript of $x_l^{(k)}$ denotes the k-th transmission layers of the l-th PSK/QAM symbol. To design this LSSTC system using our L-GSTSK system, consider $P = Q$ and $K = 2$ as well as the following dispersion matrices

$$\begin{aligned} \boldsymbol{S}_k &= \begin{bmatrix} x_1^{(k)} & x_2^{(k)} \\ -x_2^{(k)*} & x_1^{(k)*} \end{bmatrix}, \\ &= \begin{bmatrix} \frac{1}{2} & 0 \\ 0 & \frac{1}{2} \end{bmatrix} \sqrt{2}\beta_1^{(k)} + j \begin{bmatrix} \frac{1}{2} & 0 \\ 0 & -\frac{1}{2} \end{bmatrix} \sqrt{2}\beta_1^{(k)} \\ &\quad + \begin{bmatrix} 0 & \frac{1}{2} \\ -\frac{1}{2} & 0 \end{bmatrix} \sqrt{2}\alpha_2^{(k)} + j \begin{bmatrix} 0 & \frac{1}{2} \\ \frac{1}{2} & 0 \end{bmatrix} \sqrt{2}\beta_2^{(k)}, \end{aligned} \tag{74}$$

where $x_l^{(k)} = \alpha_1^{(k)} + j\beta_1^{(k)}$ denotes the PSK/QAM symbol transmitted over the k-th antenna layer. Observe that the four dispersion matrices seen in (74) resemble four STSK matrices $\boldsymbol{A}_1$, $\boldsymbol{A}_2$, $\boldsymbol{A}_3$ and $\boldsymbol{A}_4$ out of $Q = 4$ matrices, which are activated with the aid of four symbols $\alpha_1^{(k)}$, $\beta_1^{(k)}$, $\alpha_2^{(k)}$ and $\beta_2^{(k)}$, respectively, in a GSTSK system, given that the set of matrices belongs to the set $\{\boldsymbol{A}_q\}_{q=1}^{Q}$ formulated as

$$\{\boldsymbol{A}_q\}_{q=1}^{Q} \in \left\{ \begin{bmatrix} \frac{1}{2} & 0 \\ 0 & \frac{1}{2} \end{bmatrix}, \begin{bmatrix} \frac{1}{2} & 0 \\ 0 & -\frac{1}{2} \end{bmatrix}, \tag{75}$$

$$\begin{bmatrix} 0 & \frac{1}{2} \\ -\frac{1}{2} & 0 \end{bmatrix}, \begin{bmatrix} 0 & \frac{1}{2} \\ \frac{1}{2} & 0 \end{bmatrix} \right\}. \tag{76}$$

Equation (74) can now be expressed as

$$\begin{aligned} \boldsymbol{S}_k &= \boldsymbol{A}_1\left(\sqrt{2}\alpha_1^{(k)}\right) + \boldsymbol{A}_2\left(j\sqrt{2}\beta_1^{(k)}\right) \\ &\quad + \boldsymbol{A}_3\left(\sqrt{2}\alpha_2^{(k)}\right) + \boldsymbol{A}_4\left(j\sqrt{2}\beta_2^{(k)}\right). \end{aligned} \tag{77}$$

In a nutshell, the LSSTC arrangement of Figure 12 can be considered as a special case of the aforementioned L-GSTSK, which can in turn be considered as a generalized LSSTC structure. Furthermore, the system scales down to the conventional STC scheme employed, when a single-layer LSSTC scheme is employed, where in the case of employing STBC and/or OSTBC the system can be viewed as an STBC and/or OSTBC system.

5) L-SM(SSK)/SM(SSK) AND L-GSM/GSM

Our LMS-GSTSK scheme can be viewed as a classical SM, by setting $K = 1$, $P = 1$ and $T = 1$. The q-th AE is activated by selecting the single-layered dispersion matrices $\{\boldsymbol{A}_q\}_{q=1}^{Q}$ formulated as

$$\boldsymbol{A}_q = \left[\underbrace{0, \ldots, 0}_{q-1}, \; 1, \underbrace{0, \ldots, 0}_{Q-q}\right]^T, \tag{78}$$

given that the number of dispersion matrices is equal to the spactial dimension of $\boldsymbol{A}_q \in \mathbb{C}^{M\times 1}$, yielding $Q = M$. The desired dispersion matrix and/or AE is activated by simply setting the q-th coefficient of (78) to one. Hence, the transmitted symbol can be expressed as

$$\bar{\boldsymbol{S}} = \left[\underbrace{0, \ldots, 0}_{q-1}, \; x_l, \underbrace{0, \ldots, 0}_{Q-q}\right]^T. \tag{79}$$

This system scales down to SSK when no PSK/QAM symbol is transmitted, corresponding to using $x_l = 1$ – 1PSK – and only the implicit index of the activated antenna is transmitted. Furthermore, a layered structure of SM, referred to as L-SM/L-SSK, can be constructed by utilizing the aforementioned SM configurations, while additionally increasing the number of layers to $K > 1$. The resultant system would then resemble either the L-SM scheme proposed for multi-user scenarios by Maleki *et al.* [94], or to the conventional GSM of Figure 7(a) when employed in a single-user scenario.

Furthermore, our LMS-GSTSK scheme of Figure 14 and Table 2 may mimic the GSM scheme of Figure 7(a), by setting $K \geq 1$, $Q = M$, $P > 1$ and $T = 1$, where the p-th dispersion matrix of the k-th layer GSTSK codeword of (49) activates a specific AE to transmit P PSK/QAM symbols.

For example, consider a single-layered LMS-GSTSK system associated with the aforementioned GSM settings under the assumption of $Q = M = N_t = 4$ and $P = 2$. Based on the dispersion matrix structure of SM seen in (78),

a GSM-equivalent GSTSK codeword can be expressed as

$$\boldsymbol{S}_1 = \sum_{p=1}^{P=2} \left(\underbrace{\begin{bmatrix} 0 \\ 1 \\ 0 \\ 0 \end{bmatrix}}_{\boldsymbol{A}(1)} x(1) + \underbrace{\begin{bmatrix} 0 \\ 0 \\ 1 \\ 0 \end{bmatrix}}_{\boldsymbol{A}(2)} x(2) \right) = \begin{bmatrix} 0 \\ x(1) \\ x(2) \\ 0 \end{bmatrix}, \tag{80}$$

where both the 2-nd and 3-rd rows (or transmit AEs) of $\boldsymbol{S}_1$ are activated to transmit $x(1)$ and $x(2)$, respectively. $\boldsymbol{S}_1$can be considered as an SSK codeword, when $x(p) = 1$ $\forall p = 1, \ldots, P$.

Our LMS-GSTSK scheme is equivalent to an ordinary GSM scheme, especially when $K = 1$. However, upon increasing the number of layers to $K > 1$ the system can be further generalized to a multi-layered system represented as L-GSM.

6) L-QSM/QSM

The above-mentioned GSM configurations of our LMS-GSTSK system can be further evolved in order to incorporate QSM as a special case, as shown both in Figure 14 and Table 2. More specifically, by applying the same settings of $K \geq 1$, $Q = M$ and $T = 1$, but with $P = 2$, the GSM-equivalent LMS-GSTSK system can be viewed as a QSM system, if and only if the in-phase and quadrature components are separated in space.

For further clarification, consider the single-layered LMS-GSTSK system of Figure 14 associated with $Q = M = N_t = 4$ dispersion matrices as well as transmit AEs and $P = 2$ for representing a QSM symbol. Based on the example of (80), a generated QSM-equivalent GSTSK codeword $\boldsymbol{S}_1$ can be expressed as

$$\boldsymbol{S}_1 = \sum_{p=1}^{P=2} \left(\begin{bmatrix} 0 \\ 1 \\ 0 \\ 0 \end{bmatrix} \alpha_1^{(k)} + j \begin{bmatrix} 0 \\ 0 \\ 1 \\ 0 \end{bmatrix} \beta_1^{(k)} \right) = \begin{bmatrix} 0 \\ \alpha_1^{(k)} \\ j \cdot \beta_1^{(k)} \\ 0 \end{bmatrix}, \tag{81}$$

where the real part and imaginary part are transmitted by the second and third AEs, respectively. This scheme can be further generalized by utilizing multiple layers with the aid of $K \geq 1$, where multiple QSM symbols can be transmitted over different layers.

7) LMS-LDC/LDC

In LDC, all of the available Q dispersion matrices are utilized for transmitting a linear combination of Q PSK/QAM symbols. By considering the single-layered LMS-GSTSK system of Figure 14 relying on N_t AEs equivalent to the number of RF chains $N_t = N_c^t$ leading to $N_c = 1$, the system is scaled down into an LDC system upon selecting $P = Q$ dispersion matrices, as depicted in Figure 14 and Table 2. Hence, the LDC-equivalent output of the GSTSK encoder of Figure 14 and Figure 15 may be expressed as:

$$\begin{aligned} \boldsymbol{S}_1 &= \sum_{p=1}^{P=Q} \boldsymbol{A}(p)\, x(p) \\ &= \boldsymbol{A}(1)\, x(1) + \cdots + \boldsymbol{A}(Q)\, x(Q). \end{aligned} \tag{82}$$

Given that $P = Q$ and $N_c^t = N_t$, the number of bits implicitly transmitted over both the P combinations of dispersion matrices selected and the activated AC is nil, since both $\log_2(f(Q, P)) = 1$ and $\log_2(N_c = 1)$ of (68) are equal to zero. Nonetheless, the system can be viewed both as an L-LDC system upon increasing the number of layers to $K > 1$ and as an LMS-LDC system by using higher number of AEs than that of the RF chains, yielding $N_t > N_c^t$.

8) BLAST

BLAST is another special case of the LMS-GSTSK system, which can be constituted using two techniques. In the first technique, we start by scaling the system down to a GSTSK system and then we set the number of dispersion matrices to the number of transmit antennas according to $Q = M$, where we have $M = N_c^t$ as well as $N_c^t = N_t$ and then we select all of the Q dispersion matrices by setting $P = Q$. Furthermore, the dispersion matrices used here are equivalent to those used for GSM in (80), where a degenerated single-time slot dispersion matrix is used in conjunction with $T = 1$, as illustrated in Figure 14 and Table 2.

For example, consider a single-layered LMS-GSTSK system equipped with $N_c = 4$ RF chains and $N_t = 4$ transmit AEs. The GSTSK encoder relying on $Q = 4$ dispersion matrices and $T = 1$ time slots generates a BLAST-equivalent LMS-GSTSK codeword as

$$\boldsymbol{S}_1 = \sum_{p=1}^{P=2} \left(\underbrace{\begin{bmatrix} 1 \\ 0 \\ 0 \\ 0 \end{bmatrix}}_{\boldsymbol{A}(1)} x(1) + \underbrace{\begin{bmatrix} 0 \\ 1 \\ 0 \\ 0 \end{bmatrix}}_{\boldsymbol{A}(2)} x(2) + \underbrace{\begin{bmatrix} 0 \\ 0 \\ 1 \\ 0 \end{bmatrix}}_{\boldsymbol{A}(3)} x(3) + \underbrace{\begin{bmatrix} 0 \\ 0 \\ 0 \\ 1 \end{bmatrix}}_{\boldsymbol{A}(4)} x(4) \right) = \begin{bmatrix} x(1) \\ x(2) \\ x(3) \\ x(4) \end{bmatrix}, \tag{83}$$

which is transmitted by $N_t = M = 4$ transmit AEs as $\bar{\boldsymbol{S}} = \boldsymbol{S}_1$.

According to the other technique, the number of layers is set to the number of symbols multiplexed in a BLAST system, yielding $K = M$. Then, a single unity dispersion matrix is selected by relying on $P = Q = 1$ and $T = 1$ time slots. The codeword generated by each layer's GSTSK encoder may be

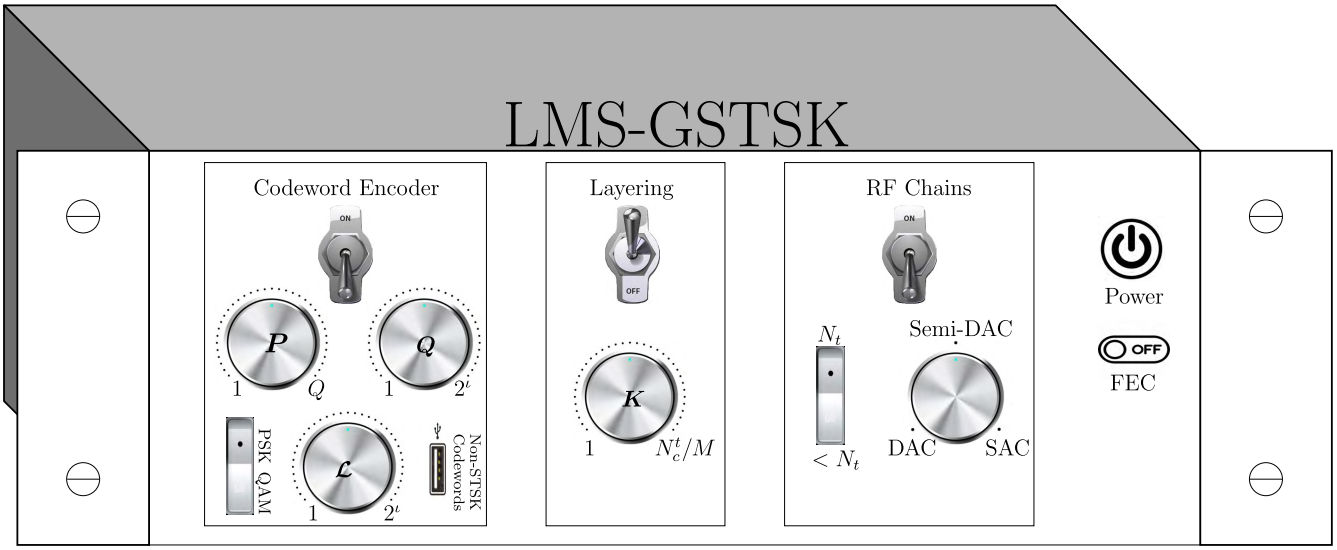

FIGURE 19. A illustration of the LMS-GSTSK 'device', which is constituted by three main components, namely the Encoder part, the Layering part as well as the RF-Chains part.

expressed as

$$\begin{aligned} \boldsymbol{S}_k &= \boldsymbol{A}^{(k)} x^{(k)} \\ &= [1]\, x^{(k)} \\ &= x^{(k)}, \end{aligned} \tag{84}$$

and the layered codeword of (51) is then formulated as

$$\begin{aligned} \bar{\boldsymbol{S}} &= \sum_{k=1}^{K=4} \left(\underbrace{\begin{bmatrix} x^{(1)} \\ 0 \\ 0 \\ 0 \end{bmatrix}}_{\bar{\boldsymbol{s}}_1} + \underbrace{\begin{bmatrix} 0 \\ x^{(2)} \\ 0 \\ 0 \end{bmatrix}}_{\bar{\boldsymbol{s}}_2} + \underbrace{\begin{bmatrix} 0 \\ 0 \\ x^{(3)} \\ 0 \end{bmatrix}}_{\bar{\boldsymbol{s}}_3} + \underbrace{\begin{bmatrix} 0 \\ 0 \\ 0 \\ x^{(4)} \end{bmatrix}}_{\bar{\boldsymbol{s}}_4} \right) \\ &= \begin{bmatrix} x^{(1)} \\ x^{(2)} \\ x^{(3)} \\ x^{(4)} \end{bmatrix}, \end{aligned} \tag{85}$$

E. LMS-GSTSK SYSTEM SUMMARY

A stylized illustration of our LMS-GSTSK system as an 'electronic device' is depicted in Figure 19. The device of Figure 19 has three main components, namely the Codeword Encoder, the Layering and the RF Chain components, as well as the Forward Error Correction (FEC) scheme of the system, which is detailed in the following section. This illustration perfectly resembles the behavior of our LMS system, where each of its parts can be both digitally tuned as well as switched on and/or off based on the system requirements as follows.

The Codeword Encoder of Figure 19 is responsible for adjusting the core LMS codeword configurations shown in Figure 14 and formulated in Equation (49). More specifically, after toggling the Codeword Encoder switch to on, we can adjust its three main elements; (1) the number of dispersion matrices generated according to Equation (14) and shown by the Q-tuning wheel of Figure 19, (2) the number of selected dispersion matrices P having a maximum of Q, as shown on its corresponding tuning wheel in Figure 19 in order to encode the $\log_2 f(Q, P)$ bits formulated in (27), (3) the PSK/QAM constellation size $\mathcal{L}$ and its associated PSK/QAM switch to select either of the two constellation types. Furthermore, an input port is included in the Codeword Encoder part to allow using other types of codewords, such as the OSTBC, B-BLAST and LSSTC codewords presented in Figure III-D. On the other hand, in the Layering part of Figure 19, the number of layers K spans between 1 and N_c^t/M, which is indicated by the associated tuning wheel of Figure 19. Finally, the number of RF chains determines the total number of ACs N_c, where the switch in the RF Chains part of Figure 19 decides whether the number of RF chains N_c^t is equal or less than N_t, namely the number of transmit AEs. The tuning wheel in this segment of Figure 19 activates one of three antenna allocation techniques, particularly the DAC, SAC and Semi-DAC defined in Equations (58), (62) as well as (64), respectively. The system also includes the FEC functionality and can be switched on using the on/off switch located below the power button. In the following section, we present our uncoded and coded LMS-GSTSK receivers designed based on both Hard-Decision (HD)-aided as well as on Soft-Decision (SD)-aided detection. On a side note, a summary of the complexity order, diversity order and data rate of various MIMO arrangements in comparison to our LMS scheme, namely the OSTBC, LSSTC, V-BLAST, SM/SSK, GSM, LDC, STSK, GSTSK and MS-STSK schemes is shown in Table 3. It is also worth mentioning in Table 3 that the attainable diversity gain of GSM (marked with the asterisk symbol) relies on the GSM approach employed. More

TABLE 3. A summary of the complexity order, diversity order and data rate of various MIMO arrangements, namely the OSTBC, LSSTC, V-BLAST, SM/SSK, GSM, LDC, STSK, GSTSK and MS-STSK schemes in comparison to our LMS scheme. *Note here that the diversity order of GSM may vary depending on the transmission approach employed.

Scheme	Complexity	Diversity	Rate	RF Chains
OSTBC [33]	$\mathcal{O}(\mathcal{L})$	$(N_t \cdot N_r)$	$\leq \log_2(\mathcal{L})$	N_t
LSSTC [75]	$\mathcal{O}(\mathcal{L}^K)$	$((N_t/K) \cdot N_r)$	$\leq K \cdot \log_2(\mathcal{L})$	N_t
V-BLAST [52]	$\mathcal{O}(\mathcal{L}^{N_t})$	$(N_t - N_r + 1)$	$N_t \cdot \log_2(\mathcal{L})$	N_t
SM/SSK [32], [56]	$\mathcal{O}(N_t \cdot \mathcal{L})$	N_r	Equation (2)	1
GSM [89], [90]	$\mathcal{O}(f(N_t, P) \cdot \mathcal{L}^P)$	$(N_c^t \cdot N_r)$ or $(N_r)^*$	Equation (8)	P
LDC [46]	$\mathcal{O}(\mathcal{L}^Q)$	$N_r \cdot \min(M, T)$	$Q \cdot \log_2(\mathcal{L})/T$	$N_t = M$
STSK [78]	$\mathcal{O}(Q \cdot \mathcal{L})$	$N_r \cdot \min(M, T)$	Equation (16)	$N_t = M$
GSTSK [76]	$\mathcal{O}(f(Q, P) \cdot \mathcal{L}^P)$	$N_r \cdot \min(M, T)$	Equation (27)	$N_t = M$
MS-STSK [85]	$\mathcal{O}(Q \cdot \mathcal{L} \cdot N_c)$	$N_r \cdot \min(M, T)$	Equation (32)	$M < N_t$
LMS-GSTSK	$\mathcal{O}\left(\left(f(Q, P) \cdot \mathcal{L}^P\right)^K \cdot N_c\right)$	$N_r \cdot \min(M, T)$	Equation (68)	$N_c^t \leq N_t$

specifically, when P symbols are transmitted over the P activated AEs, no transmit diversity is obtained, hence the diversity order of the system relies on the number of receive AEs, yielding $\mathcal{D} = N_r$. However, when transmitting a single symbol over the P activated AEs, as discussed in Section II-B, the achievable diversity gain is increased to $\mathcal{D} = (N_t \cdot N_r)$.

IV. DETECTION TECHNIQUES

In this section, we present a HD-aided detector based on the optimal ML full-search method for the LMS-GSTSK system of Figure 14. We then introduce our two-stage serially concatenated SD-aided decoder for LMS-GSTSK, which iteratively exchanges extrinsic information between the LMS detector and the channel decoder.

A. THE LMS-GSTSK RECEIVER

The LMS receiver depicted in Figure 13 is equipped both with N_r receive AEs and an LMS detector. The LMS detector matches the LMS encoder of the transmitter, which in our LMS-GSTSK case can be digitally adjusted to resemble any of the special cases seen both in Figure 17 and in Table 2, in addition to the LMS-GSTSK scheme itself.

Consider a $(N_t \times N_r)$-element LMS-GSTSK system based on the schematic of Figure 13 and let $\boldsymbol{H} \in \mathbb{C}^{N_r \times N_t}$ describe the zero-mean and unity-power MIMO channel matrix between the system's transmit and receive AEs and $\boldsymbol{V} \in \mathbb{C}^{N_r \times T}$ the zero-mean Additive White Gaussian Noise (AWGN) obeying $\mathcal{CN}(0, N_0)$ with N_0 being the noise power. The $(N_r \times T)$-element block-based received signal $\boldsymbol{Y}$ can be formulated as

$$\boldsymbol{Y} = \boldsymbol{H}\,\mathring{\boldsymbol{S}} + \boldsymbol{V}. \tag{86}$$

Having demonstrated that our LMS system characterizes a higher-hierarchy SM MIMO system, the classical MIMO system model of (86) can be reformulated to resemble the SM-equivalent system models presented in Section II with the aid of a linear matrix vectorization operation.

By examining the system models presented in Section II, we deduce that each system model encompasses a specific parameter that epitomizes the system's distinctive feature. More specifically, the matrix of vectorized dispersion matrices $\mathcal{X}$ of (18) and its size Q are particularly specific to STSK, while the vector of activated PSK/QAM symbols $\mathbf{K}$ of (28) is rather specified for GSTSK. Furthermore, the AC activation matrix $\mathcal{I}$ of (33) or $\boldsymbol{F}_c$ of (40) are specifically designed for MS-STSK. It is also observed from those system models that the systems that subsumes other systems' characteristics additionally utilize their parameters. For example, the STSK component $\mathcal{X}$ of (18) is additionally used for both GSTSK and MS-STSK, given that the latter systems exploit the dispersion matrix functionality.

In the context of LMS systems, which exhibit all of the aforementioned system characteristics, the eminent feature of our proposed system is its layered architecture. Hence, the LMS system model is characterized by: Q dispersion matrices, N_c ACs, the vector of modulated symbols $\mathbf{K}$ as well as by the number of layers K. This can be achieved both by inheriting the preceding system models' characteristics[9] and by introducing the proposed scheme's distinctive feature.[10]

Based on the above-mentioned STSK, GSTSK and MS-STSK system models conversion methods, the $(N_r T \times 1)$-element vector-based representation of the received LMS-GSTSK signal can be arranged by applying the vectorization operation to its block MIMO representation. Here, we opt for the second MS-STSK system model defined in (40) for characterizing the AC selection operation, since the first model defined in (33) would require a huge dispersion matrix $\mathcal{X}$ in order to represent all the dispersion matrices, ACs and layers. Hence, the $(N_r T \times 1)$-element vector-based representation $\bar{\boldsymbol{Y}}$ of (86) of the LMS system can be expressed as

$$\bar{\boldsymbol{Y}} = \bar{\boldsymbol{H}}_c \mathcal{X} \mathbf{K} + \bar{\boldsymbol{V}}, \tag{87}$$

given that

$$\bar{\boldsymbol{Y}} = vec(\boldsymbol{Y}) \in \mathbb{C}^{N_r T \times 1}, \tag{88}$$

$$\bar{\boldsymbol{H}}_c = \boldsymbol{I}_T \otimes (\boldsymbol{H}\mathbf{F}_c) \in \mathbb{C}^{N_r T \times N_c^t T}, \tag{89}$$

$$\bar{\boldsymbol{V}} = vec(\boldsymbol{V}) \in \mathbb{C}^{N_r T \times 1}, \tag{90}$$

[9] Such as, $\mathcal{X}$ and $\mathbf{K}$.
[10] Number of layers K.

where $\bar{\boldsymbol{H}}_c$ is the vectorized representation of $(\boldsymbol{H}\mathbf{F}_c) \in \mathbb{C}^{N_r \times N_c^t}$ denoting the channel between the N_c^t activated transmit AEs[11] and all of the N_r receive AEs, with $\boldsymbol{I}_T$ being an $(T \times T)$-element identity matrix. The AC activation matrix $\boldsymbol{F}_c \in \mathbb{C}^{N_t \times N_c^t}$ is a matrix containing ones-and-zeros that produces the channel matrix $(\boldsymbol{H}\boldsymbol{F}_c)$ between the N_c^t activated transmit AEs and the N_r receive AEs, when multiplied by $\boldsymbol{H} \in \mathbb{C}^{N_r \times N_t}$. The AC activation matrix $\boldsymbol{F}_c$ is defined here as

$$\begin{aligned}\boldsymbol{F}_c &= \left[\boldsymbol{f}_{c,1} \quad \cdots \quad \boldsymbol{f}_{c,n_c^t} \quad \cdots \quad \boldsymbol{f}_{c,N_c^t}\right] \\ &= \left[\boldsymbol{f}_c^{(1)} \quad \cdots \quad \boldsymbol{f}_c^{(k)} \quad \cdots \quad \boldsymbol{f}_c^{(K)}\right] \\ &= \left[\begin{array}{ccc} \cdots & \underbrace{\left[\boldsymbol{f}_{c,n_c^t} \quad \cdots \quad \boldsymbol{f}_{c,(n_c^t+M)}\right]}_{\boldsymbol{f}_c(k)} & \cdots \end{array}\right] \\ &= \begin{bmatrix} \vdots & \vdots & \cdots & \vdots \\ 0 & 1 & \cdots & 0 \\ \vdots & \vdots & \cdots & \vdots \\ 1 & 0 & \cdots & 0 \\ \vdots & \vdots & \cdots & \vdots \\ 0 & 0 & \cdots & 1 \\ \vdots & \vdots & \cdots & \vdots \end{bmatrix}, \end{aligned} \tag{91}$$

where the n_c^t-th column vector $\boldsymbol{f}_{c,n_c^t} \in \mathbb{C}^{N_t \times 1}$ activates the n_t-th AE when a value of 1 is located on its n_t-th index, given that each column vector $\boldsymbol{f}_{c,n_c^t}$ has one and only one non-zero coefficient. Furthermore, the sub-matrix $\boldsymbol{f}_c^{(k)} \in \mathbb{C}^{N_t \times M}$ of (91), which contains the k-th group of M column vectors in $\boldsymbol{F}_c$ activates the a specific potion of M AEs in the c-th AC in order to transmit the GSTSK codeword of the k-th layer.

The dispersion matrix agglomerate $\mathcal{X} \in \mathbb{C}^{(MT)\times(QK)}$ in (87) is constituted by K recurrences of the Q STSK dispersion matrices as

$$\begin{aligned}\mathcal{X} &= \left[\mathcal{X}^{(1)} \quad \cdots \quad \mathcal{X}^{(k)} \quad \cdots \quad \mathcal{X}^{(K)}\right] \\ &= \left[\begin{array}{ccc} \cdots & \underbrace{\left[vec\left(\boldsymbol{A}_1\right), \ldots, vec(\boldsymbol{A}_Q)\right]}_{\mathcal{X}^{(k)}} & \cdots \end{array}\right], \end{aligned} \tag{92}$$

where $\mathcal{X}^{(k)}$ is exact for every $k = 1, \ldots, K$.

Furthermore, the equivalent K-layered transmit symbol vector used for activating P out of Q dispersion matrices in each layer $\mathbf{K} \in \mathbb{C}^{KQ\times 1}$ is expressed as

$$\begin{aligned}\mathbf{K} &= \left[\left(\mathbf{K}^{(1)}\right)^T \quad \cdots \quad \left(\mathbf{K}^{(k)}\right)^T \quad \cdots \quad \left(\mathbf{K}^{K}\right)^T\right]^T \\ &= \left[\begin{array}{ccc} \cdots & \underbrace{\left[a_1^{(k)}, \ldots, a_q^{(k)}, \ldots, a_Q^{(k)}\right]}_{\left(\mathbf{K}^{(k)}\right)^T} & \cdots \end{array}\right]^T, \end{aligned} \tag{93}$$

where the q-th dispersion matrix in the k-th layer is activated, when $a_q^{(k)} \neq 0$, given that the total number of non-zero components of $\mathbf{K}^{(k)}$ is P and that of $\mathbf{K}$ is KP, which are equal to the number of dispersion matrices activated per layer and per all layers, respectively. In the following, we introduce an example for further illustrating the concept of LMS-GSTSK.

Example: consider the LMS-GSTSK($N_t = 6, N_c = 4, K = 2, M = 2, N_r = 4, T = 2, P = 2{:}Q = 4$, $\mathcal{L}$-PSK/QAM)[12] of Figure 14 system associated with a Semi-DAC arrangement, where a distinct group of M AEs are shared amongst the ACs. Assume furthermore that the $(N_r = 4 \times N_t = 6)$-element channel matrix is defined as

$$\boldsymbol{H} = \begin{bmatrix} h_{1,1} & h_{1,2} & h_{1,3} & h_{1,4} & h_{1,5} & h_{1,6} \\ h_{2,1} & h_{2,2} & h_{2,3} & h_{2,4} & h_{2,5} & h_{2,6} \\ h_{3,1} & h_{3,2} & h_{3,3} & h_{3,4} & h_{3,5} & h_{3,6} \\ h_{4,1} & h_{4,2} & h_{4,3} & h_{4,4} & h_{4,5} & h_{4,6} \end{bmatrix}. \tag{94}$$

Let us select the third and fourth dispersion matrices in the first layer by placing the PSK/QAM symbols $x^1(1)$ and $x^1(2)$ in $\mathbf{K}_1$ as

$$\mathbf{K}^{(1)} = \begin{bmatrix} 0 & 0 & x^1(1) & x^1(2) \end{bmatrix}^T, \tag{95}$$

and the first and third dispersion matrices in the second layer by placing $x^2(1)$ and $x^2(2)$ PSK/QAM symbols in $\mathbf{K}_2$ as

$$\mathbf{K}^{(2)} = \begin{bmatrix} x^2(1) & 0 & x^2(2) & 0 \end{bmatrix}^T, \tag{96}$$

where the overall transmitted symbol vector $\mathbf{K}$ is given by

$$\mathbf{K} = \begin{bmatrix} \mathbf{K}^{(1)} \\ \mathbf{K}^{(2)} \end{bmatrix}. \tag{97}$$

Now, we select the first AC, which assigns for instance the first and second transmit AEs for transmitting the GSTSK codeword of the first layer and the fifth and sixth transmit AEs to transmit that of the second layer by setting their corresponding AC activation matrix to

$$\boldsymbol{F}_1 = \left[\begin{array}{cccc} 1 & 0 & 0 & 0 \\ 0 & 1 & 0 & 0 \\ 0 & 0 & 0 & 0 \\ 0 & 0 & 0 & 0 \\ 0 & 0 & 1 & 0 \\ 0 & 0 & 0 & 1 \end{array}\right] \begin{array}{l} \\ \\ \\ \\ \\ \\ \end{array} \begin{array}{cc} \\ \\ \\ \\ \underbrace{}_{\boldsymbol{f}_1^{(1)}} & \underbrace{}_{\boldsymbol{f}_1^{(2)}} \end{array}. \tag{98}$$

Next, by applying the AC activation matrix $\boldsymbol{F}_1$[13] to the channel matrix $\boldsymbol{H}$, the $\left(N_r = 4 \times N_c^t = 4\right)$-element channel matrix between the $N_c^t = 4$ activated transmit AEs and the $N_r = 4$ receive AEs arrives at

$$(\boldsymbol{H}\boldsymbol{F}_1) = \begin{bmatrix} h_{1,1} & h_{1,2} & h_{1,5} & h_{1,6} \\ h_{2,1} & h_{2,2} & h_{2,5} & h_{2,6} \\ h_{3,1} & h_{3,2} & h_{3,5} & h_{3,6} \\ h_{4,1} & h_{4,2} & h_{4,5} & h_{4,6} \end{bmatrix}, \tag{99}$$

[11] The number of activated transmit AEs is equivalent to the number of available RF chains.

[12] Again, LMS-GSTSK($N_t, N_c, K, M, N_r, T, P{:}Q$, $\mathcal{L}$-PSK/QAM)

[13] Note that $\boldsymbol{f}_c^{(k)}$ is defined in (91).

where based on the LMS system model of (87), the SM-equivalent signal can be expressed as

$$\bar{\boldsymbol{Y}} = \underbrace{\begin{bmatrix} h_{1,1} & h_{1,2} & h_{1,5} & h_{1,6} & 0 & 0 & 0 & 0 \\ h_{2,1} & h_{2,2} & h_{2,5} & h_{2,6} & 0 & 0 & 0 & 0 \\ h_{3,1} & h_{3,2} & h_{3,5} & h_{3,6} & 0 & 0 & 0 & 0 \\ h_{4,1} & h_{4,2} & h_{4,5} & h_{4,6} & 0 & 0 & 0 & 0 \\ 0 & 0 & 0 & 0 & h_{1,1} & h_{1,2} & h_{1,5} & h_{1,6} \\ 0 & 0 & 0 & 0 & h_{2,1} & h_{2,2} & h_{2,5} & h_{2,6} \\ 0 & 0 & 0 & 0 & h_{3,1} & h_{3,2} & h_{3,5} & h_{3,6} \\ 0 & 0 & 0 & 0 & h_{4,1} & h_{4,2} & h_{4,5} & h_{4,6} \end{bmatrix}}_{\bar{\boldsymbol{H}}_c} \cdot \underbrace{\left[\begin{array}{cccc|cccc} \underbrace{a_{1,1} & a_{1,2} & a_{1,3} & a_{1,4}}_{\mathcal{X}^{(1)}} & \underbrace{a_{1,1} & a_{1,2} & a_{1,3} & a_{1,4}}_{\mathcal{X}^{(2)}} \\ a_{2,1} & a_{2,2} & a_{2,3} & a_{2,4} & a_{2,1} & a_{2,2} & a_{2,3} & a_{2,4} \\ a_{3,1} & a_{3,2} & a_{3,3} & a_{3,4} & a_{3,1} & a_{3,2} & a_{3,3} & a_{3,4} \\ a_{4,1} & a_{4,2} & a_{4,3} & a_{4,4} & a_{4,1} & a_{4,2} & a_{4,3} & a_{4,4} \end{array}\right]}_{\mathcal{X}} \cdot \underbrace{\left[\underbrace{0 \quad 0 \quad x^1(1) \quad x^1(2)}_{\mathbf{K}^{(1)}} \underbrace{x^2(1) \quad 0 \quad x^2(2) \quad 0}_{\mathbf{K}^{(2)}}\right]^T}_{\mathbf{K}} + \bar{\boldsymbol{V}}, \tag{100}$$

and after converting $\bar{\boldsymbol{Y}}$ back into its matrix form, the received block $\boldsymbol{Y}$ can viewed as

$$\boldsymbol{Y} = \frac{1}{\sqrt{2}} (\boldsymbol{H}\boldsymbol{F}_1) \cdot \left[\underbrace{\left(\boldsymbol{A}_3 x^{(1)}(1) + \boldsymbol{A}_4 x^{(1)}(2)\right)}_{layer-1} \quad \underbrace{\left(\boldsymbol{A}_1 x^{(2)}(1) + \boldsymbol{A}_3 x^{(2)}(2)\right)}_{layer-2} \right] + \boldsymbol{V}, \tag{101}$$

where the first-layer GSTSK codeword $\left(\boldsymbol{A}_3 x^{(1)}(1) + \boldsymbol{A}_4 x^{(1)}(2)\right)$ occupying the first two columns of the transmitted agglomerate is transmitted over the 1-st and 2-nd transmit AEs, while the second layer GSTSK codeword $\left(\boldsymbol{A}_1 x^{(2)}(1) + \boldsymbol{A}_3 x^{(2)}(2)\right)$ occupying the next two columns of the transmitted agglomerate is transmitted over the 5-th and 6-th transmit AEs.

B. HARD DECISION-AIDED DETECTION

By recalling the system model of (87), the vector-based representation of the received LMS-GSTSK signal can be expressed as

$$\bar{\boldsymbol{Y}} = \bar{\boldsymbol{H}}_c \mathcal{X} \mathbf{K} + \bar{\boldsymbol{V}}. \tag{102}$$

In a single-layered LMS system associated with a non-generalized and ICI-free encoder, such as SM/SSK, STSK and MS-STSK, we may invoke the low-complexity single-stream-based ML detection for detecting the LMS signal of [61]. However, by introducing generalized structures, such as GSM/GSSK, GSTSK, LDC and V-BLAST, or by increasing the number of layers, the LMS system endures an excessive level of ICI, which requires an extra complexity at the receiver for mitigating its effect. The level of ICI in the LMS-GSTSK scheme is proportional to both the number of layers K as well as to the number of P GSTSK selected codewords and it is typically equivalent to $(KP-1)$. Hence, when any of the red, blue and green acronyms of Figure 17 are switched off, except for BLAST and LDC that inherently impose ICI, our system benefits from low-complexity single-stream-based ML detection.

Prior to elaborating on the detection process, here we introduce the specific parameters representing the transmitted information, namely the GSTSK codeword agglomerate and the activated AC. For instance, $\boldsymbol{A}_{q_{k,p}}$ is the p-th dispersion matrix selected in the GSTSK codeword at the k-th layer, given that $q_{k,p} = 1, \ldots, Q$ is the dispersion matrix index in $\{\boldsymbol{A}_{q_{k,p}}\}_{q_{k,p}=1}^{Q}$. Additionally, the $\boldsymbol{A}_{q_{k,p}}$ dispersion matrix is selected with the aid of $x_{l_{k,p}}$ designating the $l_{k,p}$-th PSK/QAM symbol, whereas the c-th AC is activated for transmitting the K-layered agglomerate. Hence, the receiver has to estimate $\bar{q}$ as

$$\bar{q} = \left\{ \left\{ \{q_{k,p}\}_{p=1}^{P} \right\}_{k=1}^{K} \right\}_{q=1}^{Q}, \tag{103}$$

used for characterizing the dispersion matrix $\boldsymbol{A}_{q_{k,p}}$ selected as $\boldsymbol{A}_{\bar{q}}$, and $\bar{l}$ as

$$\bar{l} = \left\{ \left\{ \{l_{k,p}\}_{p=1}^{P} \right\}_{k=1}^{K} \right\}_{l=1}^{\mathcal{L}}, \tag{104}$$

used for representing the PSK/QAM symbol $x_{l_{k,p}}$ as $x_{\bar{l}}$, in addition to c describing the AC selected. Let us consider that $\hat{\bar{q}}$, $\hat{\bar{l}}$ and $\hat{c}$ correspond to the estimates of $\bar{q}$, $\bar{l}$ and c, respectively.

The optimum Bahl-Cocke-Jelinek-Raviv (BCJR) decoding algorithm [95] aims for maximizing the *a posteriori* probability $p\left(\left\{\mathbf{K}_{\bar{q},\bar{l}}\right\}_c \middle| \bar{\boldsymbol{Y}}\right)$ based on Bayes' Law as

$$p\left(\left\{\mathbf{K}_{\bar{q},\bar{l}}\right\}_c \middle| \bar{\boldsymbol{Y}}\right) = \frac{p\left(\bar{\boldsymbol{Y}} \middle| \left\{\mathbf{K}_{\bar{q},\bar{l}}\right\}_c\right) p\left(\left\{\mathbf{K}_{\bar{q},\bar{l}}\right\}_c\right)}{\sum_{\forall \mathbf{K} \in \mathcal{K}} p\left(\bar{\boldsymbol{Y}} \middle| \left\{\mathbf{K}_{\bar{q},\bar{l}}\right\}_c\right) p\left(\left\{\mathbf{K}_{\bar{q},\bar{l}}\right\}_c\right)}, \tag{105}$$

where $\left\{\mathbf{K}_{\bar{q},\bar{l}}\right\}_c$ is the $(KQ \times 1)$-element transmitted symbol vector defined in (93) that is associated with the c-th AC for $\bar{\boldsymbol{H}}_c$. Now, under the assumption of equiprobable *a priori* probabilities characterizing the transmitted symbol

$\left\{p\left(\left\{\mathbf{K}_{\bar{q},\bar{l}}\right\}_c\right)=\frac{1}{2^B}\right\}_{\forall\bar{q},\bar{l},c}$ in HD-aided detection and by substituting $\left\{\mathbf{K}_{\bar{q},\bar{l}}\right\}_c$ by $\overline{\mathbf{K}}$ for easier representation, the conditional probability of receiving $\bar{\boldsymbol{Y}}$ provided that $\overline{\mathbf{K}}$ was transmitted can be formulated as

$$p\left(\bar{\boldsymbol{Y}}\middle|\,\overline{\mathbf{K}}\right)=\frac{1}{(\pi N_0)^{N_r T}}\exp\left(-\frac{\left\|\bar{\boldsymbol{Y}}-\bar{\boldsymbol{H}}_c\mathcal{X}\overline{\mathbf{K}}\right\|^2}{N_0}\right), \quad (106)$$

which may be invoked for maximizing $p\left(\overline{\mathbf{K}}|\bar{\boldsymbol{Y}}\right)$ of (105) in order to determine the estimates $\hat{\bar{q}}$, $\hat{\bar{l}}$ and $\hat{c}$ using an optimal ML detector as

$$\begin{aligned}\left\langle\hat{\bar{q}},\hat{\bar{l}},\hat{c}\right\rangle&=\arg\max_{\langle\bar{q},\bar{l},c\rangle}\ p\left(\bar{\boldsymbol{Y}}\middle|\,\overline{\mathbf{K}}\right)\\&=\arg\max_{\langle\bar{q},\bar{l},c\rangle}\ \exp\left(-\frac{\left\|\bar{\boldsymbol{Y}}-\bar{\boldsymbol{H}}_c\mathcal{X}\overline{\mathbf{K}}\right\|^2}{N_0}\right). \quad (107)\end{aligned}$$

The exp function of (107) can be ignored in order to simplify the detection problem according to

$$\begin{aligned}\left\langle\hat{\bar{q}},\hat{\bar{l}},\hat{c}\right\rangle&=\arg\min_{\langle\bar{q},\bar{l},c\rangle}\left\|\bar{\boldsymbol{Y}}-\bar{\boldsymbol{H}}_c\mathcal{X}\overline{\mathbf{K}}\right\|^2\\&=\arg\min_{\langle\bar{q},\bar{l},c\rangle}\left\|\bar{\boldsymbol{Y}}-\sum_{q'=1}^{KQ}a_{q'}^{(k)}\left\{\bar{\boldsymbol{H}}_c\mathcal{X}\right\}_{q'}\right\|^2, \quad (108)\end{aligned}$$

where $\left\{\bar{\boldsymbol{H}}_c\mathcal{X}\right\}_{q'}$ denotes the q'-th column vector of $\left(\bar{\boldsymbol{H}}_c\mathcal{X}\right)$ and $a_{q'}^{(k)}$ the q'-th coefficient of $\mathbf{K}$ given that $q'=1,\ldots,(KQ)$. The ML search-space in the LMS-GSTSK system relies on $f(Q,P)$, $\mathcal{L}$, K as well as on N_c, where the complexity order achieved is $\mathcal{O}\left(\left(f(Q,P)\cdot\mathcal{L}^P\right)^K\cdot N_c\right)$.

C. SOFT DECISION-AIDED DETECTION

In this section, we extend the aforementioned HD-aided receiver for supporting SD-aided detection. Rather than being an exact logical 1 or an exact logical 0 as in HD-aided detection, soft-bit based detection is characterized with the aid of a Log Likelihood Ratio (LLR) defined by [96] and [97]:

$$\begin{aligned}L(b)&=\log\frac{p(b=1)}{p(b=0)} \quad (109)\\&=\log\frac{p(b=1)}{1-p(b=1)}, \quad (110)\end{aligned}$$

where a positive or a negative sign of $L(b)$ indicates, whether the bit b is a logical 1 or a logical 0, respectively, while its magnitude $|L(b)|$ determines the confidence level of either decisions. The corresponding probabilities of having a logical 1 bit $p(b=1)$ and a logical 0 bit $p(b=0)$ in terms of the LLR $L(b)$ can be determined based on Equations (109) and (110) as:

$$p(b=1)=\frac{e^{L(b)}}{1+e^{L(b)}}, \quad (111)$$

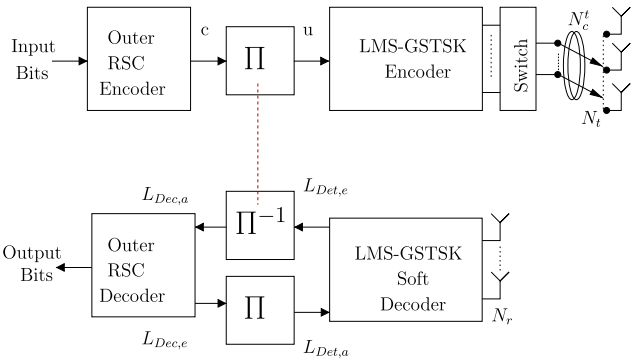

FIGURE 20. The transceiver block diagram of the SD-aided LMS-GSTSK system, which is extended from the LMS schematic of Figure 14.

and

$$p(b=0)=\frac{1}{1+e^{L(b)}}, \quad (112)$$

respectively. The *a priori* probabilities $\left\{p\left(\overline{\mathbf{K}}\right)\right\}_{\forall\bar{q},\bar{l},c}$ that were considered equiprobable in HD-aided detection are no longer equiprobable here and they may be obtained from the channel decoder as

$$p\left(\overline{\mathbf{K}}\right)=\prod_{i=1}^{B}\frac{e^{\widetilde{b}_i L_a(b_i)}}{1+e^{L_a(b_i)}}, \quad (113)$$

where $\left\{\widetilde{b}_i\right\}_{i=1}^{B}$ represents the bit sequence of a specific LMS symbol $\overline{\mathbf{K}}\in\mathcal{K}$ and $\{L_a(b_i)\}_{i=1}^{B}$ denotes the *a priori* LLRs at the channel decoder's output, given that $i=1,\ldots,B$.

The block diagram of the SD-aided LMS system is depicted in Figure 20. At the transmitter, the input bits are fed into the Recursive Systematic Convolutional (RSC)[14] encoder of Figure 20 that produces the coded bits sequence c. The RSC decoder invokes the BCJR algorithm in order to convert the multiplication operations to additions by relying on the logarithmic operations. The coded bits are then scrambled with the aid of the interleaver $\prod$ of Figure 20, in order to disperse the error bursts imposed by deep channel fades over a longer period of time. Afterwards, the interleaved sequence u is fed into the LMS-GSTSK encoder, which is detailed in Section III-A and based on the schematic of Figure 14, in order to transmit the coded agglomerate over the specified AC.

After receiving the coded agglomerate, the inner LMS Soft-Input Soft-Output (SI-SO) decoder iteratively exchanges its soft extrinsic information with the outer RSC decoder, as shown in Figure 20. To expound a little further, the LMS decoder of Figure 20 decodes the received signal in order to produce the extrinsic LLR $L_{Det,e}$ by relying on the *a priori* LLRs $L_{Dec,e}$ of (113) gleaned from the channel decoder. By considering the received signal $\bar{\boldsymbol{Y}}$ of (102), which

[14]RSC codes belong to the class of convolutional codes, which are commonly used in iterative and concatenated coding designs, such as in Turbo codes [39].

carries B coded bits $\mathbf{b} = [b_1, b_2, \ldots, b_B]$, the extrinsic LLR of $b_i \in \mathbf{b}$ can be defined as [39]

$$L_{Det,e}(b_i) = \log\left(\frac{\sum_{\overline{\mathbf{K}}\in\mathbf{K}_1^{b_i}} \exp\left(\lambda_{\overline{q},\overline{l},c}\right)}{\sum_{\overline{\mathbf{K}}\in\mathbf{K}_0^{b_i}} \exp\left(\lambda_{\overline{q},\overline{l},c}\right)}\right), \tag{114}$$

where $\mathbf{K}_1^{b_i}$ and $\mathbf{K}_0^{b_i}$ denote the LMS-GSTSK agglomerate sets satisfying the conditions of $\mathbf{K}_1^{b_i} \doteq \left\{\overline{\mathbf{K}} \in \mathbf{K} : b_i = 1\right\}$ and $\mathbf{K}_0^{b_i} \doteq \left\{\overline{\mathbf{K}} \in \mathbf{K} : b_i = 0\right\}$, respectively, while $\lambda_{\overline{q},\overline{l},c}$ denotes the intrinsic soft metric that may be expressed as

$$\lambda_{\overline{q},\overline{l},c} = -\frac{\left\|\bar{\mathbf{Y}} - \sum_{q'=1}^{KQ} a_{q'}^{(k)} \left\{\bar{\boldsymbol{H}}_c \mathcal{X}\right\}_{q'}\right\|^2}{N_0} + \sum_{j\neq i} b_j L_{Det,a}(b_j). \tag{115}$$

The extrinsic LLRs at the LMS decoder's output are fed into the RSC decoder after being deinterleaved with the aid of $\prod^{-1}$ that reinstates the original bit order of the *a priori* LLR $L_{Dec,a}$, as depicted in Figure 20. The RSC decoder applies the Log-MAP algorithm, which relies on addition operations instead of multiplication operations by switching to the logarithmic domain, in order to produce the extrinsic LLR $L_{Dec,e}$. Then, the extrinsic LLRs output $L_{Dec,e}$ of the RSC decoder are interleaved again and fed as *a priori* LLRs into the LMS decoder as $L_{Det,a}$, which are invoked for producing improved extrinsic LLR values $L_{Det,e}$ for the next iteration. The LMS decoder employed in Figure 20 uses two SD algorithms, namely the Approximate Log-MAP (Approx-Log-MAP) algorithm of [96] and [98], and the Maximum Log-MAP (Max-Log-MAP) algorithm of [39], where the extrinsic LLRs are obtained based on

$$L_{Det,e}(b_k) = \underset{\mathbf{K}_{q,l,c}\in\mathbf{K}_1^k}{\text{jac}}\left(\lambda_{q,l,c}\right) - \underset{\mathbf{K}_{q,l,c}\in\mathbf{K}_0^k}{\text{jac}}\left(\lambda_{q,l,c}\right), \tag{116}$$

and

$$L_{Det,e}(b_k) = \max_{\mathbf{K}_{q,l,c}\in\mathbf{K}_1^k}\left(\lambda_{q,l,c}\right) - \max_{\mathbf{K}_{q,l,c}\in\mathbf{K}_0^k}\left(\lambda_{q,l,c}\right), \tag{117}$$

for Approx-Log-MAP and Max-Log-MAP algorithms, respectively, given that jac represents the Jacobian maximum operation[15] [99], while max represents the ordinary maximum operation [100]. In the following section, we device the Discrete-input Continuous-output Memoryless Channel (DCMC) capacity formula of the LMS-GSTSK system of Figure 14.

V. LMS SYSTEM CAPACITY

In this section, we formulate the DCMC capacity [101] of our LMS-GSTSK system, which can be considered as a generalized DCMC framework for all of its subsidiary systems of Section III-D.

[15]The Jacobian maximum utilizes an additional parameter using a look-up table with the maximum operation.

The DCMC capacity of our LMS-GSTSK system using $\mathcal{L}$-PSK/QAM signaling can be formulated as

$$C = \frac{1}{T}\max_{\left\{p\left(\overline{\mathbf{K}}\right)\right\}_{\forall\overline{q},\overline{l},c}} \sum \int_{-\infty}^{+\infty}\cdots\int_{-\infty}^{+\infty} p\left(\bar{\mathbf{Y}}\middle|\overline{\mathbf{K}}\right) p\left(\overline{\mathbf{K}}\right) \cdot\left[\frac{p\left(\bar{\mathbf{Y}}\middle|\overline{\mathbf{K}}\right)}{\sum_{\forall\mathbf{K}\in\mathcal{K}} p\left(\bar{\mathbf{Y}}\middle|\overline{\mathbf{K}}'\right) p\left(\overline{\mathbf{K}}'\right)}\right] d\bar{\mathbf{Y}}, \tag{118}$$

which is maximized when the transmitted $\mathcal{L}$-PSK/QAM symbols $p\left(\overline{\mathbf{K}}\right)$ are equiprobable.

Now, based on the conditional probability given by (106), the DCMC capacity can be further simplified as

$$C = \frac{1}{T}\left(B - \frac{1}{\left(2^B\right)} \times \sum_{\overline{q},\overline{l},c} E\left[\log_2\left\{\sum_{\overline{q}',\overline{l}'}\exp\left(\overline{\psi}\right)\middle|\overline{\mathbf{K}}\right\}\right]\right), \tag{119}$$

where the intrinsic metric of the exponent $\overline{\psi}$ denoting the difference between two symbols may be expressed as

$$\overline{\psi} = -\left\|\bar{\boldsymbol{H}}_c\mathcal{X}\left(\overline{\mathbf{K}} - \overline{\mathbf{K}}'\right) + \bar{\boldsymbol{V}}\right\|^2 + \left\|\bar{\boldsymbol{V}}\right\|^2, \tag{120}$$

with $\overline{\mathbf{K}}'$ denoting the transmitted symbol vector $\mathbf{K}_{\overline{q}',\overline{l}'}$.[16]

To characterize the DCMC limits of our system, we present multiple DCMC plots of the proposed LMS system associated with various configurations. More specifically, the DCMC capacity of multiple configurations of LMS systems having throughputs of 2, 2.5, 3, 3.5, 4, 4.5 and 5 bpcu associated with the DAC, Semi-DAC and SAC techniques are shown in Figure 21, Figure 22 and Figure 23, respectively. The figures show that as the SNR increases, the capacity curve of each system converges to its maximum attainable throughput R given in Equation (69). More specifically, it is shown in Figure 21 that the same capacity can be achieved by employing different LMS configurations, such as the 4 bpcu LMS-GSTSK(64:4, 16, 2, 2, 2, 2, 1:2, BPSK) and LMS-GSTSK(4:4, 1, 2, 2, 2, 2, 1:4, 4QAM) systems. Furthermore, it is shown in the three figures that the DCMC capacity increases as the three main parameters of the LMS system increase, namely the ratio of N_c^t RF chains to AEs N_t, the number of layers K, the STSK's Q and $\mathcal{L}$ coefficient and the number P of selected dispersion matrices.

Furthermore, in Figure 24 we compared the DCMC capacities of LMS systems associated with DAC to that with Semi-DAC and SAC techniques. It is shown in this figure that the DCMC capacity of the DAC is slightly higher than that of both Semi-DAC and SAC, respectively, which is due to the correlation imposed both by the Inter-AGglomerate Correlation (I-AgC) and by the Inter-COdeword Correlation

[16]$\mathbf{K}_{\overline{q}',\overline{l}'}$ is a symbol vector based on Equation (93) but with the $\overline{q}'$ and $\overline{l}'$ indices.

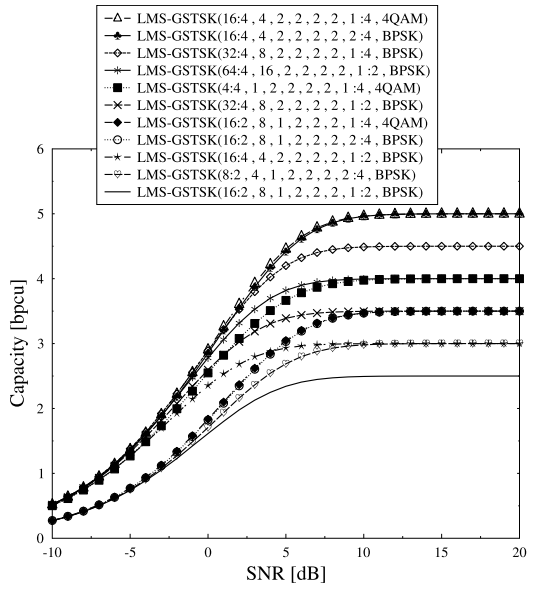

FIGURE 21. The DCMC capacity of LMS systems associated with the DAC technique.

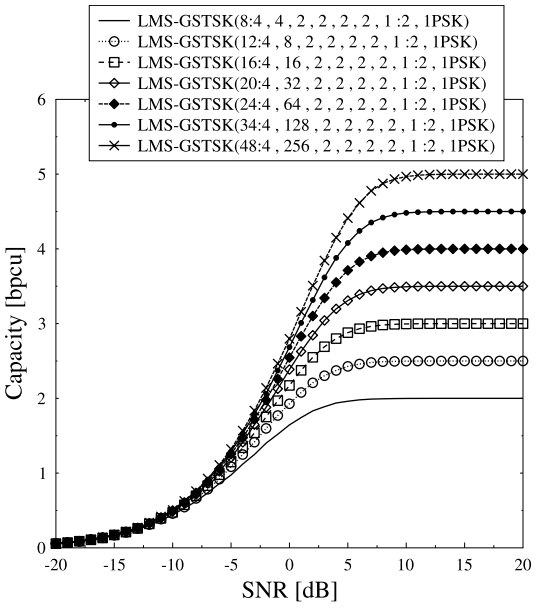

FIGURE 22. The DCMC capacity of LMS systems associated with the Semi-DAC technique.

(I-CoC) discussed in Section VI-A. This in fact suggests that all systems are capable of achieving an infinitesimally low BER at near-capacity SNR levels, especially when appropriate precoding techniques are used for SAC and Semi-DAC.

To elaborate further on the effect of the number of layers in the LMS system, a comparison of the DCMC capacities of four 4-bpcu LMS systems having the same throughput and associated with the DAC technique having $K = 1, 2, 3$ and 4 layers is shown in Figure 25, where the LMS systems share the same GSTSK codeword. These are the LMS-GSTSK(8:8, 1, 4, 2, 2, 2, 1:2, BPSK), LMS-GSTSK(32:6, 4, 3, 2, 2, 2, 1:2, BPSK), LMS-GSTSK(64:4, 16, 2, 2, 2, 2, 1:2, BPSK) and LMS-GSTSK(128:2, 64, 1, 2, 2, 2, 1:2, BPSK) systems. Observe that the capacity tends to increase as the number of layers increases, although the capacity curves converge to the same level. This capacity enhancement is an explicit benefit of the increased number of RF chains required by the additional layers, which comes however at the cost of an increased computational complexity required for mitigating the effect of the $(K-1)$ ICI[17] contribution detailed in Section IV-B. In the following section, we provide the BER performance results for our LMS-GSTSK system, where the simulations were based on the Monte-Carlo approach.

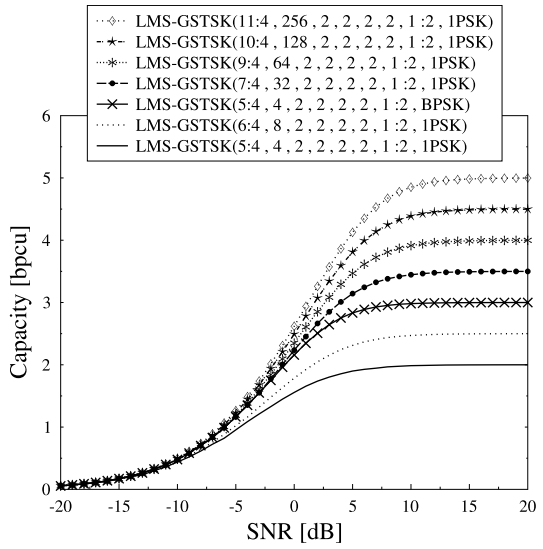

FIGURE 23. The DCMC capacity of LMS systems associated with the SAC technique.

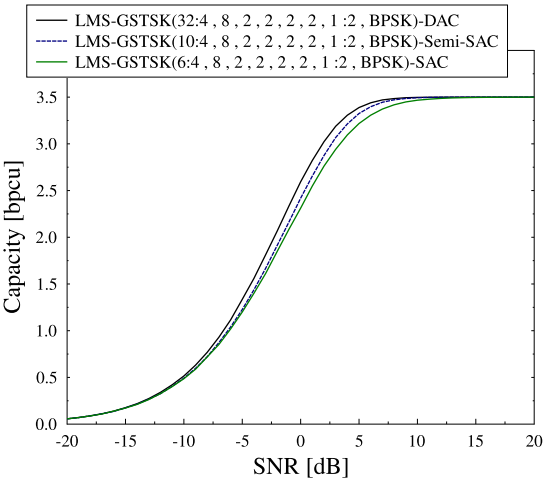

FIGURE 24. A comparison of the DCMC capacities of 3.5 bpcu equivalent-throughput LMS systems associated with the DAC, Semi-DAC and SAC techniques.

[17] The LMS system typically endures $(KP-1)$ ICI contributions, however all the LMS systems utilized in Figure 25 select a single dispersion matrix, yielding $P = 1$.

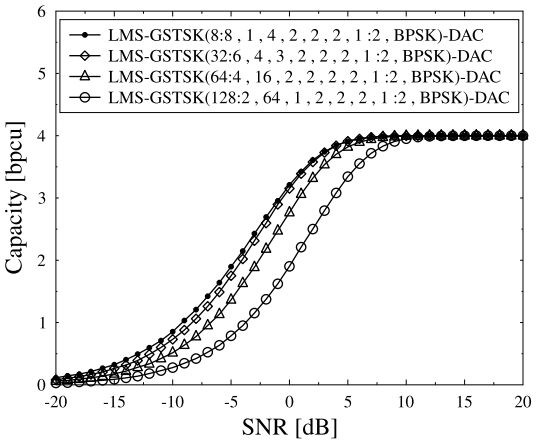

FIGURE 25. The DCMC capacity of four equivalent-throughput LMS systems of 4 bpcu associated with the DAC technique having $K = 1, 2, 3$ and 4 layers and sharing the same GSTSK codeword, namely the LMS-GSTSK(8:8, 1, 4, 2, 2, 2, 1:2, BPSK), LMS-GSTSK(32:6, 4, 3, 2, 2, 2, 1:2, BPSK), LMS-GSTSK(64:4, 16, 2, 2, 2, 2, 1:2, BPSK) and LMS-GSTSK(128:2, 64, 1, 2, 2, 2, 1:2, BPSK) systems.

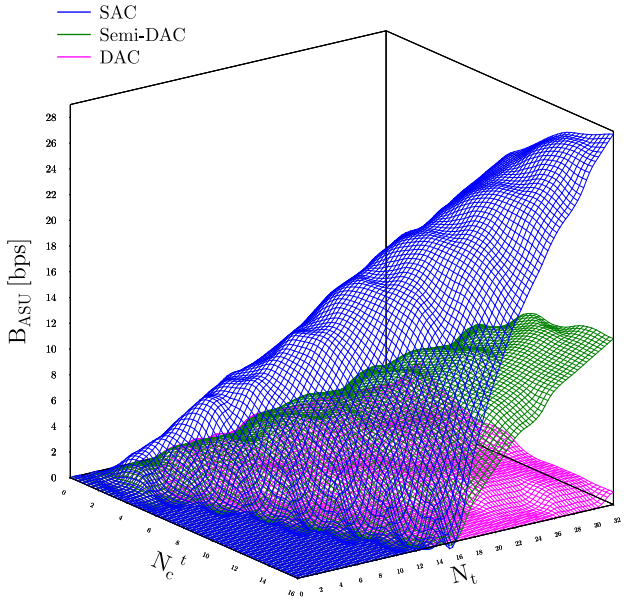

FIGURE 26. Number of B_{ASU} bits implicitly transmitted over the activated transmit antenna elements.

VI. PERFORMANCE RESULTS AND DISCUSSIONS

Again, we provide simulation results based on the Monte-Carlo approach. We commence by analyzing the AC allocation techniques presented in Section III-B and studying their performances, followed by presenting the BER performances of both the HD-aided and of the SD-aided detectors presented in Sections IV-B and IV-C, respectively.

A. ANTENNA ALLOCATION TECHNIQUES

DAC vs SAC vs SEMI-DAC

In this section, we expound further on both the achievable throughput and on the BER performance of our LMS scheme associated with the three AC allocation techniques presented in Section III-B, namely the SAC, DAC and Semi-DAC techniques.

The LMS agglomerate is formed by a linear combination of multi-layered codewords that are transmitted over the activated AC out of the available N_c ACs. The total number of ACs, which contributes $\log_2(N_c)$ bits to B in (68), is mainly determined by the number of available RF chains and by the choice of the AC allocation technique employed. At a fixed number of RF chains, the value of AC only relies on the choice of the AC allocation technique based on Equations (58), (62) and (64) for DAC, SAC and Semi-DAC techniques, respectively. For instance, we depict in Figure 26 the number of bits transmitted over the AC indices with the aid of the ASU of Figure 14. We may observe in Figure 26 that the number B_{ASU} of implicitly conveyed bits of the activated AC of the LMS system associated with SAC exceeds that with Semi-DAC and DAC, where the Semi-DAC curve is between both curves. This is by the virtue of having N_c^t-combinations of N_t AEs in SAC, N_c^t-combinations of $\left(N_t/N_c^t\right)$ denoting the distinct multiples of N_c^t-AEs in Semi-DAC and N_c^t-distinct-combinations of N_t in DAC.

To elaborate further, let us assume that we project the surfaces shown in Figure 26 onto the $(N_t,\ B_{ASU})$ plane, as shown in Figure 27(a), Figure 27(b) and Figure 27(c) representing the pink (DAC), green (Semi-DAC) and blue (SAC) curves of Figure 26, respectively. For example, based on the subfigures of Figure 27, and considering the case of $N_t = 16$ AEs as well as $N_c^t = 4$ RF chains, the value of B_{ASU} for DAC is 2 bits, for Semi-DAC is 4 bits, while for SAC is 10 bits.

This improved throughput of the SAC technique, attained by sharing the N_t AEs over the legitimate 2^ι ACs comes however at the cost of a degraded BER performance. In Figure 28, we show a comparison of equivalent-throughput LMS systems associated with the three AC allocation techniques. More specifically, the BER performances of the LMS-GSTSK(32 : 4, 8, 2, 2, 2, 2, 1:2, BPSK), LMS-GSTSK(10 : 4, 8, 2, 2, 2, 2, 1:2, BPSK) and LMS-GSTSK(6 : 4, 8, 2, 2, 2, 2, 1:2, BPSK) systems of Figure 14 associated with the DAC, Semi-DAC and SAC techniques are shown. Quantitatively, each of them achieves a throughput of 3.5 bpcu.

All systems are associated with $N_c^t = 4$ RF chains and $K = 2$ layers of GSTSK(2, 2, 2, 1:2, BPSK) encoders, where each layer carries $B_{GSTSK} = 2$ bits over $T = 2$ time slots and $B_{L-GSTSK} = 4$ bits over all layers. In order to achieve an overall throughput of 3.5 bpcu, the LMS system associated with the DAC technique requires $N_t = 32$ AEs for implicitly conveying $B_{ASU} = 3$ bits over the activated AC index. In total, the number of bits conveyed over the LMS agglomerate is $B = 4 + 3 = 7$ bits and the throughput of the system is $R = 3.5$ bpcu. Now, to achieve the same throughput as the DAC system, the semi-DAC system requires $N_t = 10$ AEs, while the SAC system needs only $N_t = 6$ AEs.

We can observe in Figure 28 that the DAC system outperforms both the Semi-DAC and the SAC systems, while the SAC exhibits the worst performance. The Semi-DAC system shows an approximately 1dB performance erosion compared to the DAC system at a BER of 10^{-5}, while the

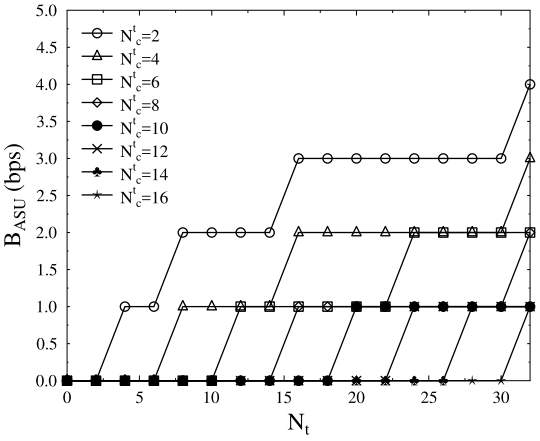

(a)

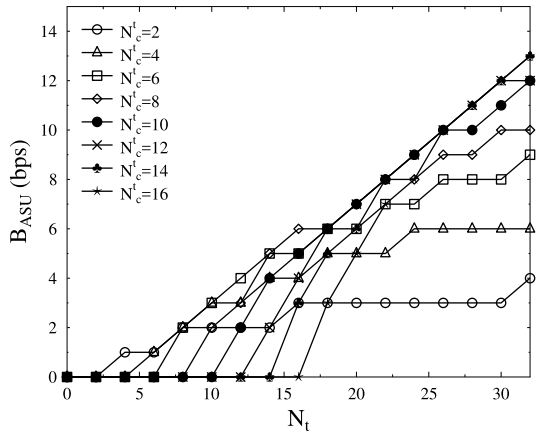

(b)

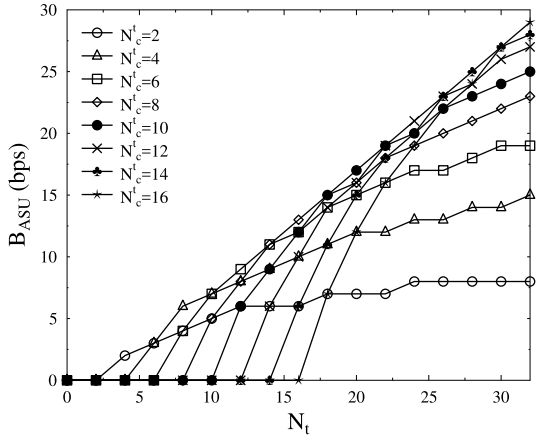

(c)

FIGURE 27. Projection of Figure 26 on to the $(N_t B_{ASU})$-plane showing the B_{ASU} value of the LMS system associated with the (a) DAC (b) Semi-DAC and (c) SAC techniques.

SAC scheme's performance is degraded by ∼9 dB and ∼8 dB at a BER of 10^{-5} compared to the DAC and Semi-DAC systems, respectively.

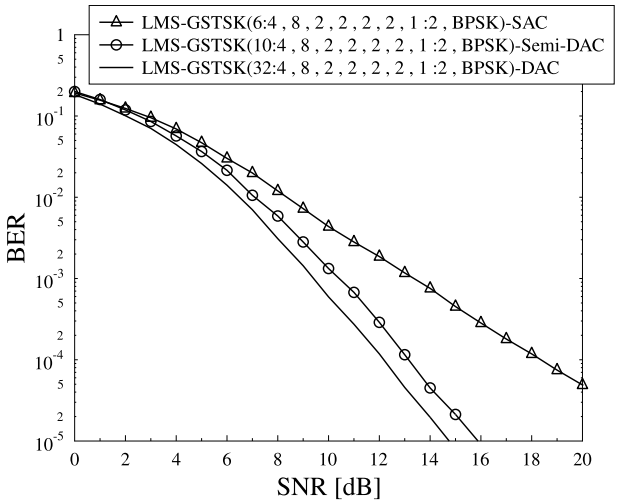

FIGURE 28. A BER performance comparison of equivalent-throughput LMS systems of 3.5 bpcu, namely the LMS-GSTSK(32 : 4, 8, 2, 2, 2, 2, 1:2, BPSK), LMS-GSTSK(10 : 4, 8, 2, 2, 2, 2, 1:2, BPSK) and LMS-GSTSK(6 : 4, 8, 2, 2, 2, 2, 1:2, BPSK) systems associated with the DAC, Semi-DAC and SAC techniques.

This performance degradation of the SAC allocation schemes is due to the increased levels of two types of correlations, namely of the I-AgC and of the I-CoC correlations. More specifically, the I-AgC is imposed by repeatedly activating similar AEs for transmitting different agglomerates, while the I-CoC is constituted by activating the same AEs in different layers within an agglomerate and over different agglomerates. In fact, the existence of the I-CoC amongst transmitted agglomerates may be expected to degrade the achievable diversity order of the LMS system associated with the SAC technique. A good agreement is observed between what has been mentioned here and the slope of the SAC curve in Figure 28, which defines the diversity gain of the system. Explicitly, observe that the steepness of the SAC curve is lower than that of the DAC and Semi-DAC curves.

On the other hand, the Semi-DAC technique explicitly demonstrates the relationship between the BER performance and the diversity gain attained in Figure 28. As for the Semi-DAC, only groups of M AEs are shared amongst the $N_c^t = (K \cdot M)$-sized N_c ACs, which guarantees that each layer's codeword of each agglomerate is always transmitted over a distinct group of M AEs, as opposed to SAC that allows sharing all AEs over all layers. Hence, Semi-DAC is an I-CoC-free technique and the Semi-DAC curve of Figure 28 is parallel to that of DAC's and its diversity order is equal to $\mathcal{D}$ of Equation (70). However, due to the fact that M-groups of AEs are shared over different agglomerates, the BER performance degradation of the Semi-DAC technique is inflicted by the I-AgC.

In the spirit of the above-mentioned throughput and BER performance comparisons of the DAC, Semi-DAC and SAC techniques, we summarize the AC allocation trade-offs in Figure 29. To expound a little further, the SAC technique attained the highest throughput, followed by the Semi-DAC

TABLE 4. The DAC, Semi-DAC and SAC trade-offs.

Allocation Technique	DAC	$\leq, \geq, =$	Semi-DAC	$\leq, \geq, =$	SAC
Throughput	N_t/N_c^t	$\leq$	$\left\lfloor \binom{N_t/M}{N_c^t/M} \right\rfloor_{2^\iota}$	$\leq$	$\left\lfloor \binom{N_t}{N_c^t} \right\rfloor_{2^\iota}$
Diversity	$\mathcal{D}$	$=$	$\mathcal{D}$	$\geq$	$\{\leq \mathcal{D}\}$
			I-CoC/I-AgC		
Performance	Best	$\geq$	intermediate	$\geq$	acute/imperfect/inexact

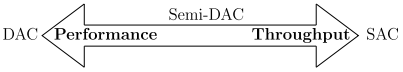

FIGURE 29. Antenna allocation techniques trade-offs.

and then the DAC techniques, given the same number of RF chains and AEs. Furthermore, observe in Figure 28 that more AEs are required for the Semi-DAC and DAC techniques to achieve a specific throughput than by the SAC technique. However, the LMS system associated with the DAC technique achieved a better BER performance than the Semi-DAC and SAC techniques. The Semi-DAC technique showed a slight performance degradation in Figure 28 compared to the DAC performance. The SAC technique endured a more grave performance degradation. Our comparison between the three techniques and their trade-offs is summarized in Table 4.

Its should be noted that to mitigate the effect of I-CoC when employing SAC, transmit precoding can be applied to the GSTSK/STSK codewords before their transmission. For example, we employ a simple precoding technique at the transmitter of Figure 14 by imposing a phase-shift on the codewords prior to transmission following the concept proposed in [8], [9], [23], [24], and [85]. To elaborate further on the precoding technique employed, a phase-shift θ_c is imposed on each of the codewords $\boldsymbol{S}_k$ of (121) formulated as

$$\boldsymbol{S}_k = \sum_{p=1}^{P} \boldsymbol{A}^{(k)}(p)\, x^{(k)}(p)\, e^{j\theta_c}, \tag{121}$$

given that the difference between two concurrent combinations of the same codeword[18] is defined by $\bigtriangleup\theta_c = \theta_{c+1} - \theta_c$, and hence the phase-shift is given as [85]

$$\theta_c = \bigtriangleup\theta_c \cdot \left(-\frac{N_c}{2} + c - 1\right). \tag{122}$$

To examine the beneficial effect of the phase-shift precoding, we portray the BER performance of an LMS system associated with SAC in Figure 30, namely that of the LMS-GSTSK(6 : 4, 8, 2, 2, 2, 2, 1:2, BPSK) system of Figure 14 as shown in Figure 28, when imposing phase-shifts of $\bigtriangleup\theta_c = \pi/36, \pi/18, \pi/14, \pi/12, \pi/2, \pi$, and $5\pi/4$ as well as a randomly-generated phase-shift (Rand) compared both to the LMS-GSTSK(32 : 4, 8, 2, 2, 2, 2, 1:2, BPSK) system associated with DAC and to the LMS-GSTSK(10 : 4, 8, 2, 2, 2, 2, 1:2, BPSK) arrangement associated with Semi-DAC of Figure 28. We note here that the randomly-generated phase-shift was utilized by generating a random phase-shift within 0 and 2π in each run of our Monte-Carlo simulation. It is shown in Figure 30 that the SAC arrangement's performance has been enhanced by ∼7.5 dB at a BER of 10^{-5}, when using a phase-shift of $\bigtriangleup\theta_c = 5\pi/4$, but it was degraded, when using $\bigtriangleup\theta_c = \pi$. Furthermore, the SAC arrangement relying on $\bigtriangleup\theta_c = 5\pi/4$ now shows in Figure 30 a slight performance degradation compared to the Semi-DAC and DAC system at nearly ∼1 dB and ∼2 dB, respectively, at a BER of 10^{-5}. Nonetheless, the performance of the SAC system can be further enhanced by considering more sophisticated precoding techniques [63], [65].

[18] In LMS, the same GSTSK/STSK codeword is transmitted on more than one AC to implicitly convey the index of the activated AC. Hence, each codeword is multiplied by the corresponding c-th phase-shift of the activated AC.

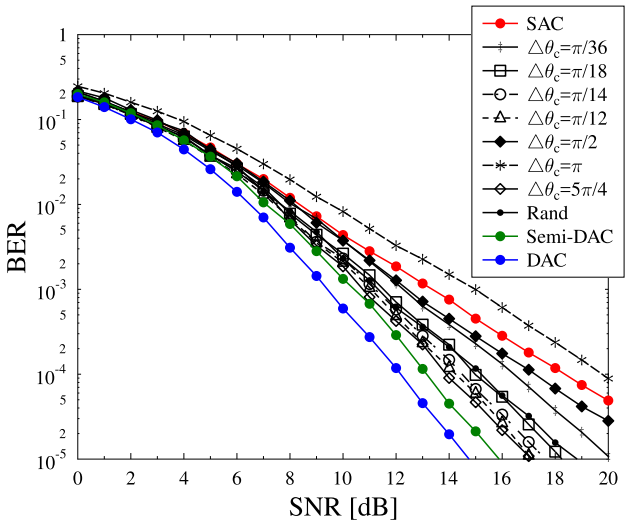

FIGURE 30. The BER performance of the LMS-GSTSK(6 : 4, 8, 2, 2, 2, 2, 1:2, BPSK) system of Figure 28 associated with SAC and a phase-shift $\bigtriangleup\theta_c$ of $\pi/36, \pi/18, \pi/14, \pi/12, \pi/2, \pi$, and $5\pi/4$ as well as a randomly-generated phase-shift compared to the LMS-GSTSK(32 : 4, 8, 2, 2, 2, 2, 1:2, BPSK) system and the LMS-GSTSK(10 : 4, 8, 2, 2, 2, 2, 1:2, BPSK) system associate with the DAC and Semi-DAC arrangements, respectively, of Figure 28.

B. BER PERFORMANCE OF HD-AIDED LMS SYSTEM

In this section, we characterize the BER performance of our LMS-GSTSK system by conducting Monte-Carlo simulations. The GSTSK dispersion matrices are generated based

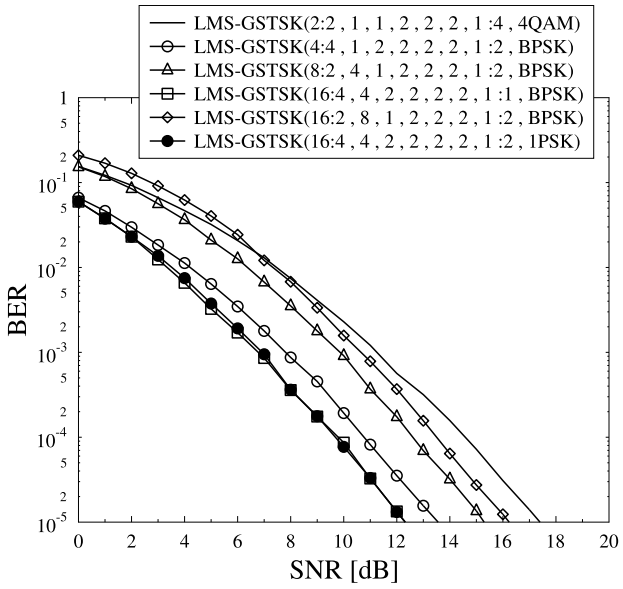

FIGURE 31. The BER performance of various LMS-GSTSK systems achieving a throughput of $R = 2$ bpcu. The results are based on the schematic of Figure 14.

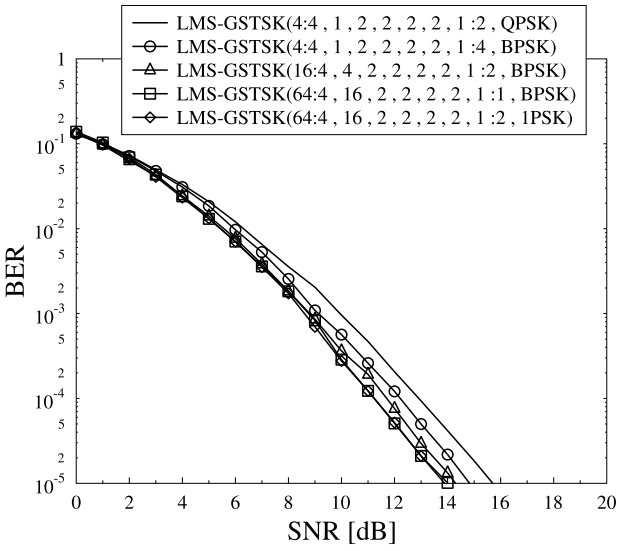

FIGURE 32. The BER performance of various LMS-GSTSK systems achieving a throughput of $R = 3$ bpcu. The results are based on the schematic of Figure 14.

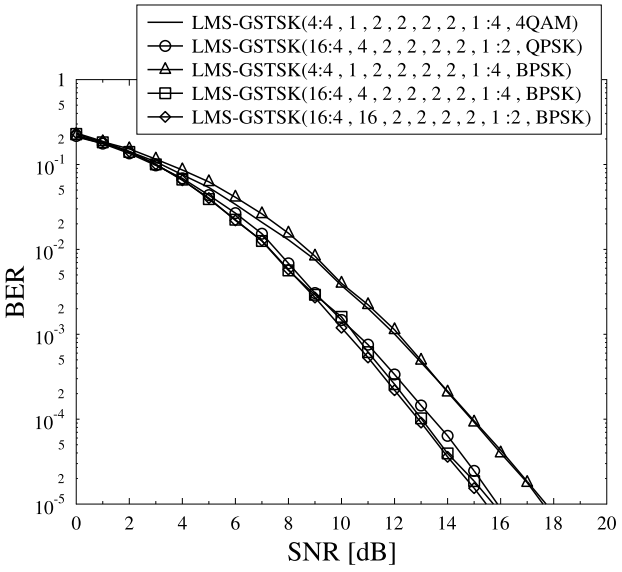

FIGURE 33. The BER performance of various LMS-GSTSK systems achieving a throughput of $R = 4$ bpcu. The results are based on the schematic of Figure 14.

on the random-search approach of [78] under the power constraint formulated in Equation (26). More specifically, the best out of 10^6 dispersion matrices were selected for dispersing P PSK/QAM symbols in each encoder.

Let us now consider the LMS-GSTSK(N_t:N_c^t, N_c, K, M, N_r, T, P:Q, $\mathcal{L}$-PSK/QAM) system of Figure 14 having a throughput of $R = 2$ bpcu, which can be achieved using various system parameters arrangements. For instance, the LMS-GSTSK(2:2, 1, 1, 2, 2, 2, 1 :4, 4QAM), LMS-GSTSK(4:4, 1, 2, 2, 2, 2, 1 :2, BPSK), LMS-GSTSK(8:2, 4, 1, 2, 2, 2, 1 :2, BPSK), LMS-GSTSK(16:4, 4, 2, 2, 2, 2, 1 :1, BPSK), LMS-GSTSK(16:2, 8, 1, 2, 2, 2, 1 :2, BPSK) and LMS-GSTSK(16:4, 4, 2, 2, 2, 2, 1 :2, 1PSK)[19] systems associated with DAC are all capable of achieving 2 bpcu. The BER performance of those equivalent-throughput systems is depicted in Figure 31. As shown in the figure, the BER performance of the LMS system varies based on the parameters used, at the same throughput of 2 bpcu. Furthermore, the LMS systems of Figure 31 that are associated with $K > 1$ layers are capable of outperforming single-layered systems, as a benefit of their enhanced degrees of freedom attained by the increased number of RF chains. Similarly, we present the BER performance of various LMS systems achieving a throughput of 3 bpcu and 4 bpcu in Figure 32 and Figure 33, respectively. It is shown in both figures that the BER performance can be enhanced by increasing the implicit information conveyed by the AC index in favor of other system's parameters, given that the same number of RF chains is employed.

To expound a little further on the performance of the LMS system compared to other conventional MIMO schemes, consider a MIMO system that is capable of achieving 4 bpcu. Based on the special cases of LMS presented in Section III-D, we appropriately tune our LMS-GSTSK(N_t:N_c^t, N_c, K, M, N_r, T, P:Q, $\mathcal{L}$-PSK/QAM) to mimic the following arrangements.

- A V-BLAST system with the aid of the LMS-GSTSK(4:4, 1, 1, 4, 4, 1, 4:4, BPSK) arrangement, which is equivalent to an ($N_t = 4 \times N_r = 4$) BLAST MIMO system, where each transmit AE conveys a BPSK symbol;
- A GSM system by relying on the LMS-GSTSK(4:2, 4, 1, 4, 4, 1, 2 :4, BPSK) arrangement. This system is

[19]The 1PSK modulation denotes an information-free single-symbol constellation.

equivalent to a ($N_t = 4 \times N_r = 4$) GSM system associated with $N_c^t = 2$ RF chains;
- An SM system depending on the LMS-GSTSK(4:1, 4, 1, 4, 4, 1, 1 :4, QPSK) arrangement, which is equivalent to an ($N_t = 4 \times N_r = 4$) SM system incorporated with a single RF chain;
- An SSK system by relying on the LMS-GSTSK(16:1, 16, 1, 16, 4, 1, 1 :16, QPSK) arrangement, which is comparable to an ($N_t = 16 \times N_r = 4$) SSK system associated with a single RF chain;
- An LSSTC system with the aid of the LMS-GSTSK(4:4, 1, 1, 4, 4, 2, 4 :4, QPSK) arrangement, where a special type of dispersion matrices is used as detailed in Section III-D. This system is equivalent to a 2-layered ($N_t = 4 \times N_r = 4$) LSSTC system, where each layer is associated with an G_2 OSTBC encoder and a QPSK modulator;
- A GSTSK system depending on the LMS-GSTSK(4:4, 1, 1, 4, 4, 2, 3 :4, 4QAM) arrangement;
- An STSK system using the LMS-GSTSK(4:4, 1, 1, 4, 4, 2, 1 :16, 16QAM) arrangement;
- An LDC system employing the LMS-GSTSK(4:4, 1, 1, 4, 4, 2, 4 :4, 4QAM) arrangement;
- An MS-STSK system using the LMS-GSTSK(64:4, 16, 1, 4, 4, 2, 1 :4, 4QAM) arrangement;

The BER performance of these systems is presented in Figure 34 in comparison to four equivalent-throughput LMS systems that do not belong to any of the special cases of Section III-D. More specifically, the following LMS configurations that are all associated with the DAC technique are considered:

- LMS1: LMS-GSTSK(32:4, 8, 2, 2, 4, 2, 3 :4, BPSK);
- LMS2: LMS-GSTSK(4:4, 1, 2, 2, 4, 2, 2 :4, BPSK);
- LMS3: LMS-GSTSK(16:4, 4, 2, 2, 4, 2, 1 :4, BPSK);
- LMS4: LMS-GSTSK(64:4, 16, 2, 2, 4, 2, 1 :2, BPSK);

Observe in Figure 34 that the LMS systems relying on the above-mentioned four arrangements are capable of outperforming all of the conventional MIMO schemes presented. Our LMS systems achieved a higher BER performance, than the other conventional MIMO schemes for different reasons. For instance, the V-BLAST has a diversity order of $(4 - 4 + 1) = 1$, which is the lowest amongst all other employed schemes. By contrast, the single-RF chain SM and SSK systems used in the comparisons of Figure 34 achieve a diversity order of 4. On the other hand, the LMS systems employed achieve a diversity order of $\mathcal{D} = 4 \times \min(M = 2, T = 2) = 8$ based on Equation (70), which is equivalent to that of the STSK, GSTSK, LDC and LSSTC systems utilized in the comparisons of Figure 34. The LMS systems of Figure 34 outperformed the V-BLAST due to their capability of spreading the information over both space and time, which improved both its attainable diversity order and its BER performance. Moreover, the LMS systems used outperformed the single-RF chain systems as a benefit of their higher diversity order and grade of freedom granted by

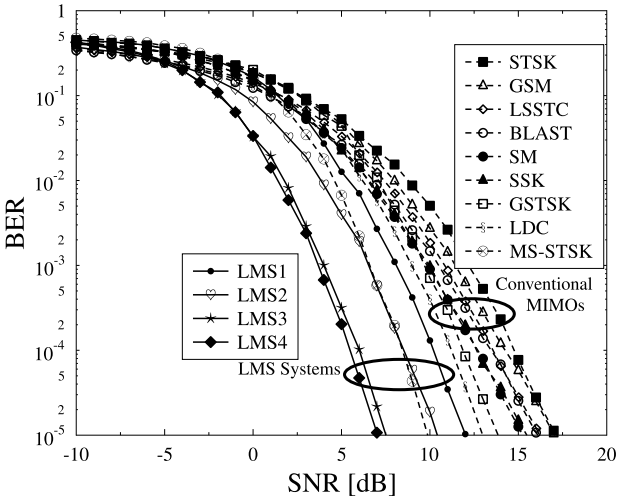

FIGURE 34. BER vs SNR comparison based on the schematic of Figure 14.

the increased number of RF chains. Furthermore, the STSK system of Figure 34 required a high modulation order to attain the desired transmission rate of 4 bpcu, whilst using a comparable number of RF chains to that of the LMS systems. Furthermore, the layered architecture of our LMS system leads to an enhanced BER performance over the other LDC and GSTSK systems. additionally, since randomly-generated dispersion matrices are used for LMS rather than the space-time matrices of STBC, the LMS systems outperformed their LSSTC counterpart. Furthermore, the MS-STSK system employed was capable of outperforming LMS1 and LMS2, since it implicitly transmits 2 out of 4 bpcu over its 64 AEs and relies on 16 ACs indices, while LMS1 and LMS2 transmit only 1.5 and 0 bpcu by relying on 8 and 1 ACs, respectively. However, LMS3 and LMS4 exhibited a better BER performance.

A comparison between all the simulated systems of Figure 34 is explicitly summarized in Table 5, in terms of the complexity order, diversity order, SNR required at BER = 10^{-5} as well as the number of RF chains. The table shows that the diversity order of all system is equivalent to $\mathcal{D} = 8$, except for V-BLAST, SM and SSK, which achieve diversity orders of $\mathcal{D} = 1$, 4 and 4, respectively. Furthermore, Table 5 shows that all systems require an equivalent number of RF $N_c^t = 4$, except that of SM, SSK as well as GSM, which require $N_c^t = 1$, 1 and 2 RF chains, respectively. Additionally, all the multiplexing-based systems, namely the SM, SSK, V-BLAST and GSM arrangements of Table 5 achieves a complexity order of $\mathcal{O}$ (16). On the other hand, the dispersion matrix-based systems achieve a complexity order of $\mathcal{O}$ (256) in return of their improved BER performance, except for LMS1, which achieves a complexity order of $\mathcal{O}$ (8192), albeit obtaining the worst BER performance amongst its LMS2, LMS3 and LMS4 counterparts, while still outperforming the conventional systems. Hence, the system configurations of our LMS system should be carefully choosed at the system design level for the sake of maintaining a striking trade-off

TABLE 5. Comparison between all the simulated LMS systems of Figure 34, namely the V-BLAST, SM, SSK, GSM, LDC, STSK, GSTSK, MS-STSK and LSSTC schemes as well as the LMS1, LMS2, LMS3 and LMS3 system, in terms of the complexity order, diversity order, SNR required at BER = 10^{-5} as well as the number of RF chains.

Scheme	Complexity	Diversity	$\text{SNR}_{10^{-5}}$ [dB]	N_c^t
V-BLAST	$\mathcal{O}\left(2^4\right) = \mathcal{O}\left(16\right)$	$(4-4+1)=1$	16.11	4
SM	$\mathcal{O}\left(4\cdot 4\right) = \mathcal{O}\left(16\right)$	$N_r = 4$	15.24	1
SSK	$\mathcal{O}\left(16\right)$	$N_r = 4$	15.48	1
GSM	$\mathcal{O}\left(4\cdot 2^2\right) = \mathcal{O}\left(16\right)$	$(2\cdot 4)=8$	17.07	2
LDC	$\mathcal{O}\left(4^4\right) = \mathcal{O}\left(256\right)$	$4\cdot\min\left(4,\,2\right)=8$	12.98	4
STSK	$\mathcal{O}\left(16\cdot 16\right) = \mathcal{O}\left(256\right)$	$4\cdot\min\left(4,\,2\right)=8$	17.09	4
GSTSK	$\mathcal{O}\left(f\left(4,\,3\right)\cdot 4^3\right) = \mathcal{O}\left(256\right)$	$4\cdot\min\left(4,\,2\right)=8$	13.86	4
MS-STSK	$\mathcal{O}\left(4\cdot 4\cdot 16\right) = \mathcal{O}\left(256\right)$	$4\cdot\min\left(4,\,2\right)=8$	9.875	4
LSSTC	$\mathcal{O}\left(4^2\right) = \mathcal{O}\left(16\right)$	$(2\cdot 4)=8$	16.19	4
LMS1	$\mathcal{O}\left(\left(4\cdot 2^3\right)^2\cdot 8\right) = \mathcal{O}\left(8192\right)$	$4\cdot\min\left(4,\,2\right)=8$	12	4
LMS2	$\mathcal{O}\left(\left(4\cdot 2^2\right)^2\cdot 1\right) = \mathcal{O}\left(256\right)$	$4\cdot\min\left(4,\,2\right)=8$	10.42	4
LMS3	$\mathcal{O}\left(\left(4\cdot 2^1\right)^2\cdot 4\right) = \mathcal{O}\left(256\right)$	$4\cdot\min\left(4,\,2\right)=8$	7.513	4
LMS4	$\mathcal{O}\left(\left(2\cdot 2^1\right)^2\cdot 16\right) = \mathcal{O}\left(256\right)$	$4\cdot\min\left(4,\,2\right)=8$	7.031	4

between the achievable BER performance and the attainable complexity order.

C. BER PERFORMANCE OF SD-AIDED CODED LMS SYSTEMS

Here, we investigate the BER performance of our SD-aided coded LMS system. Consider the SD-aided LMS-GSTSK(64:4, 16, 2, 2, 2, 2, 1:2, BPSK) system of Figure 14 associated with DAC that can attain a throughput of 4-bpcu based on the two-stage serially concatenated schematic of Figure 20. The outer encoder employed relies on a half-rate RSC(2, 1, 3) channel code having a constraint length of $L = 3$ and with a decimal generator polynomial of $(G_1, G_2) = (13, 6)_{10}$.

The BER performance of this system is shown in Figure 35, where the LMS decoder iteratively exchanges its extrinsic information over four iterations with the RSC decoder. The attainable throughput of the system is 2 bpcu. The LMS system achieves an infinitesimally low BER at SNR = 0 dB with the aid of four outer iterations. Furthermore, observe in Figure 35 that upon increasing the number of outer iterations, the BER performance of the LMS system substantially improves. However, the extra enhancement gradually reduces as the number of iterations increases. Explicitly, we observe a 3.5 dB enhancement between 1 and 2 outer iterations, compared to less than 1 dB enhancement between 3 and 4 iterations.

The number of iterations required for the system both to converge and to attain a near-capacity performance, given a specific type of outer decoder can be visually analyzed using the EXIT chart tool, which is detailed in the next section. For a tutorial on EXIt charts you may consult [97].

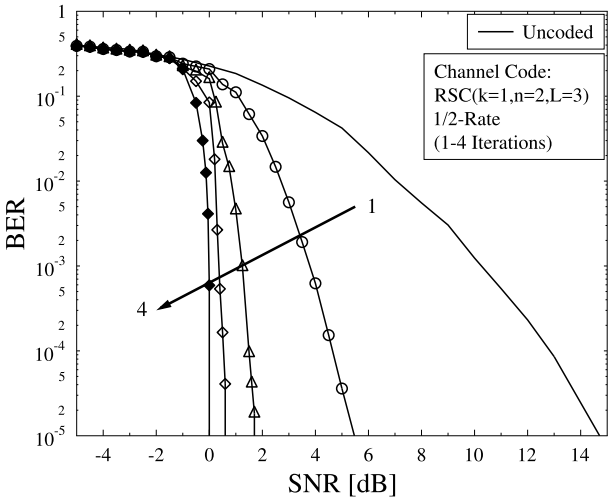

FIGURE 35. The BER performance of an LMS-GSTSK(64:4, 16, 2, 2, 2, 2, 1:2, BPSK) associated with DAC that conveys 4 bpcu. The LMS decoder intrinsically exchanges its extrinsic information over four iterations with a half-rate RSC(2, 1, 3) channel decoder, where the attainable normalized throughput of the system is 2 bpcu. The results are based on the schematic of Figure 20.

VII. EXIT CHARTS ANALYSIS

In this section, we utilize the EXIT chart tool [97] in order to analyze the convergence behavior of our SD-aided LMS decoder of Figure 20, which is presented in Section IV-C. The EXIT chart is a powerful analysis tool that can be conceived both for visually evaluating the extrinsic information iteratively exchanged between the concatenated decoders and for predicting the convergence behavior of an encoded system by relying on the mutual information between the system's decoders [23], [96], [102], rather than instinctively choosing the number of iterations as per Figure 35.

To begin with, the iterative exchange of extrinsic information between the RSC outer decoder and the LMS inner detector portrayed in Figure 20 can be used for describing the EXIT characteristics of each of the systems' components. More specifically, the EXIT characteristics of the RSC decoder of

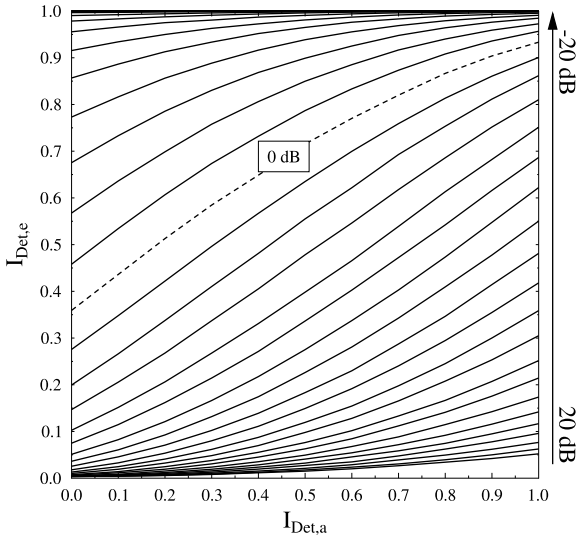

FIGURE 36. LMS-GSTSK(64:4, 16, 2, 2, 2, 2, 1:2, BPSK)-DAC EXIT charts from -20 -> 20 dB. The results are based on the schematic of Figure 20.

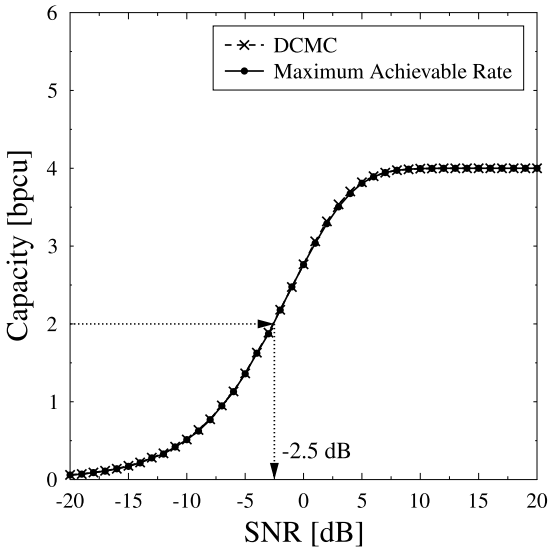

FIGURE 37. LMS-GSTSK(64:4, 16, 2, 2, 2, 2, 1:2, BPSK)-DAC EXIT charts from −20 -> 20 dB. The results are based on the schematic of Figure 20.

Figure 20 indicates the relationship between its input *a priori* LLRs and its output extrinsic LLRs denoted as $L_{Dec,a}$ and $L_{Dec,e}$, respectively. Similarly, the EXIT characteristics of the LMS detector of Figure 20 portray the relationship between its input *a priori* LLRs and its output extrinsic LLRs denoted by $L_{Det,a}$ and $L_{Det,e}$, respectively.

The information exchange between the inner and outer decoders can be characterized using their input mutual information $I_{Det,a}$ and $I_{Dec,a}$, respectively, and their output mutual information $I_{Det,e}$ and $I_{Dec,e}$, respectively. More specifically, $I_{Det,a}$ denotes the mutual information between the interleaved coded bit sequence u and the LLRs input to the LMS decoder $L_{Det,a}$, while $I_{Det,e}$ characterizes the mutual information between the output LLRs of the LMS decoder $L_{Det,e}$ and the interleaved coded bit sequence u. On the other hand, $I_{Dec,a}$ represents the mutual information between the LLRs input to the RSC decoder $L_{Dec,a}$ and the coded bits sequence c, while $I_{Dec,e}$ defines the mutual information between the output LLRs of the RSC decoder $L_{Dec,e}$ and the coded bits sequence c. Note that when the EXIT curves of both the inner and the outer decoders are depicted on the same plot, the representation of $I_{Dec,a}$ and $I_{Dec,e}$ is swapped between the x-axis and y-axis for ease of observation.

Let us consider the LMS-GSTSK(64:4, 16, 2, 2, 2, 2, 1:2, BPSK) system of Figure 14 associated with DAC used in Figure 35, which is configured for transmitting 4 bpcu. The EXIT curves of this system are portrayed in Figure 36, which are recorded at SNR values ranging between −20 dB to 20 dB with a step size of 1 dB, where the 0 dB EXIT curve is shown by the dashed line. These EXIT curves can be used for determining the maximum achievable rate at the i-th SNR value, simply by calculating the area $\mathcal{A}(\text{SNR}_i)$ below SNR_i-th EXIT curve of Figure 36 [97], [103]. Hence, the maximum achievable rate at the SNR_i-th value of our LMS system associated with an R_c-rate outer encoder can be formulated as [97]

$$R_{max}(\text{SNR}_i) = R \times R_c \times \mathcal{A}(\text{SNR}_i). \tag{123}$$

After applying Equation (123) to each of the EXIT charts of Figure 36, we arrive at the maximum achievable limit of the system depicted in Figure 37 compared to the DCMC capacity determined according to Equation (119). Each of the points of the "Maximum Achievable Rate" curve is calculated using Equation (123) incorporated in the corresponding EXIT curve of Figure 36.

In the light of the above, the maximum achievable rate of the LMS-GSTSK(64:4, 16, 2, 2, 2, 2, 1:2, BPSK) system, after employing the half-rate RSC(2, 1, 3) decoder used previously in Figure 35, is displayed at SNR $= -2.5$ dB, where the LMS system achieves its half-rate of 2 bpcu.

Now, the convergence behavior of this LMS system can be characterized using the EXIT chart tool. The EXIT tool can be used to analyze the exchange of the extrinsic information between the inner and outer decoders, in order to determine the closest SNR value to the capacity limit, where a vanishingly low BER can be attained. More specifically, an open-tunnel between the inner and the outer decoder's EXIT curves ensures that an output mutual information of $I_{Dec,e} = 1.0$ is achieved. For instance, observe the open-tunnel seen between the inner decoder curve at SNR= −0.5 dB and the outer decoder's EXIT curves in Figure 38. The system is expected to produce an infinitesimally low BER at SNR= −0.5 dB, which is 2 dB away from the achievable capacity limit. Furthermore, the stair-case-shaped trajectory of Figure 38 characterizes the convergence behavior of the system, which was obtained using a Monte-Carlo simulation with an input interleaver length of 10^6 bits. Observe that the output mutual information of $I_{Dec,e} = 1.0$ is achieved and the system converges after 8 iterations.

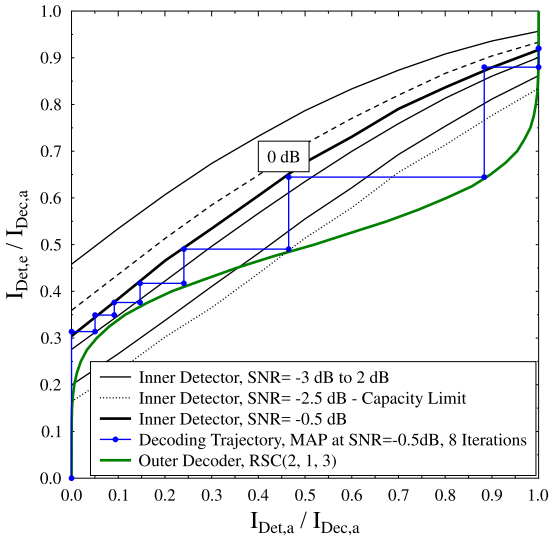

FIGURE 38. The EXIT charts of an LMS-GSTSK(64:4, 16, 2, 2, 2, 2, 1:2, BPSK) system associated with the DAC configuration and a half-rate RSC(2, 1, 3) outer decoder. An open-tunnel is shown between the outer decoder's EXIT curve and the inner decoder's EXIT curve at SNR = −0.5 dB, where 8 iterations iterations are required in order for the system to converge. The results are based on the schematic of Figure 20.

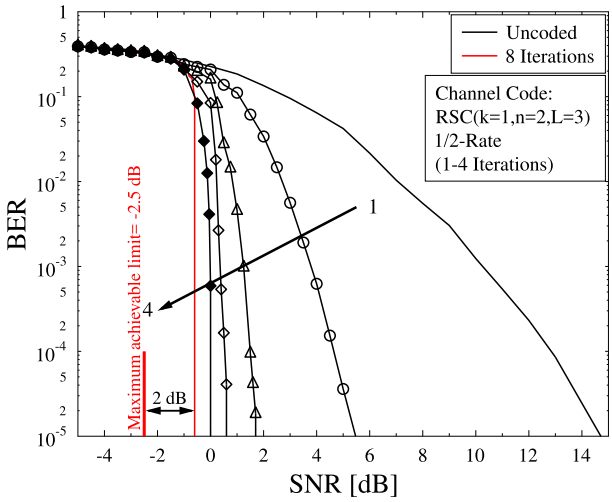

FIGURE 39. The BER performance of the LMS-GSTSK(64:4, 16, 2, 2, 2, 2, 1:2, BPSK) system associated with a half-rate RSC(2, 1, 3) decoder. The simulation was carried out using an input code length of 10^6 bits and 8 iterations between the outer decoder and the inner decoder. The results are based on the schematic of Figure 20.

To further illustrate the system's convergence behavior, the BER performance of the above LMS-GSTSK(64:4, 16, 2, 2, 2, 2, 1:2, BPSK) system associated with the half-rate RSC(2, 1, 3) decoder and using 8 iterations is shown in Figure 39. The performance curves of Figure 35 are also included in this figure for comparison. As expected, the system achieves a vanishingly low BER at SNR= −0.5 dB after applying 8 iterations between the outer and the inner decoder of Figure 20.

VIII. CONCLUSION

In this treatise, we proposed a novel LMS architecture, as a highly-evolved hierarchical MF framework that subsumes various conventional MIMO schemes as special cases, such as SM, SSK, GSM, QSM, STSK, GSTSK, MS-STSK, STBC, LDC, BLAST as well as LSSTCs. Our LMS concept is an amalgam of three constituents, namely of the GSTSK scheme, of the layered or stacked GSTSK codewords as well as of the activated AC. In the LMS of Figure 14, information is stacked into a compact agglomerate of codewords for the sake of transmitting a chunk of information in a single channel use. In a nutshell, our LMS invokes the index-modulation-based on/off mechanism both in time and space, as follows. In the GSTSK encoder of each layer, P out of Q dispersion matrices are selected to disperse the P non-zero components of the symbol vector over time and space. Then, the codewords of the K layers available are stacked into compact GSTSK codewords, which are transmitted over a specific combination of N_c^t out of N_t transmit AEs. Hence, the SM-based on/off mechanism is realized by: (1) the appropriately selected dispersion matrices of the GSTSK codewords, (2) the activated combination of dispersion matrices within each layer of the agglomerate and (3) the activated portion of AEs. We also proposed a two-stage serially concatenated SD-aided LMS detector, which is composed of a pair of an inner and an outer decoders that iteratively exchange their extrinsic information in order to achieve a near-capacity performance. Furthermore, we derived the DCMC capacity of our LMS system, which incorporates the capacity limit of all its derivatives. Finally, we utilized the EXIT chart tool for the sake of visually analyzing the LMS iterative decoding convergence.

REFERENCES

[1] L. L. Hanzo, O. Alamri, M. El-Hajjar, and N. Wu, *Near-Capacity Multi-Functional MIMO Systems: Sphere-Packing, Iterative Detection and Cooperation*. Hoboken, NJ, USA: Wiley, 2009. [Online]. Available: http://books.google.co.uk/books?id=590-JItOJREC

[2] L. Hanzo, M. El-Hajjar, and O. Alamri, "Near-capacity wireless transceivers and cooperative communications in the MIMO era: Evolution of standards, waveform design, and future perspectives," *Proc. IEEE*, vol. 99, no. 8, pp. 1343–1385, Aug. 2011.

[3] M. Di Renzo, H. Haas, A. Ghrayeb, S. Sugiura, and L. Hanzo, "Spatial modulation for generalized MIMO: Challenges, opportunities, and implementation," *Proc. IEEE*, vol. 102, no. 1, pp. 56–103, Jan. 2014.

[4] S. Sun, T. S. Rappaport, R. W. Heath, Jr., A. Nix, and S. Rangan, "MIMO for millimeter-wave wireless communications: Beamforming, spatial multiplexing, or both?" *IEEE Commun. Mag.*, vol. 52, no. 12, pp. 110–121, Dec. 2014.

[5] A. Adhikary *et al.*, "Joint spatial division and multiplexing for mm-Wave channels," *IEEE J. Sel. Areas Commun.*, vol. 32, no. 6, pp. 1239–1255, Jun. 2014.

[6] I. A. Hemadeh, M. El-Hajjar, S. Won, and L. Hanzo, "Layered multi-group steered space-time shift-keying for millimeter-wave communications," *IEEE Access*, vol. 4, pp. 3708–3718, 2016.

[7] R. W. Heath, N. González-Prelcic, S. Rangan, W. Roh, and A. M. Sayeed, "An overview of signal processing techniques for millimeter wave MIMO systems," *IEEE J. Sel. Topics Signal Process.*, vol. 10, no. 3, pp. 436–453, Apr. 2016.

[8] I. A. Hemadeh, M. El-Hajjar, S. Won, and L. Hanzo, "Multiuser steered multiset space-time shift keying for millimeter-wave communications," *IEEE Trans. Veh. Technol.*, vol. 66, no. 6, pp. 5491–5495, Jun. 2017.

[9] I. A. Hemadeh, M. El-Hajjar, S. Won, and L. Hanzo, "Multi-set space-time shift keying and space- frequency space-time shift keying for millimeter-wave communications," *IEEE Access*, vol. 5, pp. 8324–8342, 2017.

[10] S. Kutty and D. Sen, "Beamforming for millimeter wave communications: An inclusive survey," *IEEE Commun. Surveys Tuts.*, vol. 18, no. 2, pp. 949–973, 2nd Quart., 2016.

[11] M. Xiao *et al.*, "Millimeter wave communications for future mobile networks," *IEEE J. Sel. Areas Commun.*, vol. 35, no. 9, pp. 1909–1935, Sep. 2017.

[12] I. Hemadeh, K. Satyanarayana, M. El-Hajjar, and L. Hanzo, "Millimeter-wave communications: Physical channel models, design considerations, antenna constructions and link-budget," *IEEE Commun. Surveys Tuts.*, to be published.

[13] E. G. Larsson, O. Edfors, F. Tufvesson, and T. L. Marzetta, "Massive MIMO for next generation wireless systems," *IEEE Commun. Mag.*, vol. 52, no. 2, pp. 186–195, Feb. 2014.

[14] A. F. Molisch *et al.*, "Hybrid beamforming for massive MIMO: A survey," *IEEE Commun. Mag.*, vol. 55, no. 9, pp. 134–141, Sep. 2017.

[15] R. Vannithamby and S. Talwar, *Massive MIMO Communications*. Hoboken, NJ, USA: Wiley, 2017, p. 472. [Online]. Available: http://ieeexplore.ieee.org/xpl/articleDetails.jsp?arnumber=8042298

[16] J. G. Andrews, H. Claussen, M. Dohler, S. Rangan, and M. C. Reed, "Femtocells: Past, present, and future," *IEEE J. Sel. Areas Commun.*, vol. 30, no. 3, pp. 497–508, Apr. 2012.

[17] N. Zhang, N. Cheng, A. T. Gamage, K. Zhang, J. W. Mark, and X. Shen, "Cloud assisted HetNets toward 5G wireless networks," *IEEE Commun. Mag.*, vol. 53, no. 6, pp. 59–65, Jun. 2015.

[18] M. Agiwal, A. Roy, and N. Saxena, "Next generation 5G wireless networks: A comprehensive survey," *IEEE Commun. Surveys Tut.*, vol. 18, no. 3, pp. 1617–1655, 3rd Quart., 2016.

[19] M. El-Hajjar and L. Hanzo, "Multifunctional MIMO systems: A combined diversity and multiplexing design perspective," *IEEE Wireless Commun.*, vol. 17, no. 2, pp. 73–79, Apr. 2010.

[20] H. Mehrpouyan, M. Matthaiou, R. Wang, G. K. Karagiannidis, and Y. Hua, "Hybrid millimeter-wave systems: A novel paradigm for HetNets," *IEEE Commun. Mag.*, vol. 53, no. 1, pp. 216–221, Jan. 2015.

[21] A. Alkhateeb, J. Mo, N. Gonzalez-Prelcic, and R. W. Heath, Jr., "MIMO precoding and combining solutions for millimeter-wave systems," *IEEE Commun. Mag.*, vol. 52, no. 12, pp. 122–131, Dec. 2014.

[22] J. Brady, N. Behdad, and A. M. Sayeed, "Beamspace MIMO for millimeter-wave communications: System architecture, modeling, analysis, and measurements," *IEEE Trans. Antennas Propag.*, vol. 61, no. 7, pp. 3814–3827, Jul. 2013.

[23] I. A. Hemadeh, P. Botsinis, M. El-Hajjar, S. Won, and L. Hanzo, "Reduced-RF-chain aided soft-decision multi-set steered space-time shift-keying for millimeter-wave communications," *IEEE Access*, vol. 5, pp. 7223–7243, 2017.

[24] E. Başar, U. Aygolu, E. Panayirci, and H. V. Poor, "Space-time block coded spatial modulation," *IEEE Trans. Commun.*, vol. 59, no. 3, pp. 823–832, Mar. 2011.

[25] J. Li, M. Wen, M. Zhang, and X. Cheng, "Virtual spatial modulation," *IEEE Access*, vol. 4, pp. 6929–6938, 2016.

[26] E. Basar, "On multiple-input multiple-output OFDM with index modulation for next generation wireless networks," *IEEE Trans. Signal Process.*, vol. 64, no. 15, pp. 3868–3878, Aug. 2016.

[27] N. Ishikawa, S. Sugiura, and L. Hanzo, "Subcarrier-index modulation aided OFDM—Will it work?" *IEEE Access*, vol. 4, pp. 2580–2593, 2016.

[28] E. Basar, M. Wen, R. Mesleh, M. Di Renzo, Y. Xiao, and H. Haas, "Index modulation techniques for next-generation wireless networks," *IEEE Access*, vol. 5, pp. 16693–16746, 2017.

[29] C. Sacchi, T. Rahman, I. A. Hemadeh, and M. El-Hajjar, "Millimeter-wave transmission for small-cell backhaul in dense urban environment: A solution based on MIMO-OFDM and space-time shift keying (STSK)," *IEEE Access*, vol. 5, pp. 4000–4017, 2017.

[30] L. Hanzo, M. Münster, B. Choi, and T. Keller, *OFDM and MC-CDMA for Broadband Multi-User Communications, WLANs and Broadcasting*. Hoboken, NJ, USA: Wiley, May 2003. [Online]. Available: http://eprints.soton.ac.uk/258228/

[31] P. W. Wolniansky, G. J. Foschini, G. D. Golden, and R. A. Valenzuela, "V-BLAST: An architecture for realizing very high data rates over the rich-scattering wireless channel," in *Proc. URSI Int. Symp. Signals, Syst., Electron.*, Oct. 1998, pp. 295–300.

[32] R. Y. Mesleh, H. Haas, S. Sinanovic, C. W. Ahn, and S. Yun, "Spatial modulation," *IEEE Trans. Veh. Technol.*, vol. 57, no. 4, pp. 2228–2241, Jul. 2008.

[33] S. Alamouti, "A simple transmit diversity technique for wireless communications," *IEEE J. Sel. Areas Commun.*, vol. 16, no. 8, pp. 1451–1458, Oct. 1998.

[34] V. Tarokh, H. Jafarkhani, and A. R. Calderbank, "Space-time block codes from orthogonal designs," *IEEE Trans. Inf. Theory*, vol. 45, no. 5, pp. 1456–1467, Jul. 1999.

[35] L. Hanzo, J. Blogh, and S. Ni, *3G, HSPA and FDD versus TDD Networking: Smart Antennas and Adaptive Modulation*. Hoboken, NJ, USA: Wiley, 2008. [Online]. Available: https://books.google.co.uk/books?id=1-SJroa2hqsC

[36] C. Xu, S. Sugiura, S. X. Ng, P. Zhang, L. Wang, and L. Hanzo, "Two decades of MIMO design tradeoffs and reduced-complexity MIMO detection in near-capacity systems," *IEEE Access*, vol. 5, pp. 18564–18632, 2017.

[37] L. Hanzo, O. Alamri, M. El-Hajjar, and N. Wu, *Near-Capacity Multi-Functional MIMO Systems: Sphere-Packing, Iterative Detection and Cooperation*. Hoboken, NJ, USA: Wiley, 2008. [Online]. Available: http://eprints.soton.ac.uk/265783/

[38] L. Hanzo, L.-L. Yang, E.-L. Kuan, and K. Yen, *Single and Multi-Carrier DS-CDMA: Multi-User Detection, Space-Time Spreading, Synchronisation, Networking and Standards*. Hoboken, NJ, USA: Wiley, 2003. [Online]. Available: https://books.google.co.uk/books?id=04QSiM_Mzx8C

[39] L. Hanzo, T. H. Liew, and B. L. Yeap, *Turbo Coding, Turbo Equalisation and Space-Time Coding: For Transmission Over Fading Channels*. Hoboken, NJ, USA: Wiley, 2002. [Online]. Available: http://books.google.co.uk/books?id=3mOhrvMWTwQC

[40] D. G. Brennan, "Linear diversity combining techniques," *Proc. IRE*, vol. 47, no. 6, pp. 1075–1102, Jun. 1959.

[41] D. G. Brennan, "Linear diversity combining techniques," *Proc. IEEE*, vol. 91, no. 2, pp. 331–356, Feb. 2003.

[42] T. K. Y. Lo, "Maximum ratio transmission," *IEEE Trans. Commun.*, vol. 47, no. 10, pp. 1458–1461, Oct. 1999.

[43] N. Seshadri, V. Tarokh, and A. R. Calderbank, "Space-time codes for wireless communication: Code construction," in *Proc. IEEE 47th Veh. Technol. Conf.*, vol. 2. May 1997, pp. 637–641.

[44] V. Tarokh, N. Seshadri, and A. R. Calderbank, "Space-time codes for high data rate wireless communication: Performance criterion and code construction," *IEEE Trans. Inf. Theory*, vol. 44, no. 2, pp. 744–765, Mar. 1998.

[45] B. Hassibi and B. Hochwald, "Linear dispersion codes," in *Proc. IEEE Int. Symp. Inf. Theory*, Jun. 2001, p. 325.

[46] R. W. Heath, Jr., and A. Paulraj, "Linear dispersion codes for MIMO systems based on frame theory," *IEEE Trans. Signal Process.*, vol. 50, no. 10, pp. 2429–2441, Oct. 2002.

[47] H. El Gamal, A. R. J. Hammons, Y. Liu, M. P. Fitz, and O. Y. Takeshita, "On the design of space-time and space-frequency codes for MIMO frequency-selective fading channels," *IEEE Trans. Inf. Theory*, vol. 49, no. 9, pp. 2277–2292, Sep. 2003.

[48] E. Akay and E. Ayanoglu, "Achieving full frequency and space diversity in wireless systems via BICM, OFDM, STBC, and Viterbi decoding," *IEEE Trans. Commun.*, vol. 54, no. 12, pp. 2164–2172, Dec. 2006.

[49] Y. Yang, T. H. Chang, W. K. Ma, J. Ge, C. Y. Chi, and P. C. Ching, "Non-coherent bit-interleaved coded OSTBC-OFDM with maximum spatial-frequency diversity," *IEEE Trans. Wireless Commun.*, vol. 11, no. 9, pp. 3335–3347, Sep. 2012.

[50] Y. A. Eldemerdash, O. A. Dobre, and M. Öner, "Signal identification for multiple-antenna wireless systems: Achievements and challenges," *IEEE Commun. Surveys Tuts.*, vol. 18, no. 3, pp. 1524–1551, 3rd Quart., 2016.

[51] A. Paulraj and T. Kailath, "Increasing capacity in wireless broadcast systems using distributed transmission/directional reception (DTDR)," U.S. Patent 5 345 599, Sep. 6, 1994. [Online]. Available: http://www.google.co.uk/patents/US5345599

[52] G. J. Foschini, "Layered space-time architecture for wireless communication in a fading environment when using multi-element antennas," *Bell Labs Tech. J.*, vol. 1, no. 2, pp. 41–59, 1996.

[53] S. Song, Y. Yang, Q. Xionq, K. Xie, B.-J. Jeong, and B. Jiao, "A channel hopping technique I: Theoretical studies on band efficiency and capacity," in *Proc. Int. Conf. Commun., Circuits Syst.*, vol. 1. Jun. 2004, pp. 229–233.

[54] E. Başar, "Index modulation techniques for 5G wireless networks," *IEEE Commun. Mag.*, vol. 54, no. 7, pp. 168–175, Jul. 2016.

[55] Y. A. Chau and S.-H. Yu, "Space modulation on wireless fading channels," in *Proc. IEEE VTS 54th Veh. Technol. Conf. (VTC Fall)*, vol. 3. Oct. 2001, pp. 1668–1671.
[56] J. Jeganathan, A. Ghrayeb, L. Szczecinski, and A. Ceron, "Space shift keying modulation for MIMO channels," *IEEE Trans. Wireless Commun.*, vol. 8, no. 7, pp. 3692–3703, Jul. 2009.
[57] C. Xu, S. Sugiura, S. X. Ng, and L. Hanzo, "Spatial modulation and space-time shift keying: Optimal performance at a reduced detection complexity," *IEEE Trans. Commun.*, vol. 61, no. 1, pp. 206–216, Jan. 2013.
[58] D. A. Basnayaka and H. Haas, "MIMO interference channel between spatial multiplexing and spatial modulation," *IEEE Trans. Commun.*, vol. 64, no. 8, pp. 3369–3381, Aug. 2016.
[59] D. Yang, C. Xu, L. L. Yang, and L. Hanzo, "Transmit-diversity-assisted space-shift keying for colocated and distributed/cooperative MIMO elements," *IEEE Trans. Veh. Technol.*, vol. 60, no. 6, pp. 2864–2869, Jul. 2011.
[60] C. Masouros and L. Hanzo, "Constellation randomization achieves transmit diversity for single-RF spatial modulation," *IEEE Trans. Veh. Technol.*, vol. 65, no. 10, pp. 8101–8111, Oct. 2016.
[61] J. Jeganathan, A. Ghrayeb, and L. Szczecinski, "Spatial modulation: Optimal detection and performance analysis," *IEEE Commun. Lett.*, vol. 12, no. 8, pp. 545–547, Aug. 2008.
[62] J. Wang, S. Jia, and J. Song, "Generalised spatial modulation system with multiple active transmit antennas and low complexity detection scheme," *IEEE Trans. Wireless Commun.*, vol. 11, no. 4, pp. 1605–1615, Apr. 2012.
[63] S. Sugiura, C. Xu, S. X. Ng, and L. Hanzo, "Reduced-complexity iterative-detection-aided generalized space-time shift keying," *IEEE Trans. Veh. Technol.*, vol. 61, no. 8, pp. 3656–3664, Oct. 2012.
[64] X. Ma, D. A. Basnayaka, H. Haas, and D. Yuan, "Solutions for the interference caused by spatial modulation," in *Proc. 83rd Veh. Technol. Conf. (VTC Spring)*, May 2016, pp. 1–5.
[65] M. C. Lee, W. H. Chung, and T. S. Lee, "Generalized precoder design formulation and iterative algorithm for spatial modulation in MIMO systems with CSIT," *IEEE Trans. Commun.*, vol. 63, no. 4, pp. 1230–1244, Apr. 2015.
[66] C. Masouros, "Improving the diversity of spatial modulation in MISO channels by phase alignment," *IEEE Commun. Lett.*, vol. 18, no. 5, pp. 729–732, May 2014.
[67] M. Jiang and L. Hanzo, "Multiuser MIMO-OFDM for next-generation wireless systems," *Proc. IEEE*, vol. 95, no. 7, pp. 1430–1469, Jul. 2007.
[68] J. S. Blogh and L. S. Hanzo, *Third-Generation Systems and Intelligent Wireless Networking: Smart Antennas and Adaptive Modulation*. Hoboken, NJ, USA: Wiley, 2002. [Online]. Available: http://books.google.co.uk/books?id=CUZNkh4QRtoC
[69] X. Huang and Y. J. Guo, "Frequency-domain AoA estimation and beamforming with wideband hybrid arrays," *IEEE Trans. Wireless Commun.*, vol. 10, no. 8, pp. 2543–2553, Aug. 2011.
[70] E. Bjornson, E. Jorswieck, and B. Ottersten, "Impact of spatial correlation and precoding design in OSTBC MIMO systems," *IEEE Trans. Wireless Commun.*, vol. 9, no. 11, pp. 3578–3589, Nov. 2010.
[71] D.-S. Shiu, G. J. Faschini, M. J. Gans, and J. M. Kahn, "Fading correlation and its effect on the capacity of multi-element antenna systems," in *Proc. Int. Conf. Universal Pers. Commun. (ICUPC)*, vol. 1. Oct. 1998, pp. 429–433.
[72] G. J. Byers and F. Takawira, "Spatially and temporally correlated MIMO channels: Modeling and capacity analysis," *IEEE Trans. Veh. Technol.*, vol. 53, no. 3, pp. 634–643, May 2004.
[73] V. Tarokh, A. Naguib, N. Seshadri, and A. R. Calderbank, "Combined array processing and space-time coding," *IEEE Trans. Inf. Theory*, vol. 45, no. 4, pp. 1121–1128, May 1999.
[74] G. Jongren, M. Skoglund, and B. Ottersten, "Combining beamforming and orthogonal space-time block coding," *IEEE Trans. Inf. Theory*, vol. 48, no. 3, pp. 611–627, Mar. 2002.
[75] M. El-Hajjar, O. Alamri, J. Wang, S. Zummo, and L. Hanzo, "Layered steered space-time codes using multi-dimensional sphere packing modulation," *IEEE Trans. Wireless Commun.*, vol. 8, no. 7, pp. 3335–3340, Jul. 2009.
[76] S. Sugiura, S. Chen, and L. Hanzo, "Generalized space-time shift keying designed for flexible diversity-, multiplexing- and complexity-tradeoffs," *IEEE Trans. Wireless Commun.*, vol. 10, no. 4, pp. 1144–1153, Apr. 2011.
[77] S. Sugiura, S. Chen, and L. Hanzo, "Space-time shift keying: A unified MIMO architecture," in *Proc. IEEE Global Telecommun. Conf.*, Dec. 2010, pp. 1–5.
[78] S. Sugiura, S. Chen, and L. Hanzo, "Coherent and differential space-time shift keying: A dispersion matrix approach," *IEEE Trans. Commun.*, vol. 58, no. 11, pp. 3219–3230, Nov. 2010.
[79] C. Xu, S. Sugiura, S. X. Ng, and L. Hanzo, "Reduced-complexity soft-decision aided space-time shift keying," *IEEE Signal Process. Lett.*, vol. 18, no. 10, pp. 547–550, Oct. 2011.
[80] S. Sugiura, "Dispersion matrix optimization for space-time shift keying," *IEEE Commun. Lett.*, vol. 15, no. 11, pp. 1152–1155, Nov. 2011.
[81] M. I. Kadir, S. Sugiura, J. Zhang, S. Chen, and L. Hanzo, "OFDMA/SC-FDMA aided space–time shift keying for dispersive multiuser scenarios," *IEEE Trans. Veh. Technol.*, vol. 62, no. 1, pp. 408–414, Jan. 2013.
[82] P. Botsinis *et al.*, "Joint-alphabet space time shift keying in mm-Wave non-orthogonal multiple access," *IEEE Access*, to be published.
[83] M. I. Kadir, S. Chen, and L. Hanzo, "A reduced-complexity detector for OFDMA/SC-FDMA-aided space-time shift keying," in *Proc. IEEE 78th Veh. Technol. Conf. (VTC Fall)*, Sep. 2013, pp. 1–5.
[84] T. Datta, H. S. Eshwaraiah, and A. Chockalingam, "Generalized space-and-frequency index modulation," *IEEE Trans. Veh. Technol.*, vol. 65, no. 7, pp. 4911–4924, Jul. 2016.
[85] I. A. Hemadeh, M. El-Hajjar, S. Won, and L. Hanzo, "Multi-set space-time shift-keying with reduced detection complexity," *IEEE Access*, vol. 4, pp. 4234–4246, 2016.
[86] R. Mesleh, S. S. Ikki, and H. M. Aggoune, "Quadrature spatial modulation," *IEEE Trans. Veh. Technol.*, vol. 64, no. 6, pp. 2738–2742, Jun. 2015.
[87] A. Younis, N. Abuzgaia, R. Mesleh, and H. Haas, "Quadrature spatial modulation for 5G outdoor millimeter–wave communications: Capacity analysis," *IEEE Trans. Wireless Commun.*, vol. 16, no. 5, pp. 2882–2890, May 2017.
[88] J. Mietzner, R. Schober, L. Lampe, W. H. Gerstacker, and P. A. Hoeher, "Multiple-antenna techniques for wireless communications—A comprehensive literature survey," *IEEE Commun. Surveys Tuts.*, vol. 11, no. 2, pp. 87–105, 2nd Quart., 2009.
[89] A. Younis, N. Serafimovski, R. Mesleh, and H. Haas, "Generalised spatial modulation," in *Proc. Conf. Rec. 44th Asilomar Conf. Signals, Syst. Comput. (ASILOMAR)*, Nov. 2010, pp. 1498–1502.
[90] J. Fu, C. Hou, W. Xiang, L. Yan, and Y. Hou, "Generalised spatial modulation with multiple active transmit antennas," in *Proc. IEEE GLOBECOM Workshops*, Dec. 2010, pp. 839–844.
[91] K. Ntontin, M. Di Renzo, A. Perez-Neira, and C. Verikoukis, "Performance analysis of multistream spatial modulation with maximum-likelihood detection," in *Proc. IEEE Global Commun. Conf. (GLOBECOM)*, Dec. 2013, pp. 1590–1594.
[92] T. L. Narasimhan, P. Raviteja, and A. Chockalingam, "Generalized spatial modulation in large-scale multiuser MIMO systems," *IEEE Trans. Wireless Commun.*, vol. 14, no. 7, pp. 3764–3779, Jul. 2015.
[93] P. Liu, M. Di Renzo, and A. Springer, "Variable-N_u generalized spatial modulation for indoor LOS mmWave communication: Performance optimization and novel switching structure," *IEEE Trans. Commun.*, vol. 65, no. 6, pp. 2625–2640, Jun. 2017.
[94] M. Maleki, H. R. Bahrami, and A. Alizadeh, "Layered spatial modulation for multiuser communications," *IEEE Trans. Wireless Commun.*, vol. 15, no. 10, pp. 7143–7159, Oct. 2016.
[95] L. Bahl, J. Cocke, F. Jelinek, and J. Raviv, "Optimal decoding of linear codes for minimizing symbol error rate," *IEEE Trans. Inf. Theory*, vol. 20, no. 2, pp. 284–287, Mar. 1974.
[96] S. ten Brink, "Convergence behavior of iteratively decoded parallel concatenated codes," *IEEE Trans. Commun.*, vol. 49, no. 10, pp. 1727–1737, Oct. 2001.
[97] M. El-Hajjar and L. Hanzo, "EXIT charts for system design and analysis," *IEEE Commun. Surveys Tuts.*, vol. 16, no. 1, pp. 127–153, Feb. 2014.
[98] Abhishek, S. Kumar, and S. Chakrabarti, "Performance evaluation of asymmetric turbo codes using log-MAP decoding technique," in *Proc. Int. Conf. Devices Commun. (ICDeCom)*, Feb. 2011, pp. 1–5.
[99] L. Hanzo, S. X. Ng, T. Keller, and W. Webb, *Quadrature Amplitude Modulation: From Basics to Adaptive Trellis-Coded, Turbo-Equalised and Space-Time Coded OFDM, CDMA and MC-CDMA Systems*. Piscataway, NJ, USA: IEEE Press, 2004. [Online]. Available: https://books.google.co.uk/books?id=g_RSAAAAMAAJ
[100] J. Hagenauer, E. Offer, and L. Papke, "Iterative decoding of binary block and convolutional codes," *IEEE Trans. Inf. Theory*, vol. 42, no. 2, pp. 429–445, Mar. 1996.
[101] S. X. Ng and L. Hanzo, "On the MIMO channel capacity of multidimensional signal sets," *IEEE Trans. Veh. Technol.*, vol. 55, no. 2, pp. 528–536, Mar. 2006.

[102] S. ten Brink, "Convergence of iterative decoding," *Electron. Lett.*, vol. 35, no. 10, pp. 806–808, May 1999.
[103] A. Ashikhmin, G. Kramer, and S. ten Brink, "Extrinsic information transfer functions: Model and erasure channel properties," *IEEE Trans. Inf. Theory*, vol. 50, no. 11, pp. 2657–2673, Nov. 2004.

IBRAHIM A. HEMADEH received the B.Eng. degree (Hons.) in computer and communications engineering from the Islamic University of Lebanon, Lebanon, in 2010, and the M.Sc. degree (Hons.) in wireless communications and the Ph.D. degree in electronics and electrical engineering from the University of Southampton, U.K., in 2012 and 2017, respectively. He is currently a Post-Doctoral Researcher with Southampton Wireless Group, University of Southampton. His research interests mainly include millimeter-wave communications, multi-functional MIMO, multi-dimensional (time-space-and frequency) transceiver designs, channel coding, and multi-user MIMO.

MOHAMMED EL-HAJJAR received the Ph.D. degree in wireless communications from the University of Southampton, U.K., in 2008. Following the Ph.D., he joined Imagination Technologies as a Design Engineer, where he involved in designing and developing Imagination's multi-standard communications platform, which resulted in three patents. He is currently an Associate Professor with the Department of Electronics and Computer Science, University of Southampton. He was a recipient of several academic awards and has published a Wiley-IEEE book and in excess of 80 journal and conference papers. His research interests include the development of intelligent communications systems, energy-efficient transceiver design, MIMO, millimeter-wave communications, and radio over fiber network design.

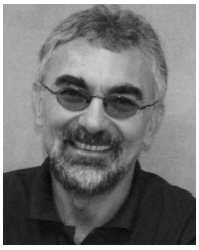

LAJOS HANZO (F'04) received the D.Sc. degree in electronics in 1976 and the Ph.D. degree in 1983. During his 40-year career in telecommunications, he has held various research and academic posts in Hungary, Germany, and U.K. Since 1986, he has been with the School of Electronics and Computer Science, University of Southampton, U.K. He is currently directing a 60-strong academic research team, working on a range of research projects in the field of wireless multimedia communications sponsored by industry, the Engineering and Physical Sciences Research Council, U.K., the European Research Council's Advanced Fellow Grant, and the Royal Society's Wolfson Research Merit Award. He is an enthusiastic supporter of industrial and academic liaison and he offers a range of industrial courses. He has successfully supervised over 110 Ph.D. students, co-authored 20 John Wiley/IEEE Press books on mobile radio communications totalling in excess of 10 000 pages, published over 1600 research entries at the IEEE Xplore. He was a FREng, FIET, and Fellow of the EURASIP. He received an Honorary Doctorate from the Technical University of Budapest in 2009. He served as the TPC Chair and the General Chair of the IEEE conferences, presented keynote lectures and has been received a number of distinctions. He is the Chair in telecommunications with the University of Southampton.